Spectral environment blind identification for PMR system the closer of analog receiver

Nicolas Grollier

UNIVERSITE BRETAGNE LOIRE / MATHSTIC

IMT Atlantique
Bretagne-Pays de la Loire
École Mines-Télécom

THESE DE DOCTORAT DE

L'ÉCOLE NATIONALE SUPERIEURE MINES-TELECOM ATLANTIQUE
BRETAGNE PAYS DE LA LOIRE - IMT ATLANTIQUE
COMUE UNIVERSITE BRETAGNE LOIRE

ECOLE DOCTORALE N° 601
Mathématiques et Sciences et Technologies de l'Information et de la Communication
Spécialité : *Télécommunications*

Par

« Nicolas GROLLIER »

« Spectral Environment Blind Identification for PMR System the Closer of Analog Receiver »

Thèse présentée et soutenue à IMT Atlantique BREST, le 13/11/2018
Unité de recherche : LAB-STICC
Thèse N° : 2018IMTA096

Rapporteurs avant soutenance :

Inbar FIJALKOW	Professeure, ENSEA – Cergy Pontoise
Philippe CIBLAT	Professeur, Télécom ParisTech

Composition du Jury :

Président :	Christophe MOY	Professeur, Université de Rennes 1
Examinateurs :	Philippe CIBLAT	Professeur, Télécom ParisTech
	Inbar FIJALKOW	Professeure, ENSEA – Cergy Pontoise
	Michaël PELISSIER	Ingénieur, CEA-Leti Minatec - Grenoble
Dir. de thèse :	Sébastien HOUCKE	Professeur, IMT Atlantique

A ma mère, Pascale

Remerciements

J'adresse tout d'abord mes sincères remerciements à mon directeur de thèse M. Sébastien Houcke, tant pour ses qualités scientifiques que personnelles. Il est certain que sans son concours, son expertise et sa patience, l'achèvement de ce travail n'aurait pas été possible. Je dois également le remercier de m'avoir accordé sa confiance, dès le début de cette thèse jusqu'à son achèvement.

Il me faut également remercier mes collègues doctorants et permanents du département Signal et Communications. Nos discussions, techniques et scientifiques entre autres, ont été essentielles pour moi tout au long de mon séjour au département.

Impossible de ne pas citer M. Vincent Gouldieff et son aide précieuse sur les problèmes cyclo-stationnaires. Je considère comme une chance et un grand plaisir d'avoir pu collaborer ensemble à la réalisation d'un travail des plus intéressants.

Je dois bien sûr remercier M. Guillaume Ferré, mon ancien professeur, de m'avoir soutenu à l'origine dans ce projet personnel orienté vers la recherche.

Je remercie aussi les partenaires du projet FITNESS, qui par leur concours financier et technique m'ont permis de progresser de cette façon. Plus spécifiquement, je remercie M. Michaël Pelissier et M. Patrick Audebert pour m'avoir reçu à plusieurs reprises au sein du CEA-LETI à Grenoble.

Enfin, je souhaite exprimer ma profonde reconnaissance à ma mère Pascale, à mon père Serge, à ma sœur Margaux et à toute ma famille pour avoir réussi à me transmettre leur affection dans les moments difficiles. Je en profite également pour remercier toute la famille Kermarrec, pour leurs attentions et leur gentillesse. Je termine plus particulièrement ces remerciements avec une mention spéciale pour Mlle. Elodie Kermarrec, ma compagne, qui a su distiller sa tendresse à chaque moment. De part son investissement et son soutien, sa contribution dans la réalisation de cette thèse est importante.

Contents

Notations

$\mathcal{D}$	Ensemble
N	Positive Integer
$\hat{x}$	Variable x Estimate
f	Function
δ_{ij}	Kronecker Symbol
$\mathbf{v}$	Vector
$\mathbf{M}$	Matrix
$\langle . \rangle_t$	Temporal Average
$(.)'$	Transpose Operation
$\lvert . \rvert$	Modulus Operation
$(.)^*$	Conjugation Operation
$\Re(.)$	Real Part
$\Im(.)$	Complex Part
$\mathcal{F}_t(.)$	Fourier Transform with respect of time
$\lfloor . \rfloor$	Floor Operator

Abbreviations

ADC	Analog to Digital Converter
APCO P25	Association of Public-Safety Communications Officials-International Project 25
AWGN	Additive White Gaussian Noise
BER	Bit Error Rate
CAF	Cyclic Autocorrelation Function
DR	Dynamic Range
IIP3	Input Interception Point of order 3
IMD	InterModulation Distortion
LNA	Low Noise Amplifier
NF	Noise Floor
PA	Power Amplifier
PMR	Professionnal Mobile Radio
PSD	Power Spectral Density
RF	Radio Frequency
ROC	Receiver Operating Characteristic
RX	Receiver
SAW	Surface Acoustic Wave
SCD	Cyclic Spectrum Density Function
SIHR	Signal to In-band Harmonic Ratio
SINR	Signal to Interference and Noise Ratio
SIR	Signal to Interference Ratio
SNR	Signal to Noise Ratio
SOI	Signal Of Interest
TEDS	TETRA Enhanced Data Service
TETRA	TerrEstrial Truncked Radio

List of Figures

List of Tables

Abstract

This document aims to present this thesis results prepared in the Lab-STICC, IMT Atlantique in the scope of the FITNESS project. FITNESS is a European project that aims to prepare the future of Professional Mobile Radio (PMR), which are secured wireless radios used by security services. Its goal is to design a new receiver compliant with the four PMR norms in Europe, while adding new functionalities such as high data rate transmission. This thesis contributions are limited to the backward compliance with current narrowband PMR standards. A new receiver architecture was defined by FITNESS preliminary work. It appears that due to the backward compliance with current PMR standards several requirements are not achievable. Amongst others, the phase noise requirement was relaxed. This tradeoff implies the presence of several powerful PMR signals close to the channel of the signal of interest. However, the presence of multiple signals in the received bandwidth raises additional issues linked to the receiver analog devices imperfections. A nonlinear phenomenon of saturation creates several unwanted harmonics that are harmful for system performance. An answer consists in making the receiver aware of its spectral environment. This methods may allow to adjust dynamically the receiver analog parameters to make it works in its linear region. A first chapter is devoted to analyze PMR radios and FITNESS constraints. As the receiver architecture is already defined, only blind detection methods could be used to sense the environment. The cyclostationary approach is the most adapted in our context. Nonetheless, state of the art methods are unable to answer FITNESS requirements. So, in a general point a view, we propose a new detection method based on second order cyclic moments. Then, this new tool is applied in a nonlinear context, to detect the presence of unwanted harmonics created by the receiver nonlinear behavior. We show that it is possible to detect early if the receiver works in a linear or in a nonlinear regime. Finally, based on the two previous studies, we propose a new method to adjust automatically the receiver analog parameters. This proof of concept improves significantly the bit error rate while allowing to relax additional analog constraints.

Résumé

Introduction

Les utilisateurs de radios PMR sont les services de sureté, de transport, des industriels ou plus largement des organismes professionnels qui ont besoin d'un système de communications sécurisé dans leur travail quotidien. Bien que l'efficacité des réseaux PMR, ainsi que leur robustesse aient été amélioré, ces professionnels réclament plus de fonctionnalités telles que celles offertes par la 4G commerciale. La thèse est réalisée dans le contexte du projet Européen FITNESS, qui a pour objectif de préparer le système PMR du futur en Europe et dans le monde. Ce projet à pour vocation d'ajouter un système de communication large bande sécurisé basé sur la technologie Long-Term-Evolution (LTE). Ses objectifs principaux sont d'étudier et de lever les principaux verrous technologiques afin de rendre possible le développement ultérieur d'un système PMR multi-standard, multi-usage à bas coût. De plus, ce nouveau récepteur devra être compatible avec les standards PMR existants pour garantir une rétro-compatibilité tout en ayant les nouvelles fonctionnalités critiques. De part le design d'un système large bande, le projet FITNESS s'inscrit dans la ligné des efforts Européens de déployer le système de communications sans fils PMR de prochaine génération.

L'IMT Atlantique est impliquée dans une petite part de ce projet. Dans la thèse, nous nous sommes concentrés sur la partie qui concerne spécifiquement la rétro-compatibilité avec les standards PMR actuels à bande étroite. Notre objectif est de proposer de nouvelles solutions permettant de garantir que le nouveau récepteur sera à-même de fonctionner dans les bandes 350-510MHz et 870-921MHz. Le problème principal rencontré lors du design de la partie analogique du nouveau récepteur est la difficulté de concilier une dynamique élevée (plus de 141dB), des canaux de communication de 12.5kHz dans un circuit tout intégré.

C'est pourquoi les spécification du nouveau récepteur sont particulièrement sévères au niveau matériel. En effet, les composants électroniques du récepteur (RX) fonctionnement en réalité de façon différente de la théorie. Certaines spécifications ne peuvent donc pas être tenues, ce qui entraine une dégradation du signal utile. Cette situation arrive lorsque certains composants utilisés en radio fréquence (RF), comme les amplificateurs à faible bruit (LNA), ou les multiplicateurs, sont utilisés en dehors de leur zone de fonctionnement nominale. Il peut alors s'agir d'une saturation du composant, ou de l'apparition d'harmoniques indésirables dues aux produit d'intermodulation. Un rapport préliminaire au projet FITNESS montre qu'il est possible de limiter certaines contraintes à l'aide d'un schéma spécifique. Cette

nouvelle architecture est supposée suffisante pour annuler les effets de divers mécanismes de dégradation tels que : appairage I/Q, signal parasite à la fréquence image ou encore des problèmes spécifiques d'architecture. Puisque le récepteur est supposé bien conçu, seules les problématiques de saturation et de non linéarités ont été traitées dans la thèse.

La nouvelle architecture ne permet toutefois pas de sélectionner le canal de communication de la même façon que les récepteurs classiques. Des contraintes supplémentaires sont donc ajoutées au niveau des convertisseurs analogiques/numériques (ADC). En effet, malgré un nouveau mécanisme de sélection de canal, la spécification de bruit de phase n'est pas atteignable. Plusieurs signaux indésirables et insuffisamment atténués peuvent alors se trouver proche de la bande du signal utile. Toute la problématique deviens alors de numériser le signal utile sans saturer la chaine, ni dégrader le signal reçu via l'intermodulation, et sans saturation des convertisseurs.

Les systèmes PMR

Cette partie est consacrée à la description rapide des systèmes PMR et du récepteur utilisé qui est décomposé en plusieurs couches hétérodynes. Nous proposons ensuite de modéliser l'ensemble du récepteur comme un système de plusieurs blocs non linéaires en série. Dans cette optique, nous définissions un modèle de non linéarités. Les conséquences sur le spectre et la création de fréquences qui en découlent sont également traitées. Enfin, le signal reçu en fréquence porteuse est modélisé comme une somme d'un signal utile et d'interféreurs qui perturbent la détection en raison du mélange induit par le modèle choisi.

Les radios professionnelles mobiles -*Professionnal Mobile Radios (PMR)*- sont plutôt inconnues du grand public. Une de leurs fonctionnalités est pourtant bien connue grâce à la première déclinaison analogique d'un standard PMR (PMR446) qui a popularisé l'usage des talkie-walkie. Les radios PMR sont des terminaux sans fils sécurisés utilisés par les services de suretés ou de travaux publics. Ses autres fonctionnalités sont par exemple : appuyer pour parler, communication point à point, positionnement GPS, appel d'urgence, multi-diffusion, etc. Les réseaux PMR sont prévu pour couvrir la plus grande surface de territoire possible, a contrario des réseaux commerciaux qui visent à couvrir la plus large portion possible de la population. Le système lui-même est conçu pour fonctionner même en cas de catastrophe naturelle (cyclone, tremblement de terre, etc.) qui pourraient impliquer la destruction partielle ou complète des différentes réseaux de communication.

Un point qui nous intéresse particulièrement est la multiplicité des réseaux PMR de nature différente sur des zones restreintes. Simplement en Europe, quatre normes PMR différentes coexistent (TETRA, TETRAPOL, P25 et leurs évolutions). Le cas de la Belgique est représentatif avec un réseau TETRAPOL à la frontière Française, et un réseau TETRA à la frontière Allemande. Le problème est la multiplicité des bandes utilisés, qui sont différentes dans chaque pays. Bien qu'il existe des passerelles entre réseaux différents, les utilisateurs en itinérance n'ont qu'un accès limité aux fonctionnalités du réseau hôte. Par conséquent, la qualité de service n'est pas assurée et les coûts multipliés par la multiplicité de réseaux hété-

rogènes. Le tableau tab.2.2 synthétise les caractéristiques principales des couches physiques et réseau des standards PMR Européens visés par FITNESS.

Pour pouvoir répondre à l'exigence de rétro-compatibilité avec tous les standards PMR actuels, une nouvelle architecture de récepteur à été définie. On notera qu'elle est de type double hétérodyne avec un système de sélection de canal basé sur l'utilisation de filtres très sélectifs et reconfigurables : les N-path filters. Ces filtres ont cependant une bande passante trop élevée pour atténuer totalement les signaux de communications PMR des canaux adjacent au signal utile. Le signal en bout de chaine est localisé sur une fréquence porteuse f_{IF_2} de 4.5MHz. Il sera constitué du signal utile et d'un ou plusieurs signaux d'interférences insuffisamment atténués. Le signal résultant est numérisé à une fréquence d'échantillonnage f_s de 18MHz.

La présence de ces signaux indésirables est problématique lorsque les composants électroniques du RX ne fonctionnent plus dans leur zone de fonctionnement optimale. Dans la thèse on a considéré que le récepteur est constitué d'une mise en série de plusieurs composants imparfait (voir [Razavi, 2011]). Celui-ci est alors modélisé par une fonction non linéaire d'ordre 3 en (2.1), tel que $e(t)$ soit le signal reçu, les coefficients $\alpha_{\{1,2,3\}}$ sont caractéristiques du récepteur et $s(t)$ le signal numérisé.

$$s(t) = \alpha_1 e(t) + \alpha_2 e^2(t) + \alpha_3 e^3(t) + \dots \tag{1}$$

Il a été montré dans [Razavi, 2011, Cripps, 2006] que suivant le modèle du signal $e(t)$, deux effets sont de nature à dégrader le signal utile et amplifié $\alpha_1 e(t)$. On peut aisément montrer que lorsque $e(t)$ est un signal sinusoïdal simple tel que $e(t) = A_1(t)cos(2\pi f_1 t)$, des harmoniques indésirables ainsi qu'un repliement dans la bande du signal utile intervient si la puissance du signal utile est trop importante (phénomène de saturation). A contrario, si $e(t)$ est une mixture d'au moins deux signaux sur porteuses différentes tel que $e(t) = A_1(t)cos(\omega_1 t) +$

	TETRAPOL	**TETRA**	**TEDS**	**P25 (phase 2)**
Frequency Band [MHz]	80, 380-490	380-390, 395-400 410-420, 420-430 450-460, 460-470 870-876, 415-921		36-174 403-512, 806-870
Channel Size [kHz]	12.5	6.25 (25-50-100-150)		6.25
Link Type	Half-Duplex	Full-Duplex		Full-Duplex
Layer Access	FDMA	TDMA (4-8-16-32 channels)		TDMA (2)
Modulation	GMSK	$\frac{\pi}{4}$-QDPSK	4 to 64 QAM	H-CPM H- DQPSK
Max. DL Speed [kbits/s]	76	36	691	12

Table 1: Synthèse des caractéristiques des standards PMR pris en compte par le projet FITNESS

$A_2(t)cos(\omega_2 t)$, alors le signal le plus puissant tends à réduire voire même annuler le gain du circuit (phénomènes de blocage et d'intermodulation).

Dans un récepteur classique, pour contrer ces phénomènes, l'amplification est limitée et d'importantes marges de numérisation sont conservées au niveau des convertisseurs. Dans le projet FITNESS, l'innovation serai de rendre le récepteur conscient de son environnement spectral, comme illustré en fig.2.7. L'idée est la suivante : dans une situation quelconque les marges d'IP3 (mesure de la non linéarité du circuit) et de bruit (NF) sont fixées comme schématisé en fig.2.7a. L'idéal serait de fixer une valeur d'IP3 la plus haute possible pour avoir un récepteur le plus linéaire possible. D'autre par on souhaiterai fixer une valeur de NF le plus bas possible pour avoir une meilleure sensibilité. Cependant ces deux paramètres sont liés par le gain du récepteur. Ainsi, la maximisation de la linéarité ne peut se faire qu'au détriment de la sensibilité. Un compromis est donc réalisé entre ces deux paramètres dans un récepteur classique.

En rendant le récepteur conscient de son environnement spectral grâce à une méthode de détection, ces bornes pourraient être ajustées. Prenons un cas ou aucun signal indésirable n'est détecté (*sensing scenario* en fig.2.7b). Dans ce cas de figure, la borne d'IP3 pourrait être relâchée, permettant d'augmenter le gain sans risquer de saturer la chaine de réception. Un autre situation serait celle de la présence de signaux interféreurs ou de saturation du circuit par le signal utile (*linearity scenario* en fig.2.7c). La borne de bruit peut alors être relâchée permettant de diminuer le gain, sans compromettre la numérisation car le signal reçu est d'amplitude importante. L'information de présence ou d'absence serait ensuite exploitée via une boucle de rétroaction pour agir sur les composants reconfigurables du RX.

Détection aveugle de signaux sur porteuse

Lorsqu'il s'agit de détecter un signal sans connaissances préalables, on parle généralement de détection aveugle. Ces méthodes sont utilisés pour des applications tant civiles que militaires. Dans un but militaire, comme dans la guerre électronique par exemple, il s'agirait d'intercepter et de décoder des messages transmis par l'ennemi, sans information (par exemple modulation, période des symboles, code, cryptage, etc.). Dans le domaine des télécommunications civiles, il existe de nombreuses applications pour les radio intelligentes. En

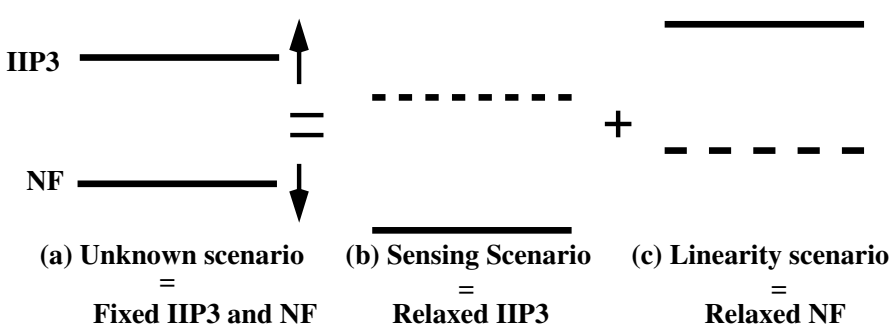

Figure 1: Scénarios d'adaptation du récepteur

effet, le spectre électromagnétique devient une ressource rare et la majeure partie de la bande passante est réservée à des utilisateurs spécifiques appelés "primaires". Ces utilisateurs sont reconnus dans l'application grâce à des "licences" payantes. Toutefois, ces utilisateurs peuvent laisser le spectre inutilisé pendant de longues périodes. Pour pallier à cette utilisation inefficace du spectre, il a été proposé par J. Mitola dans [Mitola and Maguire, 1999] et plus tard par S. Haykin dans [Haykin, 2005], de permettre à des utilisateurs "secondaires" d'accéder aux bandes non utilisés. Une telle application implique une connaissance de l'environnement spectral et, par conséquent, exige une capacité pour l'étudier. De cette façon, les utilisateurs secondaires viennent balayer le spectre à la recherche d'un canal radio exempt d'utilisateurs primaires.

Les deux applications représentent un défi, tant du point de vue du logiciel que du point de vue conception analogique. Ces problématiques sont soulevés par T. Yucek et H. Arslan dans [Yucek and Arslan, 2009], qui introduisent plusieurs méthodes statistiques de détection aveugle. Ce travail met en évidence les exigences principales des méthodes de détection : un taux d'échantillonnage élevé, une haute résolution de l'ADC, une large plage dynamique importante et enfin des capacités de calcul importantes. Ces contraintes sont très similaires à celles auxquelles nous sommes confrontés dans le cadre du projet FITNESS. Cependant, dans de nombreux cas, la détection nécessite une technique d'estimation de la puissance du bruit, ce qui n'est pas envisageable en raison des contraintes importantes imposées par FITNESS. Bien qu'il existe de nombreuses méthodes de détection, nous nous sommes concentrés sur deux méthodes en particulier : a) le détecteur d'énergie, qui est la méthode la plus simple ; b) le détecteur cyclostationnaire, qui est plus sophistiqué mais avec des inconvénients différents. La première étape identifiée est de balayer une partie de l'environnement spectral, comme dans le cas des radios intelligentes.

A notre connaissance, une grande partie des méthodes existantes proposent une détection en bande de base. Comme nous devons détecter les signaux indésirables le plus tôt possible dans la chaîne de réception, nous proposons de réaliser la détection directement à fréquence intermédiaire, juste après numérisation. Toutefois, ce traitement peut modifier les statistiques du signal reçu. Ce détail revêt une importance particulière, car les méthodes de détection reposent sur une décision statistique.

Détecteur cyclostationnaire de signaux à modulation de phase sur porteuse

Dans le chapitre 3 de la thèse, nous avons développé des outils théoriques pour détecter les signaux aléatoires. Nous proposons maintenant de les utiliser dans le cadre du projet FITNESS. Nous avons déjà souligné les avantages d'utiliser les propriétés cyclostationnaires du signal reçu dans ce contexte. En effet, la contrainte principale est de détecter des signaux à modulation de phase (c'est-à-dire O-QPSK et QAM) sur fréquence porteuse f_{ci} (avec f_{ci} la *i-ème* porteuse, $i = 1$ étant la porteuse du signal utile). Avec la connaissance du modèle cyclostationnaire du signal reçu, il a été montré dans [Gardner, 1994] qu'une détection et

même une classification est possible. Cela signifie qu'une connaissance préalable du signal étudié est nécessaire pour rechercher un modèle cyclostationnaire connu. Le problème dans notre étude est que le signal reçu est un mélange de plusieurs signaux PMR. Le détecteur doit donc obligatoirement être capable de distinguer chacun des signaux sans ambiguïté. Le seul paramètre différent pour chaque signal du mélange reçu est sa fréquence porteuse. Pour cette raison, et comme recommandé dans [Jouini et al., 2012], nous supposons connaitre a priori les fréquences porteuse des signaux possiblement reçus. Ainsi, nous nous concentrons sur les méthodes permettant de détecter une fréquence particulière dans l'ensemble étudié. Néanmoins, un autre problème se pose. Il est bien connu que les signaux modulés en phase sur porteuse ne présentent pas de fréquences cycliques multiples de f_{ci}, ce qui limite les méthodes pour effectuer un test. C'est pourquoi les détecteurs classiques, tels que le détecteur proposé par A.V. Dandawate et G.B. Giannakis qui consiste à estimer la fonction d'auto corrélation cyclique du second ordre (voir [Dandawate and Giannakis, 1994a]), ne sont pas adaptés.

Ce chapitre est donc consacré à une revue des méthodes cyclostationnaires permettant de détecter un signal modulé en phase sur porteuse. Les méthodes des moments deux ne sont pas adaptées car certaines modulations PMR n'ont pas d'énergie à des multiples de leur fréquence cyclique. Par conséquent, des statistiques cycliques d'ordre supérieur doivent être utilisées. Une autre possibilité serait d'utiliser ou la méthode de transformation non linéaire. Mais ces méthodes (qui ont des caractéristiques très similaires) nécessitent un grand nombre d'échantillons comme principal inconvénient. C'est pourquoi, nous avons proposé une nouvelle méthode pour détecter les signaux modulés en phase en utilisant une méthode de moments d'ordre deux.

Nous avons montré qu'il est possible de détecter la présence d'un signal à une fréquence cyclique où il n'y a théoriquement aucune énergie. Au moyen de simulations, nous avons exploré différentes caractéristiques de ce critère. Un avantage majeur de cette méthode est que le détecteur fonctionne bien en n'utilisant que 8 symboles, ce qui est particulièrement peu. A titre de comparaison, nous avons réalisé un test de détection avec la méthode de transformation non linéaire. Nos performances de détection sont beaucoup plus intéressantes lorsque la taille du signal d'entrée est petite, mais sont clairement inférieures lorsque le nombre de symboles est élevé. De plus, notre critère permet un ajustement de la probabilité de détection en modifiant l'un de ses paramètres. Toute amélioration du taux de détection est cependant obtenue au prix d'une augmentation du temps de calcul.

Les méthodes de détection sont souvent appliquées dans des conditions idéales, c'est-à-dire sans canal en négligeant l'effet du milieu. Dans la dernière partie de ce chapitre, nous avons essayé de répondre aux problèmes de sélectivité temporelle et fréquentielle. Nous avons montré qu'avec notre méthode, l'influence du canal est négligeable. Une brève analyse a également montré que la méthode est robuste à l'effet Doppler. Notre détecteur présente donc plusieurs avantages qui peuvent justifier une intégration dans le prototype de récepteur FITNESS. De plus, les résultats obtenus avec la modulation Q-PSK sont facilement extensibles aux signaux M-PSK ou M-QAM modulés en phase (avec $M > 2$).

Bien que qu'une étude de l'influence de l'excès de bande du filtre d'émission soit absente

de notre étude, l'influence d'un tel paramètre est connue. Plus l'excès de bande passante est proche de 1, meilleure est la probabilité de détection. A titre d'exemple, le travail réalisé dans [Houcke, 2002] est complet sur ce sujet. Refaire la même étude dans notre contexte n'est donc pas d'un grand intérêt. Nous n'avons analysé les taux de détection du critère proposé que dans le cas de signaux modulés en phase. Toutefois, il n'y a aucune raison pour que notre méthode fonctionne différemment lorsqu'il y a une énergie non nulle à la fréquence cyclique testée. Dans ce cas, des méthodes issues de l'état de l'art pourraient être utilisées, et potentiellement être plus efficaces que la méthode proposé. Cependant, l'utilisation de notre algorithme permet d'effectuer une détection sans la connaissance de la puissance du bruit, ce qui est un avantage certain.

Récepteur RF analogique conscient de son environnement spectral

Le chapitre 2 était consacré au nouveau récepteur PMR et à la description de ses contraintes. Comme nous l'avons vu, la convergence de plusieurs normes en un seul récepteur rend les spécifications de l'ADC difficiles à atteindre. Ceci est dû à la présence de signaux indésirables à l'entrée des convertisseurs, ce qui limite leur dynamique. Par conséquent, une méthode de détection de ces signaux doit être identifiée, ce qui justifie cette étude. Le modèle de signal et les méthodes de détection de base ont été développés dans le chapitre 3. La méthode de détection la plus appropriée est l'approche cyclostationnaire. Cependant, comme nous l'avons vu dans chapitre 4, certaines modulations PMR ne peuvent être détectées de manière simple. Ainsi, afin de résoudre le problème de la détection des signaux modulés en phase sur porteuse, nous avons développé une nouvelle méthode.

Dans ce chapitre, nous proposons d'utiliser ce nouvel outil pour détecter les signaux indésirables dans le contexte du projet FITNESS. Comme développé dans le chapitre 1, en raison de ses composantes analogiques internes, le récepteur n'est pas parfaitement linéaire et est modélisé comme un polynôme. En présence d'au moins deux signaux (c'est-à-dire le signal utile et un brouilleur), des harmoniques supplémentaires apparaissent en raison de la saturation. Ainsi, pour répondre aux exigences de FITNESS, nous devons déterminer quand la chaine de réception ou les convertissent commencent à saturer selon le mécanisme décrit dans la figure 2.7. Deux scénarios sont envisagés :

a) Un signal utile uniquement (scénario de sensibilité) ;

b) Un signal utile plus un signal brouilleur (scénario de linéarité).

Dans le cas a), si la puissance du signal utile est trop élevée, le récepteur peut cependant être saturer et créer des harmoniques indésirables. Dans le cas b), deux situations sont possibles :

b.i) La puissance du brouilleur est suffisamment faible, de sorte que la puissance des harmoniques indésirables sont également faibles, ce qui n'est pas gênant pour les performances du système ;

b.ii) La puissance de l'interféreur est suffisamment élevée pour créer de puissantes harmoniques et ainsi dégrader les performances de décodage.

Dans ce chapitre, nous proposons une méthode pour distinguer ces trois cas. Notre but est de réaliser plusieurs détections successives grâce à notre méthode de détection cyclostationnaire. La première étape consiste à décider si un brouilleur est présent ou non, en surveillant notre nouveau critère aux fréquences cycliques $2f_{c2}$ (avec f_{c2} est la fréquence porteuse du brouilleur). La deuxième étape, consiste à identifier si le récepteur à un comportement non linéaire ou non. On doit ensuite identifier si ce comportement est dû à la présence d'un puissant brouilleur, ou à un excès de puissance du signal utile. La surveillance des harmoniques spécifiquement créées par la fonction non linéaire à $4f_{c1}$ et $4f_{c2}$ permet l'identification du scénario.

Les densité de probabilité théoriques de ces trois tests ne sont cependant définis qu'en l'absence de signal à détecter. Dans un contexte non linéaire, il est nécessaire de souligner les différences entre une détection de signal unique et une détection de signal dans un mélange de plusieurs signaux. Comme avantage supplémentaire, cette méthode permet également de déterminer la raison pour laquelle le système fonctionne en régime non linéaire.

Comme principaux avantages, notre méthode contourne l'identification non-linéaire du modèle. En effet, en pratique aucune connaissance préalable des paramètres du modèle n'est requise (c.-à-d. ni l'ordre polynomial, ni les coefficients α_k). Une détection peut être effectuée sans aucune connaissance préalable. Comme développé dans le chapitre précédent, les mesures de performances de détection montrent que l'approche choisie est sensible et fiable. Nous considérons donc qu'elle pourrait être utilisée pour mettre en place une boucle de rétroaction. Dans un tel schéma, le gain est le paramètre à ajuster en tenant compte du scénario de travail du récepteur, ce qui est considéré dans le chapitre suivant.

Mécanisme d'ajustement automatique de gain pour un récepteur PMR

Notre objectif principal dans ce chapitre est de proposer une méthode pour assouplir les contraintes qui pèsent sur les convertisseurs. Dans le chapitre 5, nous avons montré que nous sommes capables de détecter si le récepteur fonctionne ou non en régime non linéaire. Cependant, nous n'avons évalué que la faisabilité de détection des interférences. Cela signifie qu'aucune rétroaction de cette information n'a été réalisée. Dans la continuité de cette idée, nous considérons que notre récepteur est conscient de son environnement spectral (voir chapitre 5). Nous proposons maintenant d'adapter ses paramètres en fonction de cette connaissance.

Le mécanisme de détection numérique a pour but de diminuer les contraintes sur les ADC, tout en maintenant constante la consommation d'énergie. En outre, l'exigence d'un terminal de faible encombrement que le front-end analogique doit être aussi limité que possible. Entre autres raisons, le récepteur est prévu pour être entièrement intégré et reconfigurable. L'utilisation de filtres SAW (c'est-à-dire de dispositifs externes) n'est pas possible car cela

conduirait à une stratégie de parallélisation couteuse en énergie et en encombrement. La plupart des méthodes avancées d'égalisation des non-linéarités reposent sur des termes d'intermodulation et des mécanismes de soustraction modélisés pour surmonter ce problème. Malgré l'efficacité de ces techniques, comme détaillé dans ce chapitre, leurs caractéristiques ne répondent pas aux spécifications FITNESS. Nous proposons donc une validation de principe d'une nouvelle méthode pour limiter les effets nocifs des non-linéarités. Selon la méthode d'identification spectrale proposée dans le chapitre 5, le gain du circuit pourrait être diminué si le récepteur fonctionne en régime non linéaire. A l'inverse, le gain pourrait être augmenté si aucun brouilleur et ni saturation ne sont détectés. Nous proposons d'utiliser une boucle de rétroaction comme mécanisme d'adaptation du gain qui doit fonctionner le plus rapidement possible. La modification du gain implique que la linéarité du circuit est impactée, comme cela est décrit par l'équivalent non linéaire de la formule Friis [Razavi, 2011]. Le mécanisme proposé a été grossièrement défini dans le chapitre 2.

Dans ce chapitre, nous présentons d'abord les avantages et les inconvénients des méthodes de l'état de l'art. Différentes possibilités pourraient être adaptées pour supprimer presque totalement les perturbations non linéaires indésirables dues à la présence de signaux de blocage. Cependant, chacun s'appuie sur la connaissance des paramètres du modèle non linéaire, ce qui s'avère inadéquat dans le contexte de FITNESS. Ensuite, nous avons développé une preuve de concept de récepteur PMR conscient de son environnement spectral. Ce mécanisme est basé sur le concept de boucle de rétroaction, qui permet au récepteur d'ajuster son gain pour travailler dans une région plus linéaire. Malgré l'absence d'expression théorique de notre méthode de détection, un mécanisme adaptatif a été proposé. Une analyse de la convergence de nos algorithmes a été présentée. Nous avons vu qu'après un court laps de temps, une valeur de gain stable peut être obtenue. Cependant, nous ne pouvons pas garantir que la valeur obtenue soit optimale au sens d'un critère donné pour limiter la puissance des harmoniques non linéaires. Enfin, une étude sur l'impact de cette méthode sur les performances de taux erreur binaires (TEB) à été réalisée. Les résultats les plus notables sont listés ci-dessous :

a) Avec cette preuve de concept, nous avons montré que le TEB pouvait être considérablement amélioré même lorsque le récepteur est saturé ;

b) Lorsqu'un brouilleur est présent, le mécanisme d'adaptation du gain améliore nettement les performances de TEB du récepteur. La limite d'amplification la plus élevée est la dynamique maximale admise par les ADC. La borne d'amplification inférieure est la valeur de gain qui donne le plancher de bruit maximal acceptable ;

c) Nous avons introduit la métrique SIHR qui traduit la puissance de l'harmonique indésirable repliée dans la bande passante signal utile. Nous avons montré que le gain est lié à la valeur de cette métrique.D'autre part, l'évolution du TEB est directement liée à celle du SIR. Notre relation de mise à jour de gain donne une valeur proche de la valeur SIHR optimale pour un seuil de fausse alarme de 5% ;

c) A notre connaissance, le concept de boucle de rétroaction de gain est un sujet qui n'a pas encore été exploré, dont les premiers résultats présentés dans la thèse semblent

prometteurs

Enfin, plusieurs points n'ont pas été abordés dans ce chapitre et doivent être développés succinctement. Comme preuve de concept, le mécanisme d'adaptation du gain est réalisé sur un récepteur non linéaire simple. En d'autres termes, de nombreux paramètres ont été négligés, comme par exemple : les effets de la quantification sur le taux de détection, les ajustements des marges ADC, ou le nombre fini de valeurs de gain possibles (chaque composant analogique du front-end ne peut pas être adapté à l'envie). De telles simplifications peuvent conduire à une perte d'efficacité significative de notre méthode dans un récepteur réel, en particulier à cause de la quantification. Néanmoins, le relâchement des marges des convertisseurs (qui n'ont pas été prises en compte dans nos simulations) pourrait entraîner d'autres effets positifs qui sont difficiles à évaluer pour l'instant. En effet, comme discuté dans le chapitre 2, d'importantes marges PAPR sont conservées pour assurer un signal numérique linéaire. Grâce à notre mécanisme de détection, ces marges peuvent être réduites, ce qui permettrait d'augmenter le gain dans une certaine mesure pour améliorer le SNR. C'était une exigence majeure exprimée dans le chapitre 2. Nous avons remarqué que pour maximiser l'effet de l'ajustement de gain, la meilleure façon est d'adapter le gain des premières composantes analogiques du récepteur car il affecte toute la chaîne en aval. Dans ce travail, nous avons supposé que les paramètres de plusieurs étages peuvent être ajustés pour obtenir produire un réglage plus fin, ce qui ne serait pas possible dans un récepteur réel. Un mécanisme permettant d'adapter le gain récepteur dans un ensemble de valeurs fixées pourrait être réalisé à la place. La valeur de gain idéale pourrait être approchée pour sélectionner la valeur de gain réel la plus proche. Enfin, cette méthode est capable de détecter un brouilleur, de détecter si le circuit fonctionne en régime non linéaire et d'en identifier la cause. Cette méthode semble donc être une bonne réponse aux exigences de FITNESS.

Conclusions

D'après la définition de Minolta dans [Mitola, 2000], la définition d'une radio intelligente est la suivante :

> *Radio intelligente : une radio ou un système qui analyse et est conscient de son environnement opérationnel, et qui peut ajuster ses paramètres de fonctionnement radio en conséquence de façon dynamique et autonome.*

Compte tenu de cette définition, le mécanisme de détection conçu dans cette thèse permet un ajustement autonome du gain du récepteur, ce qui limite ses interférences internes. A la lumière des travaux présentés, nous considérons que le système proposé peut donc être qualifié de radio PMR intelligente.

La première partie de cette thèse a été consacrée à l'analyse de l'environnement spectral des radios PMR. Nous avons vu au cours du chapitre 2 que les spécifications des normes PMR difficiles à adresser simplement par le design analogique seul. De plus, la conception globale du récepteur étant déjà définie, elle implique des contraintes supplémentaires sur les réponses

numériques qui pourraient être proposées (par exemple, mode aveugle, traitement rapide, etc.). Par conséquent, la nouveauté du projet est de détecter quand et pourquoi le récepteur fonctionne dans un régime non linéaire. Cet algorithme doit être réalisé dans le domaine numérique, et pourrait permettre d'adapter les paramètres analogiques du récepteur grâce à une boucle de retour. L'idée de mesurer la puissance harmonique non linéaire est nouvelle et mérite une analyse approfondie.

C'est pourquoi le chapitre 3 est consacré à un état de l'art des méthodes de détection aveugle. Comme les statistiques de puissance du signal et du bruit sont supposées inconnues, le détecteur d'énergie ne peut pas être utilisé. D'autres méthodes efficaces telles que le filtre adapté sont également écartées en raison du manque de connaissances sur le signal à détecter. Il semble que l'approche cyclostationnaire soit la plus intéressante, car elle nécessite peu d'informations et fonctionne bien à faible SNR.

Avec l'analyse précédente, nous poursuivons avec les contributions apportées par cette thèse. Nous avons vu dans le chapitre 4 que la détection de signaux à modulation de phase n'est pas possible en utilisant une méthode cyclique de moments du second ordre. Pour détecter de tels signaux, les méthodes habituelles sont : utilisation des moments d'ordre supérieur ou l'utilisation d'une transformation non linéaire. Nous avons montré que de telles méthodes nécessitent trop de symboles pour fournir de bons taux de détection et un niveau de confiance élevé. Nous avons donc proposé une nouvelle méthode de détection basée sur des statistiques de second ordre. L'originalité de notre algorithme est de pouvoir détecter la présence d'un signal en surveillant une fréquence cyclique où aucune énergie n'est présente en théorie. Cet algorithme s'est avéré capable de détecter une énergie cyclique lorsque la valeur théorique est nulle. Cette méthode peut être utilisée en mode semi-aveugle et nécessite très peu de symboles pour détecter la présence d'un signal. Nous avons évalué par simulations que cette méthode fournit de bons taux de détection à 0 dB. Notre détecteur est également résistant à la sélectivité du canal, et à une mauvaise synchronisation, comme cela a été démontré théoriquement et expérimentalement.

Ce nouvel outil est ensuite appliqué dans le contexte du projet FITNESS. Dans le chapitre 5, nous avons modélisé le récepteur comme un polynôme en raison de ses composantes analogiques, qui ont un comportement non linéaire. Nous avons vu que la présence d'un signal PMR dans un canal proche du signal de la fréquence porteuse d'intérêt crée des harmoniques supplémentaires. La méthode développée dans le chapitre 4 a été appliquée pour détecter les harmoniques cycliques dues au régime non linéaire du récepteur. Une analyse théorique de ce mécanisme est détaillée dans ce chapitre. L'utilisation de notre détecteur n'est cependant pas obligatoire. Il permet néanmoins d'effectuer une détection avec un petit nombre de symboles, sans estimation de la variance du bruit. Avec l'information de la présence d'harmoniques non linéaires, nous sommes capables de décider si le récepteur fonctionne ou non dans sa région linéaire. A travers des simulations, nous avons montré qu'une détection est possible bien avant une dégradation du signal utile. Cette étude a été réalisée en coopération avec le CEA et a donné lieu à une communication [Grollier et al., 2018].

Dans le chapitre 6, nous avons détaillé les grands principes des techniques de la littéra-

ture pour diminuer l'influence des harmonique due aux effets non linéaires. Il existe peu de solutions sur ce sujet. Plusieurs principes et méthodes sont développées succinctement au début du chapitre. Ces méthodes imposent souvent les exigences importantes sur la partie analogique des récepteurs, ce qui n'est pas acceptable dans le contexte de FITNESS. C'est pourquoi nous proposons une méthode entièrement nouvelle basée sur le principe de la boucle de rétroaction. Basé sur notre travail des chapitres 4 et 5, nous proposons une méthode pour que le récepteur adapte ses paramètres dans le chapitre 6. Le concept d'adaptation est basé sur la formule non linéaire de Friis. Cette relation implique qu'une diminution de gain engendre un circuit plus linéaire. Ensuite, nous avons présenté un mécanisme pour adapter le niveau de gain. L'efficacité de cette méthode a été démontrée par simulation, et nous avons vu qu'elle conduit à une amélioration significative du débit d'erreur binaire. Ce travail étant récent il n'a pas encore fait l'objet pas de communications scientifiques. Cependant, une article de conférence et un article de revue sont en cours de réaction à partir des résultats obtenus.

CHAPTER 1

General Introduction

1.1 Thesis Environment

Professional Mobile Radio (PMR) users are public safety, transport, industry and other professional organizations who need reliable and secured radio communication solutions in their daily work. Besides, PMR networks efficiency was improved as well as systems robustness, professionals require more feature richness as those offered by commercial networks. This thesis is realized in the context of the European project FITNESS (see [FITNESS, 2017]), which aims to prepare the future of Professional Mobile Radio in Europe and in the world. This project paves the way toward wireless broadband secured radios based on Long-Term Evolution (LTE) technology. Its mains goals are to study and unlock technological issues, to make possible the development of a multi-standard, multi-usage and low-cost PMR receiver. Moreover, this new PMR receiver has to be compliant with existing PMR standards to guarantee backward compatibility, and present new critical functionalities. By developing PMR broadband capability, FITNESS is supporting the European effort to deploy the next PMR wireless applications generation. Project partners (ADS, NXP, BeSpoon, MKR-IC, CEA, IMS, ISEP et IMT Atlantique) share interest and resources, according their respective expertise fields.

Main challenges tackled by FITNESS are the following ones:

- Study and creation of a new low-cost narrowband PMR receiver based on Complementary Metal Oxide Semiconductor(CMOS) and compliant with existing norms (TETRAPOL, TETRA, TEDS and APCO P25):
  1. Study and use of a Cartesian Feed Back Loop (CFBL);
  2. Create a new interference detection algorithm;
  3. Manage the usage in specific bandwidths.
- Integration of a highly-reconfigurable CMOS Radio Frequency (RF) transmitter:
  1. Guarantee the compliance with standards LTE PMR;
  2. Manage the usage in the 400 MHz and 700 MHz bandwidth;
  3. Antenna coupling;

4. Energy saving for mobile front-end.

- Integration of a geolocation system.
- Design of a 3D support allowing a coexistence of heterogeneous technologies and a highly integration in a low-cost terminal.

IMT Atlantique was involved in a small part of this project. In this thesis, we focused on the specific part that concerns the backward compliance with current narrowband PMR standards. Our aim is to propose new technological solutions to guarantee system performance in a narrowband multi-standard environment. More precisely, the new receiver has to be able to transmit and receive within the bandwidth 350 MHz to 510 MHz and in the bandwidth 870 MHz to 921 MHz. The encountered problem is a the edge between analog and digital domains. It appears that the main issue is to deal with a dynamic up to 141 dB with channel bandwidth of 12.5 kHz. This is a particularly severe specification for a fully integrated Receiver (RX).

Hence, the new receiver has tight analog specifications due to backwards compatibility. Due to the effective behavior of Receiver (RX) analog components, some requirements may not be hold and the signal of interest may be affected. A degradation can occur due to RF components such as Low Noise Amplifier (LNA) or mixers when they are used outside of their linear region. It might manifest through saturation, and presence of additional unwanted intermodulation products and harmonics. The FITNESS preliminary work showed that it is possible to limit analog constraints thanks to a particular design. The chosen architecture is assumed to be enough to counterbalance several analog mechanisms such as IQ imbalance, image frequency signal or architecture inherent issues. As the receiver is assumed well designed, in this document we focus on nonlinearities and saturation phenomena. However, with such a receiver analog design, the communication channel selection is not realized the same way as in classic receivers, which led to increase constraints on ADCs. Despite the new channel selection mechanism, phase noise requirements are still unachievable due to energy saving reasons and space consumption. The phase noise constraint could be released under specific conditions, which are described in the following dissertation.

1.2 Framework

The first part of this dissertation deals with general information, that are required to fully understand the raised issue. Thereby, chapter 2 is devoted to detail the FITNESS context. A short overview of PMR systems specifications is done. A description of analog issues is developed in the consideration of the FITNESS receiver architecture. As we will see, in addition to a pure analog design a digital sensing mechanism is proposed. Then, a synthesis of technological choices that led to this thesis is realized. The chapter is concluded by the list of FITNESS specifications and working assumptions. Once the analog constraints topic clarified, the problem is simplified to a blind detection in a nonlinear context.

Hence, chapter 3 deals with mathematical models that are used in following parts. Then, we go on with a blind detection state-of-the-art. A particular focus is made on the cyclostationary theory. Indeed, almost all communication signals have cyclostationary properties. Moreover, this technique allows a very fine detection and can be performed with a few working assumptions. An interesting property of such detection methods is to perform well at relatively low signal-to-noise-ratio. However, one major issue of cyclostationary techniques is the blind detection of on-carrier phase modulated signals (i.e. Phase-Shift-Keying or Quadrature-Amplitude modulations).

The second part of this document continues with answers we proposed to cope with FITNESS requirements. In chapter 4 we assume a general context, we focus on current cyclostationary methods to detect on carrier phase modulated signals. It appears that state of the art methods are either unable to work in noisy conditions, or are too costly in calculation time. Therefore, we propose a new method to detect on-carrier phase modulated signals. A theoretical analysis of this detector is conducted with a simple received signal model. Then, we propose a characterization through simulations. We show that our method is reliable in noisy conditions and requires very few symbols. Finally, several simplifying assumptions are released to show that this new detector is also efficient in a more real context. This work led to several communications [Grollier and Houcke, 2017, Grollier and Houcke, 2018], and a cooperation [Gouldieff et al., 2018].

In chapter 5, we use this new tool in the FITNESS context. The analog receiver is now modeled as a polynomial to take into account its internal electronic components behavior. We assume the presence of a PMR signal in a channel close to the signal of interest carrier frequency. Due to the receiver nonlinear behavior, is creates additional harmonics. A theoretical analysis of this mechanism is provided. We then propose to detect particular cyclic harmonics that are created only when the receiver works in a nonlinear regime. With the information of nonlinear harmonics presence, we decide if the receiver works or not in its linear region. Through simulations, we show that a detection is possible well before a degradation of the useful signal. This study was realized in cooperation with the CEA, and led to a communication [Grollier et al., 2018].

Finally, based on chapter 4 and chapter 5, we propose a method for the receiver to adapt its parameters in chapter 6. There are few state of the art solutions on this topic, that are recalled in the beginning of the chapter. Such solutions often tightens analog requirements, which is not affordable in the FITNESS context. Hence, we propose a completely new method based on the feedback loop principle. The overall adaptation concept is first developed. Then, we go on with a mechanism to adapt its parameters, to make it works in a more linear fashion. Our method efficiency is shown through simulations. We show that with our compensation method a significant Bit-Error-Rate improvement is possible. As this work is recent, there is still no scientific communications on this topic. However, a communication and a journal paper are planed based on obtained results.

1.3 Scientific Communications

The work accomplished in the second part of the dissertation led to the publication of several communications in national and international conferences.

List of publications:

- **Conferences:**

  1. (submitted)N. Grollier, S. Houcke and M. Pelissier, "Spectrally Aware RF front end Nonlinear Receiver Performance Analysis" *IEEE International Conference on Communications (ICC)*, May 2019
  2. V. Gouldieff, A. Nafkha, N. Grollier, J. Palicot and S. Daumont, "Cyclic Autocorrelation based Spectrum Sensing:Theoretical Derivation Framework", *25th International Conference on Telecommunications (ICT)*, June 2018
  3. N. Grollier, S. Houcke and M. Pelissier, "Enhanced Spectrally Aware RF front end Receiver under Non-linearity", *IEEE International Conference on Communications (ICC)*, May 2018
  4. N. Grollier and S. Houcke, "On Carrier QPSK Signal Detector Based on Second Order Cyclic-Moments", *IEEE Wireless Communications and Networking Conference (WCNC)*, April 2018
  5. N. Grollier and S. Houcke, "Détection de signaux QPSK sur porteuse en utilisant les statistiques cycliques d'ordre 2", *26ème colloque du Groupement de Recherche en Traitement du Signal et des Images (GRETSI)*, September 2017

- **Journals:**

  1. (in preparation) N. Grollier, S. Houcke and M. Pelissier, "Variable Gain Enhancement of a Nonlinear RF front end Receiver"

Part I

FITNESS Context & Blind Detection State of the Art

CHAPTER 2

FITNESS Receiver Description

2.1 Introduction

As presented in the general introduction, this document tackles the narrowband PMR receiver backward compatibility with PMR standards, which takes place in the FITNESS WP3. Hence, in this part we first focus on a brief existing PMR standard description in section 2.2. Then, we pay attention to our technical subject, which is the narrowband analog receiver. The architecture defined in the scope of FITNESS project is a discrete time doubly super-heterodyne architecture and is mainly inspired by the work realized by L. Lolis [Lolis, 2011]. He realized a very complete work of discrete time architecture synthesis in his PhD. thesis. [Razavi, 2011] is also a reference to understand the chosen analog design options. Such an architecture is a combination of two different receivers: super-heterodyne, or discrete time receiver. All issues of design, analog electronic and RF are tackled coarsly, but let us make a brief sum up of the two architectures in section 2.3. Its internal mechanisms are defined to make sense without to much useless details. We develop encountered issues and we define the receiver limits in the second part of this section. In section 2.4, FITNESS requirements, needs and assumptions are finally defined.

2.2 PMR System Overview

As it is, PMR systems are usually unknown from mainstream. However, their functionalities are well known thanks to one of its first declination: the analog standard PMR446, which popularized walky-talkies (see [Ketterling, 2004]). PMR radios are secured wireless systems that main users are security services (military, police, firefighters, airports, etc.) but also in industry or public works (power plants, transportation, etc.). Contrary to commercials communication networks (telecommunication operators), PMR networks are designed to cover the largest territory area (instead of largest customer density) to ensure a service continuity. Its main functionalities are: push-to-talk, point-to-point communication, GPS positioning, emergency call, multi-diffusion, and a relatively long range amongst others. The system is designed to work even in emergency cases as natural disaster (e.g. typhoon, earth-

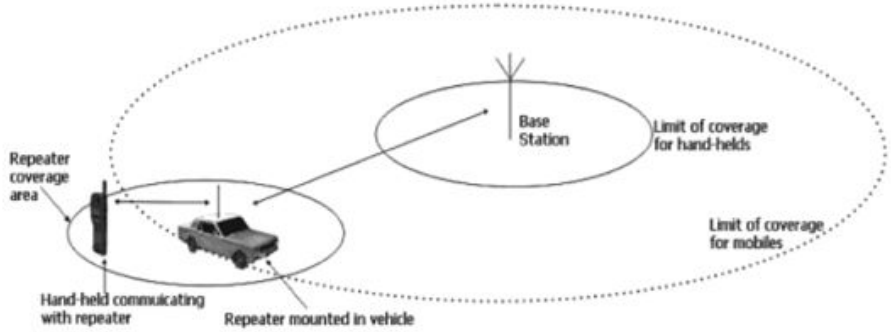

Figure 2.1: Example of the PMR network extension functionality

quake, flood, etc.) that may imply the partial or complete network destruction, thanks to its point-to-point functionality. In addition, it allows confidential communications in the case of private networks for security services, but this feature is not mandatory.

The overall communication principles can be briefly sum-up. Calls are given from a standard or directly by final users, which are gathered in two groups:

users: they use hand-held mobiles or portable terminals (e.g. embedded in a vehicle).

operators: which missions are diverse. The first is a tactical one, with the user configuration responsibility and in the field organization. The second mission is the user coordination. Finally, the last one is more technical and deals with operation and network maintenance.

Antenna networks support communications in a range of ten or so kilometers. There is also the possibility to create sub-networks or to extend the range thanks to more powerful repeaters as illustrated in fig.2.1.

Let now study PMR standards. First of them were designed in the late thirties and were based on analog technologies. Nowadays, a few of them are still in use due to their limited capacities and qualities (bad spectral efficiency, phone-tapping vulnerability, lack of data). Digital narrowband standards were introduced in the beginning of 1990, which main ones are TETRA, P25, TETRAPOL and their evolutions. Hence, they are based on old technologies as GSM. The PMR users community has new claims and requires new services offered by commercial 3G and 4G. It implies the development of a new broadband platform which guaranty the backward compatibility with current narrowband standards. In the other hand, states (main PMR users) chose different PMR solutions during the time. Therefore, several PMR standards are likely to coexist on small distances, which ask the interoperability question. The PMR system interoperability issue was analyzed and several solutions were proposed in [Baldini et al., 2011].

An interesting point is that PMR standard at borders are often different even in small areas. In Europe only, four standards are spread as shown in fig.2.2. The Belgium issue is representative: with TETRAPOL at France border and TETRA at Germany border. As each network is independent from others (even if they share the same norm), their bandwidth are

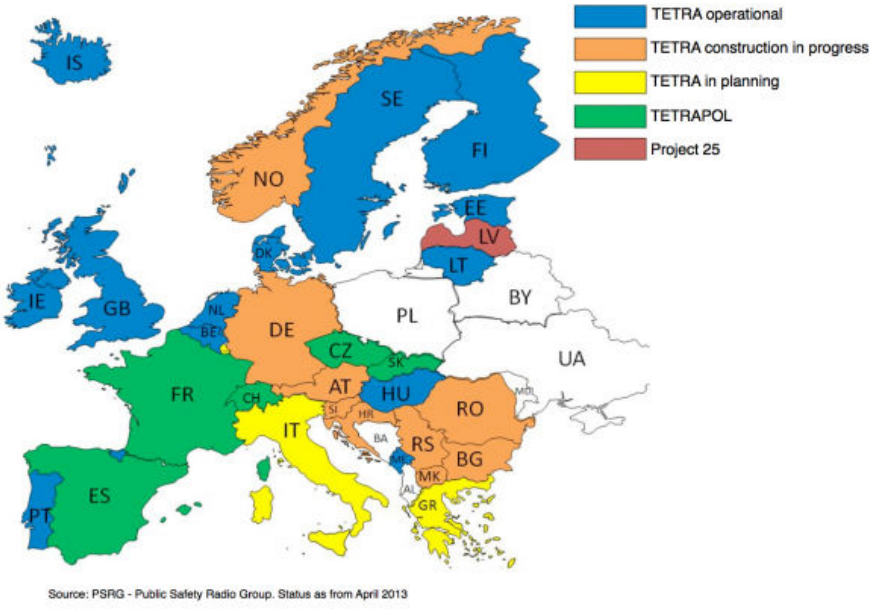

Figure 2.2: PMR standards repartition across Europe

different, which is a limiting factor for interaction between them. Besides some link can be defined, the granted user has a limited access and cannot use the full set of services. Hence, the service continuity is not insured and costs are increased due to network multiplication.

2.2.1 TETRAPOL

Initially developed by MATRA communications this standard is developed and maintained by two entities: TETRAPOL Forum and TETRAPOL User's Club. The TETRAPOL Forum Technical working group has developed TETRAPOL as a Publicly Available Specification, which makes it close to the definition of a standard. Last technical upgrades (in 2004), allowed to use IP protocol and some new functionalities such as the handover, or encrypted communications for IP based services. Deployed over 30 countries and more than 85 networks, TETRAPOL users are around 1.85 millions across the world [UC, 2018].

TETRAPOL is a digital cellular half-duplex system. Data sharing is realized through a encrypted narrowband system from user-to-user. TETRAPOL networks are designed such that covered areas are divided into 28 km side cells maximum. However, in practice communications cells are usually close to 20 km side in countryside and 6 km side in cities. The system is deployed in several frequency bands: 80 MHz and between 380 MHz to 490 MHz. Wireless communications rely on FDMA, in which every channel of 10 kHz to 12.5 kHz corresponds to a "voice user". Originally this choice allowed the adaptation of analog FM modulated PMR to new TETRAPOL networks, which are GMSK modulated. A convolutional coder is used, with an interleaving system and an error correction mechanism at reception. Maximum data speed are humble and reach 8 kbit/s. Hence, even if this system has a large range and is adapted for security services, the supported data transfer is much slower than commercial

3G or LTE (which reach in theory 42 Mbit/s and 1 Gbit/s respectively).

2.2.2 TETRA Standard and Evolution

The TETRA standard (TErrestrial Tuncked Radio) is open, developed by ETSI, and aims to tackle European PMR radios needs. Early standardization work began in 1988 to achieve a first commercial version in the middle of 90s. The system is based on resources sharing, which is very contemporary. TETRA offers same services than TETRAPOL (encrypted communication, push-to-talk, multi-cast, uni-cast, data transmission, emergency call/status, etc.).

TETRA cells have a maximum of 58 km side, which is often reduced to 8 km side depending of the network environment. Civilian networks are designed for two main bandwidth 385 MHz to 470 MHz and 870 MHz to 921 MHz. TETRA Air Interface specifications are developed in [Germain, 2014, ETSI, 2007, ETSI, 2013, ETSI, 2002]. Contrary to TETRAPOL the access layer method is based on TDMA, with 4 users interleaved within each 25 kHz frequency slot, to decrease base stations antenna number. In its first version, the modulation $\frac{\pi}{4}$-DQPSK was used. The TEDS evolution increased the channel size to 150 kHz, to improve the maximum data rate from 2.8 kbit/s to 691.2 kbit/s. However, this theoretical download speed is obtained only for more efficient modulations, which are defined to be 4 to 64-QAM. A network mechanism allows to switch to a less efficient modulation when service quality comes too low. In addition, the TETRA spectrum is managed in a semi-duplex style with the FDD duplexing method, which is a benefit compared to TETRAPOL or to VHF system. Besides its technical capabilities, the TETRA protocol cannot offer data rates as high as commercial technologies. In addition, the use of linear power amplifiers are needed to respect ETSI requirements, which is a very important aspect in this study.

2.2.3 APCO P25

Project 25 (P25) is a US standards gathering, which were developed by the cooperation of Association of Public Safety Communications Officials International (APCO): National Association of State Telecommunications Directors (NASTD), Federal Agencies and the National Communications Systems (NCS) under the lead of the Telecommunications Industry Association (TIA). This standard is used by security services and governmental organizations in north America. Hence, P25 as the same role as TETRA, but the two standards are unfortunately not compatible.

As for TETRA, a mechanism allows to tune the system if the service quality comes to low. In its first phase, the system works in analog mode, digital mode or a mix of these two options. The P25 modulation is the Continuous 4 Level FM (C4FM), which is a nonlinear modulation. The usual communication channel is 12.5 kHz, which allows a 9.6 kbit/s maximum theoretical data rate. A second development phase, which is not finalized, forecast a CQPSK modulation and a FDMA as a layer control access. One major improvement from phase one to phase two, is a better spectrum efficiency using amongst others 6.25 kHz channel size. P25 bandwidths

are located in the VHF (136 MHz to 174 MHz) and UHF (403 MHz to 512 MHz and 806 MHz to 870 MHz) spectrum part. As for TETRA and TETRAPOL, P25 offers same functionalities with more or less same drawbacks. Amongst others, the data rate is well low compared to commercial technologies.

2.3 New Narrowband PMR Receiver Environment

As developed in introduction, PMR users require new functionalities and better data rates. To answer theses requirements in the idea to address a European market, Airbus Space & Defense aims to create a new PMR receiver compliant with all European standards. The backward compliance makes the receiver highly constrained. So, let now focus on the receiver device. In this part we tackle the PMR receiver description in the FITNESS context, its limits and mains requirements that led to this thesis formulation.

2.3.1 Architecture Description

An ideal and simplified doubly heterodyne RX architecture is outlined in fig.2.3 (see [Rouphael, 2014]). Immediately after reception the signal is amplified and passes through

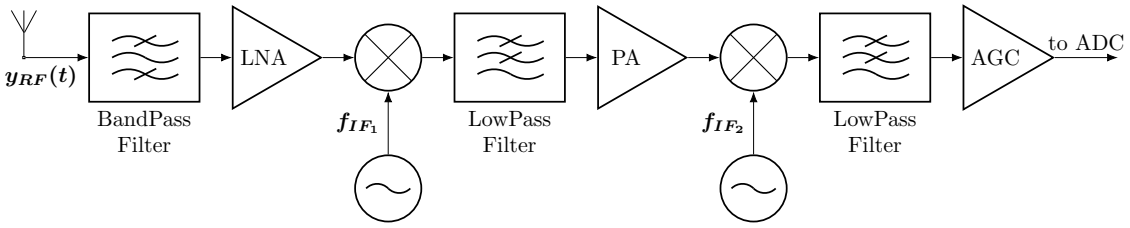

Figure 2.3: Example of double heterodyne RX architecture

a bandpass filter to select coarsely the PMR bandwidth to obtain a good attenuation of unwanted signals. A mixer and a variable oscillator are then used to down-convert the carrier frequency and choose the precise channel of communication. The first intermediate frequency, denoted as f_{IF_1} in the following document, is fixed at 126 MHz (see FITNESS report 3.3). A high enough f_{IF_1}, allows a out-of-band attenuation to be divided up in two parts (before/after f_{IF_1}). As the channel selection is realized at intermediate frequency, it allows us to decrease the bandwidth and release constraints on following components. Right after f_{IF_1}, the received signal is split into distinct ways (phase/quadrature) which are processed and digitalized separately. In fig.2.3, only one path is represented, but same operations are realized for the second path. This first down-conversion allows to suppress some unwanted signals at image frequency thanks to a smart frequency plan. Second down-conversion at f_{IF_2} (4.5 MHz) is then realized to make the ADC sampling frequency four times greater than f_{IF_1}. At this state, the useful signal has f_{IF_2} as a central frequency, and a bandwidth of 1 MHz. This operation allows us to decrease constraints on ADCs (lower sampling frequency) and to realize the

channel selection.

However, the real FITNESS RX shown in fig. 2.4 is slightly different from the ideal model. First work realized on the "discrete time architecture" was originally motivated by the need of multi-standard and multipurpose systems. Nowadays, such a receiver architecture drawn interest for its performance. An interesting work was realized by Ru and al. in [Ru et al., 2010] to clearly explain main principles. It was also shown, amongst others, by M. Muhammad et al in [Muhammad et al., 2005] that its performance reaches current communication standards. The main idea is that the useful signal bandwidth is much lower than its carrier frequency. So, operations of down-sampling and filtering are applied to reject unwanted signals and decrease ADC constraints of clock frequency and resolution. A drawback of such an operation earlier in the RX chain is the harmonics creation at sampling frequency multiples.

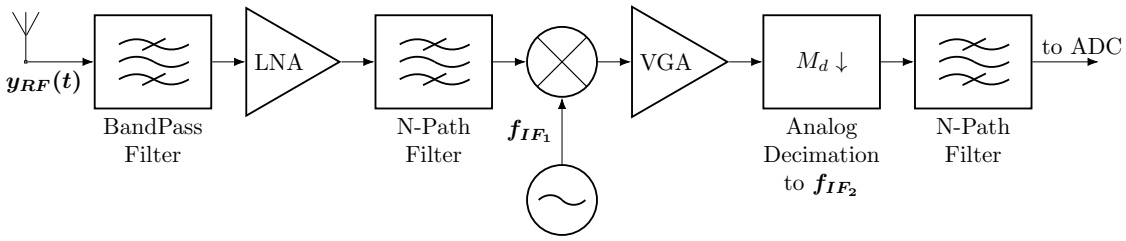

Figure 2.4: Overall Narrowband PMR Receiver Architecture for FITNESS

Another difference with the ideal architecture is the channel selection mechanism. Due to tight constraints of dynamic range, a tradeoff has to be made. Hence, two main issues happens at local oscillator and filtering stages. Indeed, in a typical RF receiver the channel is selected by downconversion of the useful signal to baseband and a filtering operation. As detailed in [Razavi, 2011], the downconversion is realized thanks to mixers and frequency adjustable oscillators. Usually, local oscillator frequency can be increased or decreased by small steps, which depends on communication channel standards requirements (e.g. 6.25 kHz in TETRAPOL standard). However, the introduced phase noise due to oscillator devices, which depends on frequency steps size, does not fit the project requirements. No commercial oscillator with a constant phase noise and able to cope with a 1 MHz bandwidth exist. A solution consists in decreasing the noise influence. This is achievable at the cost of a larger oscillator frequency step. But, if this solution is considered the RX has no channel selection mechanism.

In the other side, a 80 dB spurious attenuation is mandatory before sampling. This requirement is challenging to obtain in a fully integrated device. Moreover, to meet linearity requirements imposed by PMR standards(e.g. TETRA standard [ETSI, 2011]), the common solution is to use interstage Surface Acoustic Wave (SAW) filters. In the context of a fully integrated RX, such an option could not be considered as SAW filters are external devices. As external components SAW filters are not reconfigurable, which leads to expensive parallel filtering strategy (one filtering path peer standard at least). This is the reason of N-path filters presence in the FITNESS RX. Such filters are tunable in both central frequency and

bandpass, and allow to face three issues encountered by the new RX constraints. Their bandwidth could be adjusted to PMR channel size, which changes in every standard (see tab. 2.2). As their central frequency is tunable, it also solves the channel selection issue. Finally, the last remaining constraint is due to the small size of PMR channels (basically 12.5 kHz). So, the filter selectivity has to be sharp enough to guarantee at least 80 dB attenuation and deal with the SAW filter absence.

The proposed FITNESS architecture is able to provide a flexible and integrated solution. In order to come up with challenges, the new solution that will be tackle in the framework of FITNESS relies on the following principles:

- N-path RF filtering that enables to eliminate out of band strong interferences that exist in the wide-band range, and RF image band;
- A clock synthesis used for a coarse channel selection that provides sliding IF in order to enhance PLL cutoff frequency and facilitate Voltage Controlled Oscillator (VCO) integration;
- A high dynamic range ADC to handle strong adjacent and bi-adjacent interference scenario;
- A multi-mode configuration of the receiver to share noise and linearity constraints depending on the environment allowed by advanced signal processing method.

2.3.2 Receiver Limits

Unfortunately, architectural tradeoffs are not enough to meet stringent requirements of all PMR standards. By nature two main issues are raised from analog design: architecture limitations and nonlinear analog devices issues.

Linked to Architecture Problems

As described in the previous section, the FITNESS narrowband RX is different from a classic RX architecture. An analysis of dynamic range PMR standards shows that TETRAPOL requirements are the most stringent (the dynamic range is up to 141 dB) and linearity. To deal with it on a fully integrated RX, a design tradeoff was made. As discussed earlier, properly selecting the correct channel with respect to noise budget, is a major constraint for the overall system. So, a concession was made on local oscillator design to meet this requirement. The problem of injected noise by local oscillators and mixers was bring up in the previous part, but let us precise this problem.

As developed in [Perez, 1998], the self created noise is proportional to the PLL frequency (oscillator design) thanks to a $1/f$ relation. The lower the PLL frequency, the greater the noise power. Part of the solution is to use an heterodyne architecture: the signal is not down-converted to baseband, where the noise is maximized. According to [Razavi, 2011] chap. 7, both frequency and amplitude of oscillators are influenced by its own devices. Hence, the

oscillator is no more an ideal sinusoidal but performs instead as depicted in fig. 2.5. In fact, to meet FITNESS phase noise requirements the oscillator bandwidth has to be large enough to select almost 10 channels. The purpose of N-path filters is precisely to complete the channel selection mechanism. But, in presence of strong signals close to the Signal Of Interest (SOI), its attenuation requirements may not be hold and the SOI may be affected despite the 80 dB attenuation. Relaxing the oscillator frequency step increases device's bandwidth, but at the cost of linearity issues as we will see in the later part.

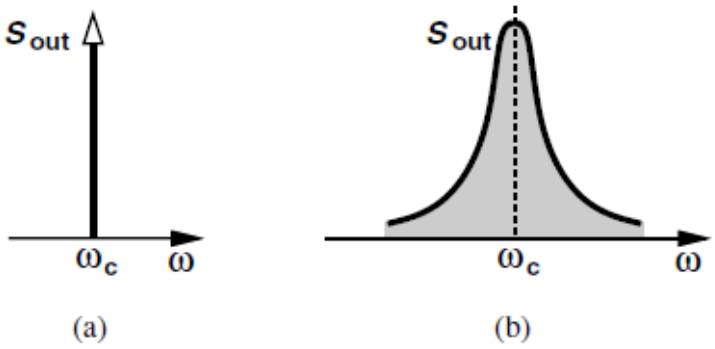

Figure 2.5: Output spectra of (a) an ideal, and (b) a noisy oscillator

Linked to Analog Devices Issues

As we consider real devices, their amplification behavior is no more ideal. If RF components such as Low Noise Amplifier (LNA) or mixers (see [Razavi, 2011, Cripps, 2006]) are considered memoryless, their output depend only on their corresponding input. Most of such devices are based on transistors, which are at the root of numerous nonlinear phenomenon. The usual state of the art model is recalled in eq. (2.1):

$$s(t) = \alpha_1 e(t) + \alpha_2 e^2(t) + \alpha_3 e^3(t) + \dots \tag{2.1}$$

where coefficients $\alpha_k, k \in \{1, 2, 3\}$ are characteristic of the considered device. In eq. (2.1), α_1 corresponds an ideal gain and α_2, α_3 to additional unwanted terms, with $\alpha_3 < 0$ the saturation coefficient. Higher order terms are often neglected as their power is insignificant. If we consider a single sinusoidal signal (e.g. $e(t) = A_1(t)cos(2\pi f_1 t)$), an input of eq. (2.1), then its output (2.2), is constituted by additional unwanted harmonics multiples of f_1 (the signal carrier frequency) and plus a continuous part.

$$\begin{aligned} s(t) \quad = \quad & \frac{\alpha_2 A_1^2(t)}{2} + (\alpha_1 A_1(t) + \frac{3\alpha_1\alpha_3 A_1^3(t)}{4})cos(2\pi f_1 t) + \frac{\alpha_2 A_1^2(t)}{2} cos(4\pi f_1 t) \\ & + \frac{3\alpha_3 A_1^3(t)}{4} cos(6\pi f_1 t) \end{aligned} \tag{2.2}$$

In eq.(2.2), there is an additional term multiple of $cos(2\pi f_1 t)$ (i.e. the SOI carrier frequency). The term $\frac{3}{4}\alpha_3 A_1^3(t)$ is an unwanted harmonic component that implies the front-end *saturation* if the $A_1(t)$ power comes too high.

Now, if we consider an input that is the sum of at least two independent signals, as described in eq. (2.3), special cases of SOI degradation can occur.

$$e(t) = A_1(t)cos(\omega_1 t) + A_2(t)cos(\omega_2 t) \tag{2.3}$$

Replacing eq.(2.3) in (2.1) leads to the creation of harmonics due to the product between the two components of $A_1(t)$ and $A_2(t)$. The complete formula, with all terms developed could be found in [Zou et al., 2009]. Harmonics frequencies depends on combinations between the SOI and the extra signal $A_2(t)$. As shown in fig. 2.6, there is many unwanted harmonics, of a smaller power than original signals. Theses harmonics are called InterModulation Distortion (IMD). Terms due to the $(.)^2$ operation are denoted IMD2, and terms due to the $(.)^3$ operation are denoted IMD3. However, even harmonics could be easily removed by a filtering operation, as they are far from the useful signal frequency. Only odd terms, which create harmonics at $2f_1 - f_2$ and at $2f_2 - f_1$ are problematic. As they are close to SOI carrier, such harmonics can't be suppressed completely and may overlap in SOI bandwidth, decreasing the Signal to Interference and Noise Ratio (SINR).

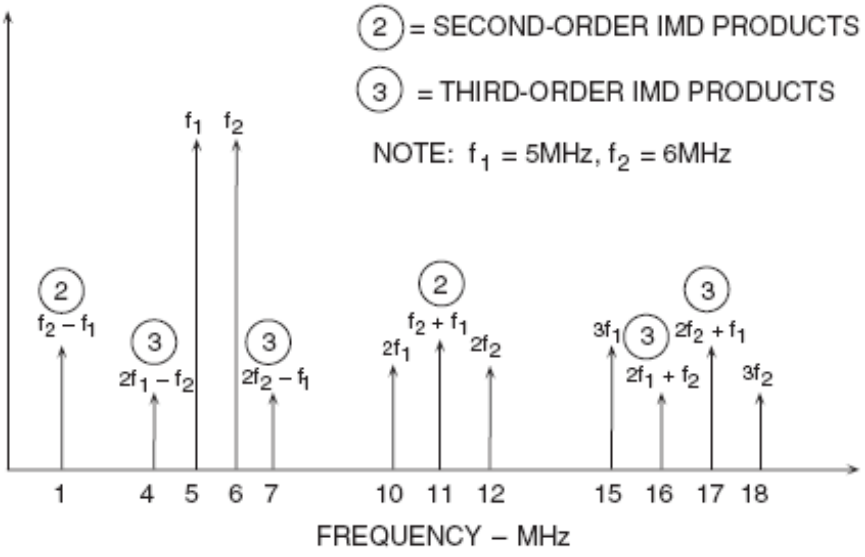

Figure 2.6: Output spectra of a nonlinear combination of two independent sinusoidal signal

If a special case of $A_1(t) << A_2(t)$ occurs, the largest signal tends to reduce the circuit gain. Hence, the weakest signal could be completely canceled. This situation is refereed as a "desensitization", and the largest signal is called a "blocker". The desensitization appears if we focus on the SOI representation in a specific sub-band, and is given in eq.(2.4):

$$s(t) = (\alpha_1 + \frac{3\alpha_3 A_2^2(t)}{2})A_1(t)cos(\omega_1 t) \tag{2.4}$$

Thus, it turns out that due to α_3, the signal $A_2(t)$ has an influence on the SOI range. Hence,

since the coefficient $\alpha_3 < 0$, this function of $A_2(t)$ could drop to zero for a larger enough $A_2(t)$ power.

There is two main scenarios, that are well known by analog designers, which can cause a blocking situation:

- a SOI and a powerful interference signal close to the SOI bandwidth. In fig.2.6, this case happens when the SOI central frequency is f_1. This is also the situation described in eq.(2.4);
- or two powerful signals far from the SOI but which central frequencies are distant of f_1, the SOI carrier frequency. This situation happens if the SOI is located at $f_2 - f_1$ with f_1 and f_2 interferers carriers.

This last situation may be really problematic since its rare for the two unwanted signals to be correctly digitized. As we saw previously, the FITNESS receiver is mainly concerned by the first of these two situations. However, this last situation has a particular interest to obtain the nonlinear parameters of eq.(2.1) during a laboratory experiment: the so called "two-tone" test. It consists precisely to create such a situation, in absence of useful signal. That way, making interferers powers grow, their unwanted contribution due to nonlinearity can be measured at $f_2 - f_1$. Then, with the interference power knowledge (which is a function of the jammer power), the model parameters can be obtained. This procedure was followed to obtain FITNESS RX nonlinear parameters exploited in chapter 5 and chapter 6.

To sum-up, the SOI degradation is the result of nonlinearities caused by analog devices used outside of their linear region. It might manifest through saturation, and presence of intermodulation harmonics and blocking. In the following development, unwanted signals are referred as blockers, jammers or interferers. Currently, important margins are left at ADC input to deal with such signals. So, limiting interferers presence could be interesting to decrease theses margins, which increases the Dynamic Range (DR).

2.4 Receiver Requirements: A Detection Issue

According to previous sections, the initial situation is presented. FITNESS RX architecture and its limitations are also clearer. In this section, FITNESS requirements are developed according to IMT Atlantique expertise. Some additional constraints as well as limiting hypothesis are then detailed.

2.4.1 FITNESS Requirements

In addition to pure analog design, a sensing mechanism performed by a digital processing could relax significantly the tight specifications of RX front end. More precisely, benefits in term of Dynamic Range (DR) and filtering requirement were quantified in the FITNESS report 3.1.

	PAPR [dB]		
	Useful Signal	Adjacent Interferer	Other Interferer
TETRAPOL	3	3	3
TETRA	6	6	3
TEDS	13	6	3

Table 2.1: PAPR requirement for PMR multi-standard depending on interference scenario

Extracted from this report, tab. 2.1 provides expected benefits on ADC PAPR specification if the system is aware of the interferer presence. A quick comparison between the useful signal PAPR requirement with other interferer PAPR margin, shows that 10 dB could be saved in the TEDS case. The main novelty proposed in this project is to detect unwanted harmonics in the analog signal that appear only if the RX works in a nonlinear regime. That way, the RX could be partially aware of its environment. Then, a mechanism to adapt its parameters dynamically to make the front-end work again in its linear region as fast as possible (see fig.2.7b) could be considered. To our best knowledge, the enhancement of a PMR receiver through a spectrum sensing method was evaluated in [Bräysy et al., 2010], but not realized. In the state-of-the-art almost all solutions implement the spectrum sensing unit and interference cancellation in the digital domain. However, in our context an adaptation in the analog domain might be useful.

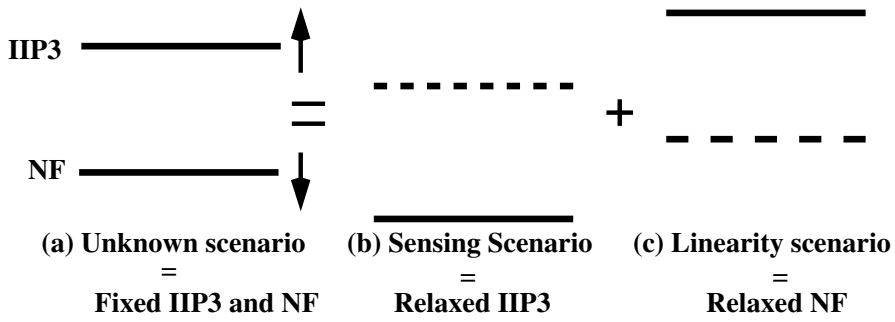

Figure 2.7: Sensing scenario cases

Providing a jammer detection, the adaptation main idea is the following one. In fig.2.7a, the unknown scenario corresponds to a classic receiver. In such a case, the RX parameters are fixed. The Input Interception Point of order 3 (IIP3) is a quantity which serves as a comparison of linearity of different circuits. It has to be the highest as possible, in order to make the receiver as linear as possible. The Noise Floor (NF) represents the noise added by the analog RX to the received signal such as in eq.(2.5),

$$NF_{|dB} = 10log_{10}(\frac{SNR_{in}}{SNR_{out}}) \tag{2.5}$$

where SNR_{in} is the SNR of the SOI before its passage through the RX system, and SNR_{out} the SNR at the RX output. So, the lower the NF, the better the Signal to Noise Ratio (SNR). However, NF and IIP3 are linked by the RX gain, and the maximization of IIP3 could be done only at the trade-off of a higher NF (see Friis formula and its nonlinear counterpart for

cascaded IIP3 in [Razavi, 2011]). We clearly understand the possible improvement if those parameters could be changed separately, which is exactly what we propose to do. Indeed, in the sensing scenario (fig.2.7b), we consider that the SOI is the only signal in presence (i.e. no jammers) and has a low power. In that particular case, NF and IIP3 could be decreased to improve the SNR. Indeed, no jammer is present, the IIP3 requirement could be relaxed. In the linearity scenario (fig.2.7c), two cases could happened: the SOI is the only signal in presence (i.e. no jammers) and has a strong power, or the SOI and jammers are present. In both cases, we are not limited by sensitivity but rather by the RX linearity. So, the RX gain could be decreased to increase the IIP3, to allow a better linearity at the cost of a NF degradation. Moreover, it would be of some use to know if the RX is close to work in its nonlinear region, and identify the reason.

If the receiver is able to detect in which scenario it has to work, it could improve significantly its dynamic by applying a quick feedback loop to set up its parameters. Another benefit is that this knowledge allows us to decrease the peak to average power ratio (PAPR) margin, and thus decrease constraints on ADCs.

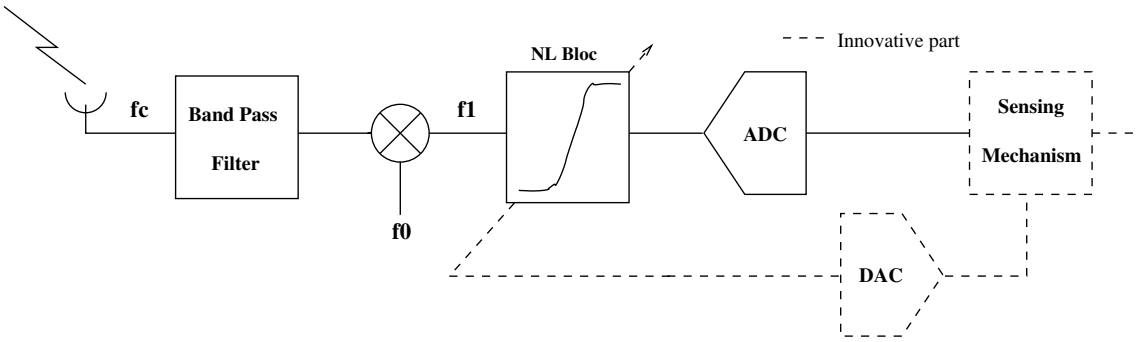

Figure 2.8: PMR Receiver scheme

This principle is depicted in fig.2.8, which represents a classic RX with the innovative part in dashed lines. To develop such a RX, the first step is to be able to detect in which scenario the RX is. The second one is the feedback loop design. The sensing mechanism allows us to:

a) detect the working region of the RX (i.e. linear or nonlinear mode);

b) detect the presence of interferer;

c) identify the reason of the nonlinear behavior : if it is due to the interferer or due to a powerful SOI.

2.4.2 Miscellaneous Constraints

PMR signals characteristics are listed below, in tab.2.2 . The first comment is that, obviously, the detection solution has to be compliant with all PMR standards. As we saw, interferers are most likely other PMR signals close to SOI carrier due to architectural tradeoffs. Hence, the detection algorithm resolution has to be sensitive enough to detect smallest

channels. Every modulated signal must be detected, which means that the detector should be modulation independent, or a least have an adaptive detection threshold.

	TETRAPOL	**TETRA**	**TEDS**	**P25 (phase 2)**
Frequency Band [MHz]	80, 380-490	380-390, 395-400 410-420, 420-430 450-460, 460-470 870-876, 415-921		36-174 403-512, 806-870
Channel Size [kHz]	12.5	6.25 (25-50-100-150)		6.25
Link Type	Half-Duplex	Full-Duplex		Full-Duplex
Layer Access	FDMA	TDMA (4-8-16-32 channels)		TDMA (2)
Modulation	GMSK	$\frac{\pi}{4}$-QDPSK	4 to 64 QAM	H-CPM H- DQPSK
Max. DL Speed [kbits/s]	76	36	691	12

Table 2.2: Characteristic of PMR standards tackled by FITNESS

Furthermore, the service quality also requests a detection as fast as possible. In other words, the number of samples needed has to be small enough to allows the feedback loop to adjust the RX parameters without loosing to much information. The ADC sampling frequency is 18 MHz, which means that working with a small number of samples is not an option. Indeed, the embedded CPU may not be able to deal with too much samples in a row. Finally, the FITNESS RX architecture can't be modified too much in order to maintain its space and energy consumption as low as possible. To save the more space and energy, the feedback could consist of a unique 3bits ADC for example. There is many detection strategies. However, some of them, could not be considered as the PMR standards and FITNESS architecture are already defined. This is typically the case of the cooperative sensing which requires either a specific architecture or information sharing strategy and protocol.

2.4.3 Additional Hypothesis

Some simplification are required to realize the following study, which must be justified. Let us begin with the analog issues hypothesis. Details on RF microelectronic and analog design are available in following books [Razavi, 2011, Cripps, 2006, Villegas, 2007, Larson, 1997] for example. In subsection 2.3.1 the image frequency issue was raised to justify architecture choices. Indeed the frequency plan is a very problematic part in a RX analog conception. However, as the architecture is well-defined thanks to the work of L. Lolis in [Lolis, 2011], we consider that image frequency issues are solved by a clever frequency planning. In the same way, it was shown in particular in [Valkama et al., 2005, Valkama et al., 2001, Tubbax et al., 2005, Windisch and Fettweis, 2007, Traverso et al., 2009] that impairment problems (also called I/Q gain mismatch) can be compensated. These papers show various methods, adapted for both narrowband or broadband systems, to make the RX independent of such

problem. Consequently, we consider that these issues are not relevant, and are not tackled as a part of the detection issue in this document.

As real devices, analog components of the RX are by definition imperfect by nature. In this study, we assume that nonlinearity is the first cause of SOI degradation. Indeed, the following work is applied to narrowband signals. As analog devices mandatory have a large bandwidth compared to SOI's, the simplification of a constant phase hold. Moreover, the chosen memoryless polynomial model in eq.(2.1) is broadly used in literature [Valkama et al., 2006,Keehr and Hajimiri, 2008,Zou et al., 2009,Turunen et al., 2016]. Other frequency almost independent models like Saleh's [Saleh, 1981], or Ghorbani's [Ghorbani and Sheikhan, 1991] were not considered for implementation consideration. Available IIP3 data were obtained through measurements on CEA demonstrator. That measure allows us to easily determine the polynomial model parameters. Moreover, most of manufacturers use this common convention, that way their products could be easily compared. On the other hand, the Volterra nonlinear model [Haykin, 1996a], is far too complex in a first approach. So, the memoryless assumption makes the study easier and could be relaxed in a future work. Finally, to limit the processing time, the detection should be processed right after ADCs at intermediate frequency. That way, all steps of down-conversion to baseband could be saved.

As developed in 2.4.1, jammers are assumed to be PMR communication signals close to the SOI. So, we have a prior information on interferer's carrier, but its others parameters are still unknown. One can consider that interferer signal has same norm as the SOI, but it may not be true in each situation. Moreover, nor the channel size, nor the modulation could be determined with such an assumption. That way the only valuable hypothesis is the prior information on carrier frequency. So, we propose a method that allows one or several close channels, to be scanned in order to get the needed information.

Interferers are PMR signal, which means that they are emitted by a different emitter. Hence, unwanted signals are independent of the SOI. Their power or probability distribution are also unknown for the RX at time t.

CHAPTER 3

On Carrier Signals Blind Detection

3.1 Introduction

When the point is to detect a signal without prior knowledge, it's usual to speak about blind detection. Such methods could be used with different aims, civilian or military. In military aims, such as in electronic warfare for example, it consists in interception and decoding of messages transmitted by the enemy, without information (e.g. modulation, symbol period, code, encryption, ...). In civilian telecommunication there is many applications in Cognitive Radio (CR). Indeed, the electromagnetic spectrum becomes a scarce resource and most of the bandwidth is reserved to specific users called "primary", which are recognized in the application thanks to "licenses". However, such users could left the spectrum unused during long periods of time. To solve this inefficient use of spectrum, it was proposed by J. Mitola in [Mitola and Maguire, 1999] and later by S. Haykin in [Haykin, 2005], to allow secondary users to access unused frequency slots. Such an application implies a spectral environment knowledge and consequently, requires an ability to sense it. That way, secondary users come to scan the spectrum to look for a radio channel free of primary users.

The two applications are challenging in a software point of view, as well as in the analog design. Problems are raised by T. Yucek, and H. Arslan in [Yucek and Arslan, 2009], where they introduce several statistical blind detection methods. This work highlights requirements of spectrum sensing: high sampling rate, high resolution of ADC, large dynamic range, and high speed signal processor. In the scope of the FITNESS project we face identical to problems. However, in many cases the detection requires a noise power estimation technique, which could not be afforded due to tights FITNESS requirements. Amongst many methods, we will focus on two detectors: a) the energy detector, which is the simpler one; b) the cyclostationary-based detector, which is more sophisticated but with different drawbacks. The first identified step is to scan a part of the spectral environment, as in CR.

To our best knowledge, a large part of existing methods propose a baseband detection. As we need to detect unwanted signals the earlier in the RX chain, the sensing mechanism input is at intermediate frequency. However, this processing may change received signal statistics. This detail has a notable importance, since detection methods rely on a statistical decision.

In this chapter, received signal and channel model are described in section 3.2. In section 3.3, we recall the detection theory basics and essential definitions for next chapters. The most classical detector is described in section 3.4, unfortunately such a method can't be used in the context of FITNESS. This chapter is concluded by the section 3.5, where concepts of cyclostationarity are developed.

3.2 Signal and Noise Models

3.2.1 Received Signal Model

Let us define the useful baseband signal continuous model in eq.(3.1).

$$z_1(t) = z_{1R}(t) + \jmath z_{1I}(t) = \beta_1 \sum_{k=-\infty}^{\infty} a_k h(t - kT_1) \tag{3.1}$$

Let T_1 be the symbol period, a_k are complex random symbols with unit variance, $h(t)$ is a continuous low-pass filter (normalized in energy) and β_1 is the square root power of $z_1(t)$. This is the classical model of a narrowband signal. The tab.2.2 defines possible modulations (i.e. values) of a_k. We consider that for a specific period of time, the standard does not change. It means that within this period, the symbols are random in one modulation (e.g. only 16-QAM symbols). In the following, the only known parameter will be $h(t)$ shape: a root raised cosine filter. However, the symbol period T_1 is unknown. $z_1(t)$ can be seen as a sum of a real and imaginary part, which are assumed independent and identically distributed. The signal $y_1(t)$ at carrier frequency f_{c1} can be expressed as:

$$y_1(t) = \Re[z_1(t - \Delta_1 t)e^{\jmath 2\pi(f_{c1}+\Delta_{f_{c1}})(t-\Delta_1 t)+\phi_1}] \tag{3.2}$$

Here $y_1(t)$ is considered as the useful signal at intermediate frequency f_{c1}, Δt is a propagation delay, $\Delta_{f_{c1}}$ is a carrier frequency shift and ϕ_1 is the initial phase of the LO emitter.

In the same way, a baseband unwanted signal $z_2(t)$ could be defined exactly as $z_1(t)$ in eq.(3.1). It should be expressed as eq.(3.3):

$$z_2(t) = z_{2R}(t) + \jmath z_{2I}(t) = \beta_2 \sum_{k=-\infty}^{\infty} b_k h(t - kT_2) \tag{3.3}$$

where the parameters can be interpreted as in eq.(3.1). Its narrowband model is the same as for the SOI:

$$y_2(t) = \Re[z_2(t - \Delta_2 t)e^{\jmath 2\pi(f_{c2}+\Delta_{f_{c2}})(t-\Delta_2 t)+\phi_2}] \tag{3.4}$$

$y_2(t)$ parameters are assumed to be unknown, as discussed in chapter 2.

When another PMR signal is present in an adjacent channel, the composite signal is the combination of SOI and jammer. This signal could be simplified as in eq.(3.5).

$$x(t) = \sum_{i=1}^{2} y_i(t) \tag{3.5}$$

3.2.2 Radio Channel Model

Now that both signal's and interferer's models are defined, let us focus on the radio channel. In every communication system, the received signal is not the same as the emitted one.

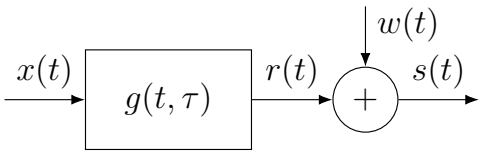

Figure 3.1: Radio channel model

Due to the channel effect and electronic induced noise, as presented in fig.3.1, the received signal is a combination of multiple perturbations ([Dunlop and Smith, 1994]). $s(t)$, the system output of fig.3.1 is expressed as:

$$s(t) = r(t) + w(t) = x(t) * g(t, \tau) + w(t) \tag{3.6}$$

where τ is a time delay, $g(t, \tau)$ is the channel impulse response, $w(t)$ is the background noise and $(u * v)$ stands for the convolution of u and v. Sources of background noise are analog components of the RX and the channel effect. This type of perturbation is often due to natural sources (i.e. thermal noise), which is the result of random moves from charged particles of materials. Some devices however, could add specific noise that could be called "artificial" and corresponds to impulse noise, which characteristics detailed in [Parsons, 2001], are very different from Gaussian noise. It's usual to neglect such a contribution, and to assume that $w(t)$ follows a normal distribution. Hence, in the following document, we assume a Additive White Gaussian Noise (AWGN) of unknown power σ_w^2, or equivalently of bilateral spectral density $\frac{N_0}{2}$.

In fig.3.1, the channel effect $g(t, \tau)$, has not be developed yet. Due to the propagation of signals, the resulting signal is subjected to several effects, which depends on the communication layer. For the considered application, the layer is obviously an electromagnetic wave. Hence, the received signal is affected by limiting factors, which complete effects description could be found in [Baudoin and Venard, 2013]:

Long term fading (path loss) is the signal fading, due to distance between emitter and receiver. Generally, the path loss is considered to be proportional to $1/d^n$, where d is the distance and $n \in \{2 - 6\}$ an index which depends on the geometry of current location.

Medium term fading (shadowing) corresponds to a fading due to obstacles (buildings, trees, etc.), since the receiver is rarely in the emitter line of sight. Usually the shadowing is taken into account by adding a gain between 0 and 1. It is almost impossible to estimate for real use cases, but measures shows that this attenuation follows a log-normal distribution with a variance between 6 dB to 12 dB.

Fast term fading (multi-path/Doppler shift) is due to two main issues:

- The multi-path effect is due to the signal reflexions. In such a case the terminal receives a random number of multiple original signal delayed echoes, which have their own magnitude and phase. Theses signals are generally a problem in reason of destructive interference. The multi-path effect is at the root of channel frequency selectivity. Hence, it is usually modeled as a low-pass filter.
- The Doppler shift, which is the root of channel time selectivity, is due to a difference of relative speed between emitter and receiver. The maximal shift Δ_{fmax} can be obtained thanks to $\Delta_{fmax} = \frac{\nu}{\lambda}$, where ν is the relative range speed between emitter and receiver, and λ is the transmitted signal wavelength. The coherence time $T_c = 1/\Delta_{fmax}$, corresponds to a moment during which the channel magnitude is constant.

$g(t, \tau)$ is the channel impulse response and the propagation could be modeled as a linear time-variant system. So, $g(t, \tau)$ is a random function of time (number of coefficients), and frequency (magnitude/phase of each path). Every communication system has to deal with such a model. However, several hypothesis are usually made to simplify receiver's design. This suppositions are: a flat fading channel (constant impulse response), slow fading (no Doppler shift), and wide sense stationary channel. That way $g(t, \tau)$ has an autocorrelation function time independent, as well as its statistical parameters.

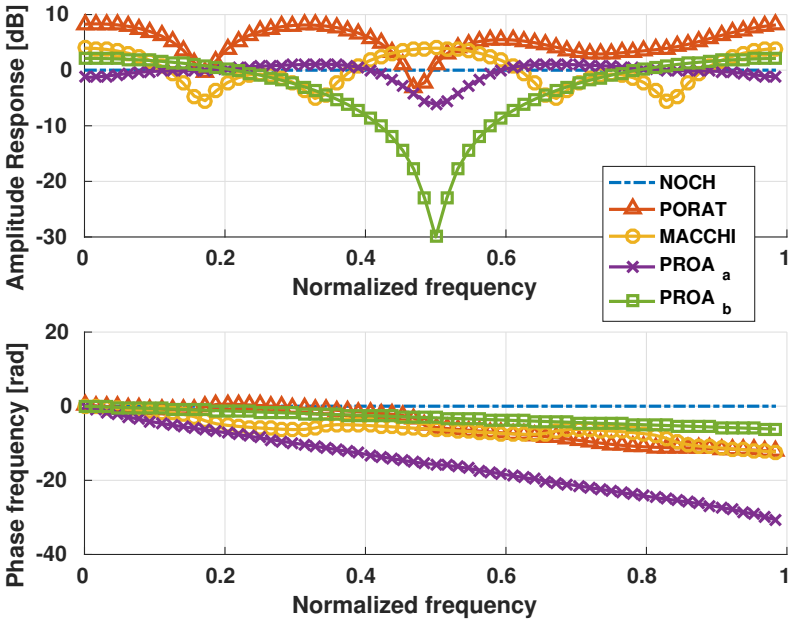

Figure 3.2: Standardized channel comparison

In the current application, such constraints are taken into account in PMR standards, which impose a particular digital baseband processing. Hence, in a first approach, we considered $g(t, \tau)$ as a dirac function such as $g(t, \tau) = \delta_0$, where δ_0 is the Kronecker symbol.

That way, the channel selectivity has no influence on the received signal. This is a strong assumption, but it simplifies greatly the study.

However, in chapter 4, these restrictive assumptions are relaxed. The multi-path channel influence is evaluated by simulation. Four discrete channel equivalent models are used: Porat and Friedlander channel, Macchi channel and Proakis "A" and "B" channels. Theses models are standard and could be found in [Laot, 1997, Porat and Friedlander, 1989, Macchi et al., 1993, Proakis, 2001]. In fig.3.2, a comparison of amplitude and phase response of such channels is provided. Each one present different characteristics in amplitude and phase. For example, the Porat and Friedlander channels present deep fading points and a nonlinear phase response when Proakis "A" characteristics are almost opposite: small fading and an almost linear phase. In facts, the number of poles and zeros of such filters are very different and theses models were chosen to be representative of most real cases.

3.3 Detection Theory Basics

Our first task is to decide if a signal is present or not, which requires a detection method. Before developing detection principles, a short part on general knowledge of detection theory has to be made. This section introduces concepts and notations, which are useful in next sections. Detection methods rely on hypothesis testing, which means to compare a criterion (i.e. make a test) to a threshold. Several statistical detection methods are synthesized by S.M. Kay in [Kay, 2009].

$$H : \begin{cases} H_0 \rightarrow s(t) = w(t), \\ H_1 \rightarrow s(t) = r(t) + w(t) \end{cases} \tag{3.7}$$

The test in eq.(3.7) is classic binary test. Here H_0 denotes the absence of signal and H_1 its presence. With that test, the question is to choose a method that select one or other case, with the minimum possible errors. There are two main solutions to decide H_1:

A Likelyhood Test Ratio which relies on the probability distributions of $P[\boldsymbol{s}|H_0]$ (understand conditional probability of $\boldsymbol{s}$ given H_0) and $P[\boldsymbol{s}|H_1]$. No additional assumption is required to realize the test. Here, $\boldsymbol{s}$ is a set of data in Ω_s the ensemble of realizations of $s(t)$;

or a Maximum Likelyhood method, which is based on a Bayesian approach of the binary system. It implies to determine the prior probability distribution of $P[H_0]$ and $P[H_1]$.

To our best knowledge, in the FITNESS project context no prior distributions of $P[H_0]$ and $P[H_1]$ could be determined. Indeed, such an hypothesis leads to the assumption that the probability to have a signal $s(t)$ or not is known, which is clearly unrealistic. Because the maximum likelihood can't be obtained, let focus on the likelihood test ratio.

Let $P[\boldsymbol{s}|H_0]$ and $P[\boldsymbol{s}|H_1]$ be marginal probability mass functions of the test eq.(3.7). These distributions are assumed unknown since we try to perform a "blind" detection. The

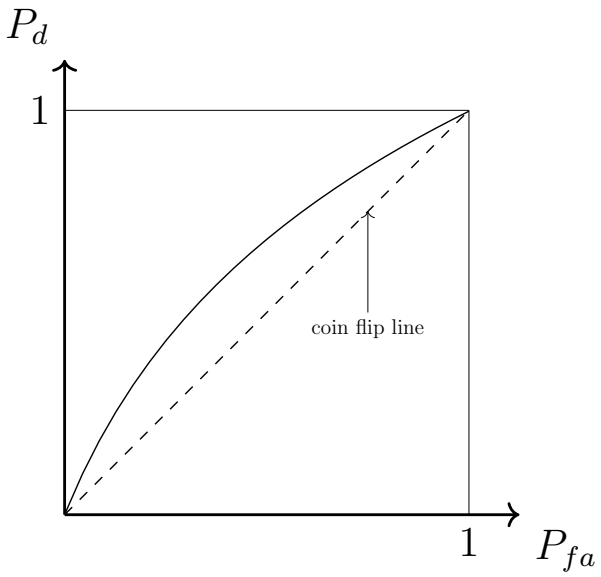

Figure 3.3: ROC Example to illustrate the detection probability P_d in function of the false alarm probability P_{fa}

question is to define a criterion able to distinguish the two distributions, thanks to a threshold. With known distributions, a theoretical expression could be determined. In the other side, it has to be set thanks to empirical densities. The most efficient way is to apply the Neyman-Pearson theorem:

Theorem 3.3.1 (Neyman-Pearson)**.** *To maximize P_d for a given $P_{fa} = \kappa$, decide H_1 if*

$$L(T(\mathbf{s})) = \frac{P[T(\mathbf{s})|H_1]}{P[T(\mathbf{s})|H_0]} > \gamma$$

where the threshold γ is found from

$$P_{fa} = \int_{\{\mathbf{s}:L(T(\mathbf{s}))>\gamma\}} P[T(\mathbf{s})|H_0]\delta s = \kappa$$

Here $\mathbf{s}$ is a set of N values $\{s(1), ..., s(N)\}$, κ is a particular value in $[0, 1]$, and $T(\mathbf{s})$ is a particular statistical test. P_d stands for the detection probability and P_{fa} represents the false alarm probability. $T(\mathbf{s})$ is chosen to summarize all the relevant information in the data (e.g. the mean operation). In such a case, the detection probability $P_d = P[H_1|H_1] = P[T(\mathbf{s}) > \gamma|H_1]$, and the probability to detect a signal presence when the test is false is $P_{fa} = P[H_1|H_0] = P[T(\mathbf{s}) > \gamma|H_0]$. Thanks to the theorem 3.3.1, we see that the theoretical threshold expression is linked to the false alarm probability. The lower the P_{fa}, the lower the detection probability.

With such a test, a 100% detection is not reachable, and two main errors can occur. The type 1 error corresponds to decide H_1 when there is no signal, which creates "false alarms" in

radar terminology. Type 2 error is the opposite of type 1. It corresponds to choose H_0 when a signal is present. Such a decision create "false negatives". The test can be optimal in terms of type 1 or type 2 errors, but the two of them can't be decreased simultaneously. In a detection system, a radar for example, the false alarm rate is often the only one specified. Indeed, it is often more interesting to minimize the number of positive matches while increasing the detection confidence.

Hence, detector efficiency is commonly visualized thanks to a Receiver Operating Characteristic (ROC) representation, as represented in fig.3.3. This is a graphical way to draw P_d evolution in function of P_{fa}. The test is considered interesting if it allows a good detection more often than a binary test (coin flip). As the detection probability generally depends on Signal to Noise Ratio (SNR) level, a comparison of several ROC is necessary. Such tests and comparisons will be useful to present algorithm efficiency in the following document.

3.4 Energy Detection

The energy detection method is the simplest and the most spread way to determine a signal presence. Its small computational time and simplicity are the reasons of such a success. Every communication requires energy to be transmitted. Hence, the idea of power consumption is fundamental. Let us consider $s(t)$ the signal defined in eq.(3.6), and a bandpass filter sharp enough to select only the useful signal. The process to detect a signal is described by the bloc diagram presented in fig.3.4.

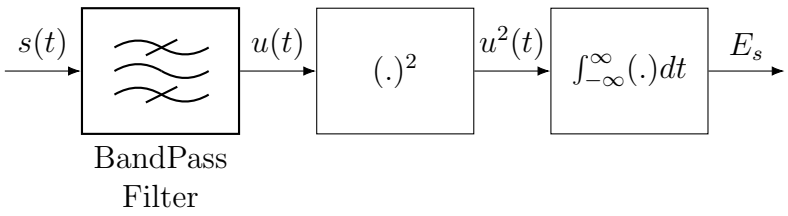

Figure 3.4: Block Diagram of a classic Energy detector

The main idea is to calculate $u^2(t)$ and its integration over a period, where $u(t) = s(t) * f_{bp}(t)$ and $f_{bp}(t)$ a bandpass filter. The filtering operation allows to limit the noise bandwidth, which spectral density is assumed constant. As defined in [Max, 1981], in the time domain for a continuous time process $u(t)$ the energy E_s is defined in eq.(3.8):

$$E_s = \int_{-\infty}^{\infty} |u(t)|^2 dt \tag{3.8}$$

A conversion of eq.(3.8) in frequency domain is possible thanks to the Parseval's Theorem and is developed below.

$$E_s = \int_{-\infty}^{\infty} S_{ss}(\nu) d\nu \tag{3.9}$$

In eq.(3.9), $S_{ss}(\nu) = |S(\nu)|^2$ is the power spectral density of $s(t)$, where $S(\nu)$ is its Fourier transform. If it exists, this transformation is defined as in eq.(3.10):

$$S(\nu) = \int_{-\infty}^{\infty} s(t)e^{-\jmath 2\pi\nu t}dt \tag{3.10}$$

From eq.(3.8) and eq.(3.10), a link could be obtained with the periodogram estimator over an integration period T, which is defined as:

$$P_T(\nu) = \frac{1}{T}S_{ss}(\nu) \tag{3.11}$$

Considering above definitions, the global signal energy does not depend on the chosen representation (i.e. in time or frequency domain). In [Urkowitz, 1967], H. Urkowitz proposes a test based on the $s(t)$ time representation. It was shown that eq.(3.12) obtained thanks to the representation in fig.3.4, is a good approximation when $N \geqslant T_1$.

$$\hat{E}_s(N) = \sum_{n=0}^{N} |u(n)|^2 \tag{3.12}$$

In such conditions and assuming that symbols distribution of $s(t)$ follows a Normal law, the test eq.(3.7) could be expressed as in eq.(3.13). Symbols are assumed random and independent, so the Normal law assumption is not restrictive in practice.

$$H : \begin{cases} H_0 \rightarrow \hat{E}_s(N) \sim \chi^2_L(0), \\ H_1 \rightarrow \hat{E}_s(N) \sim \chi^2_L(\lambda) \end{cases} \tag{3.13}$$

In eq.(3.13), $\chi^2_L(\lambda)$ is a non-central chi-square distribution of L freedom degrees, with a non-centrality parameter $\lambda = \frac{\hat{E}_s(N)}{N_0}$. For large enough N, instead of χ^2 distributions H. Urkowitz recommends to make an approximation with Normal distributions. In such a case, means and variances could be determined, as defined in eq.(3.14).

$$H : \begin{cases} H_0 \rightarrow \mathcal{N}\left(2N\sigma_w^2, 4N\sigma_w^2\right), \\ H_1 \rightarrow \mathcal{N}\left(2N\sigma_w^2 + SNR, 4N(\sigma_w^2 + SNR)\right) \end{cases} \tag{3.14}$$

With that approximation, the false alarm and miss detection rates could be expressed with the use of $\mathcal{Q}$ function, the reciprocal normal distribution. Theses expressions are obtained in eq.(3.15) and eq.(3.16):

$$P_{fa} = \mathcal{Q}\left[\frac{\gamma - \mu_0}{\sigma_0}\right] \tag{3.15}$$

$$P_{md} = \mathcal{Q}\left[-\frac{\gamma - \mu_1}{\sigma_1}\right] \tag{3.16}$$

where $\mu_0 = 2N\sigma_w^2$, $\mu_1 = 2N\sigma_w^2 + SNR$, $\sigma_0^2 = 4N\sigma_w^2$ and $\sigma_1^2 = 4N(\sigma_w^2 + SNR)$. As shown in [Tang, 2005], to minimize errors (of all types), a tradeoff between P_{fa} and P_{md} is mandatory. The threshold γ is determined when $\mathcal{Q}$ function's arguments of eq.(3.15) and eq.(3.16) are equal, making $P_{fa} = P_{md}$.

Results presented in [Yucek and Arslan, 2009, Urkowitz, 1967, Tang, 2005] show that the choice of an optimal threshold depends on N, the number of samples used in signal's energy

estimate. However, the threshold expression and distributions parameters in eq.(3.14) under H_0 and H_1 also depends on signal and noise power. Hence, a method to estimate such variables is needed. As recalled in [Yucek and Arslan, 2009], many methods exist as iterative algorithms for example, or the MUSIC algorithm. From [Hayes, 1996], details of such methods could be obtained. But, as the estimation precision depends on SNR level, estimated parameters could be far from their real values. As illustrated in [Ghozzi, 2008], even a small incertitude in power estimation leads to a significant detection performance loss. Still in [Yucek and Arslan, 2009], it is also recalled that even with a known noise power, the energy detection method gives poor results for small SNR (close to 0 dB).

In the FITNESS project context, the energy detection method face several issues. Due to space and energy savings requirements, the energy detector can't be implemented with analog devices, and should be realized completely in digital domain. Besides the MUSIC algorithm is known for its substantial estimation precision, its implementation has to be balanced by its cost in computation and storage. Finally, such a method allows the detection of a unique signal. But, the received signal may be composed of almost 10 channels, which makes it incompatible with FITNESS requirements. Another drawback is the impossibility to detect if the receiver works in its linear region. This is the major issue, as the first benefit anticipated by FITNESS for the detection algorithm is to make the RX able to change its parameters.

3.5 Cyclostationary Model: General Knowledge

In the previous section, the energy detection method was developed. We detailed its principle, and its pros and cons to show why this method is not adapted in our context. The work in [Yucek and Arslan, 2009] also proposes alternative detection solutions. But, theses methods are not really interesting due to our lack of knowledge on the received signal. As we saw, the energy detector needs the signal and noise power knowledge. Another method, the waveform sensing, needs the knowledge of emission shaping filter, which can't be assumed for adjacent channel signals. A third method, particularly efficient and very useful in RADAR context, is the matched filter detection. Unfortunately, it requires a known pattern such as pilots symbols. However, as we try to perform a detection the closer of analog chain, we have no access to such information. So, amongst all these methods, since no more prior information is required, exploiting cyclostationary properties of the received signal seems the most adapted solution. Thanks to its properties, this theory is used in several applications such as signal detection [Gardner, 1988a], source separation [Houcke, 2002], channel identification [Tong et al., 1995, Ciblat et al., 2000], or modulation type classification [Boiteau and Martret, 1998].

3.5.1 Statistical Cyclostationarity

This first part develops basic knowledge on cyclostationary properties and links it with stationary processes.

Time Domain

In signal processing a founding assumption is to assume constant properties in time of the studied signal. As developed in [Barkat, 2005] this assumption is called strict-sense stationary, and is recalled by definition 3.5.1.

Definition 3.5.1 (strict-sense stationarity)**.** A random process is strictly stationary or stationary, in the strict-sense if its statistics are unchanged by a time shift in the time domain.

Hence, a continuous time complex stochastic process $\{X_t\}$ ($t \in \mathbb{R}$) is said stationary if, for all k, all τ and for all $t_1, \ldots, t_k$, the cumulative distribution function of the unconditional joint distribution $F_X(x(t_1), \ldots, x(t_k))$ of $\{X_t\}$ is not affected by a time shift τ (i.e. $F_X(x(t_1), \ldots, x(t_k)) = F_X(x(t_1 + \tau), \ldots, x(t_k + \tau))$). It is important to underline that this definition implies ensemble statistics and not temporal statistics. However, this assumption is very restrictive in practice since it is often impossible to determine the studied signal cumulative distribution function. So, the assumption is relaxed and we consider that such a stochastic process is well described by its mean and variance.

Definition 3.5.2 (wide-sense stationarity)**.** A random process is widely stationary, or stationary in the wide-sense when its mean and autocorrelation functions vary only with the time difference $|t_1 - t_2|$.

Let us define the mean and autocorrelation in eq.(3.17) and eq.(3.18).

$$m_x(t) = E\left[\{X_t\}\right] = \int_{\mathbb{R}} x f_X(x;t) dx \tag{3.17}$$

$$r_{xx}(t_1, t_2) = E\left[\{X_{t_1}\}\{X_{t_2}\}^*\right] = \int_{\mathbb{R}}\int_{\mathbb{R}} x_1 x_2^* f_{X_1 X_2}(x_1, x_2; t_1, t_2) dx_1 dx_2 \tag{3.18}$$

In eq.(3.18), the notation $(.)^*$ stands for a complex conjugate operation. Thanks to the wide-sense stationarity definition, the autocorrelation function could be written as a function of one argument $\tau = t_1 - t_2$. So, by definition in terms of τ only, the autocorrelation function is

$$r_{xx}(t + \tau, t) = r_{xx}(\tau). \tag{3.19}$$

Hence, $\{X_t\}$ statistics are unchanged by a time shift, which means independent of time.

However, this is a major simplification. Indeed, many natural signals arise from periodic phenomena but may not be periodic functions of time. Their statistical characteristics vary periodically within time and are called cyclostationary processes. For example in physics, meteorological processes are perturbed by the earth rotation. Another example is periodical noises created by broken ball-bearings. In telecommunication, a periodic behavior could be due to modulation, sampling or filtering operations. In [Antoni, 2007], J. Antoni gives a good and simple example of a cyclostationary process in Telecommunication. He considers a periodically amplitude modulated white noise expressed as: $x(t) = s(t)w(t)$, with $s(t) = s(t+T)$ a T-periodic function and $w(t)$ a stationary white noise. This is an interesting example since it is clear that $x(t)$ may not exhibit a periodic temporal waveform, but has a random behavior synchronized with some periodic mechanism.

An excellent and complete state of the art reviewing work and explanation was conducted by W. A. Gardner and al. in [Gardner et al., 2006]. Hence, to study cyclostationary processes the wide-sense stationarity assumption is relaxed to obtain a more general framework. See fig.3.5 from [Gardner, 1994] as an illustration of different processes classes.

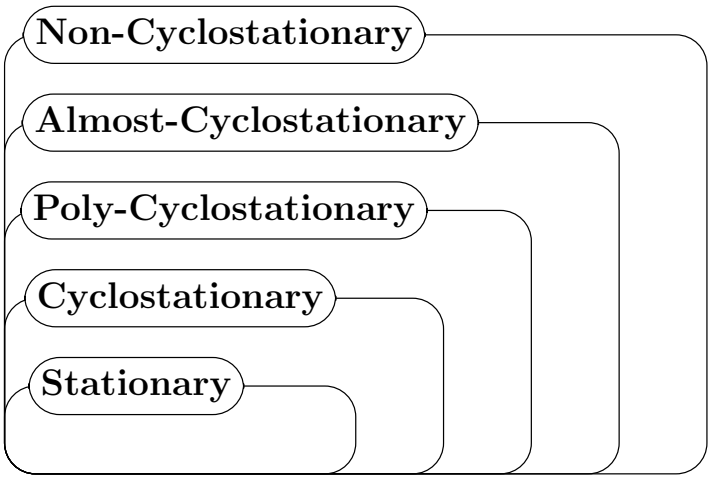

Figure 3.5: Venn diagram of classes of stochastic processes [Gardner, 1994]

In this diagram, stationary processes are a particular case of cyclostationary processes. Let us precise definitions for cyclostationary (def.3.5.3) and poly-cyclostationary processes (def.3.5.4), which are of some interest.

Definition 3.5.3. $\{X_t\}$ is a cyclostationary process with period T if and only if $F_X(x(t_1), \ldots, x(t_k))$ is periodic in t with period T.

Definition 3.5.4. $\{X_t\}$ is a poly-cyclostationary process with periods $\{T\} = T_1, T_2, \ldots$ if and only if $F_X(x(t_1), \ldots, x(t_k))$ is poly-periodic in t with periods $\{T\}$ (which is the sum of periodic functions with single periods $T_1, T_2, \ldots$) and $T_1, T_2, \ldots$ incommensurable.

Considering def.3.5.3, for a cyclostationary random process $\{X_t\}$, its autocorrelation function depends on time and on delay $\tau = t_1 - t_2$ between $x(t_1)$ and $x(t_2)$. Its means that the mean and the autocorrelation function of $\{X_t\}$ verify:

$$m_x(t+T) = m_x(t) \text{ and } r_{xx}(t+T, \tau) = r_{xx}(t, \tau). \tag{3.20}$$

In that case $\{X_t\}$ is a large-sense cyclostationary process, and T is called a *cyclic period*. As a function of time, the autocorrelation admits a Fourier series decomposition as:

$$r_{xx}(t, \tau) = E\left[x(t)x^*(t-\tau)\right] = \sum_{\alpha \in I_x} R_{xx}^{\alpha}(\tau) e^{j2\pi\alpha t} \tag{3.21}$$

In eq.(3.21), the summation is realized over integer multiples of the fundamental frequency $\alpha = \frac{1}{T}$, so α is the *cyclic frequency* (to get close to the cyclic period, its time counterpart).

Let $I_x = \{\frac{k}{T}, k \in \mathbb{Z}\}$ be the set of cyclic frequencies of $x(t)$, and Fourier series coefficients $R_{xx}^{\alpha}(\tau)$ are called *Cyclic Autocorrelation Function (CAF)*. The theoretical CAF at a cyclic frequency α is defined as the Fourier transform of $r_{xx}(t,\tau)$.

$$R_{xx}^{\alpha}(\tau) = \lim_{T_\alpha \to \infty} \frac{1}{T_\alpha} \int_0^{T_\alpha} r_{xx}(t,\tau) e^{-j2\pi\alpha t} dt \tag{3.22}$$

Coefficients $R_{xx}^{\alpha}(\tau)$ are complex continuous function in τ, but discrete variables on α. Eq.(3.22) equals zero for each $\alpha \notin I_x$. Theses coefficients are also symmetric in τ ($R_{xx}^{\alpha}(\tau) = R_{xx}^{\alpha}(-\tau)$), as the autocorrelation function in stationary field. For the special value $\alpha = 0$, the CAF becomes exactly the classic autocorrelation function in the stationary theory.

This analysis is also true for poly-cyclostationary processes, with slight differences. In that case, the set of cyclic frequencies in the sum (3.21) becomes $I_x = \{\frac{k}{T_1}, \frac{k}{T_2}, \ldots, k \in \mathbb{Z}\}$. The CAF definition is also different: as developed in [Gardner, 1994], $R_{xx}^{\alpha}(\tau)$ are Fourier-Bohr coefficients, due to the generalized Fourier series development. For the following parts, the considered signals in eq.(3.2), eq.(3.4) and (3.5) are clearly poly-cyclostationary. Indeed, they contain at least two incommensurable periods due to shaping filter and carrier frequency.

Frequency Domain

For stationary signals, the link between time and frequency domain was shown by N. Wiener for deterministic functions and A. Khinchin for its extension to stationary stochastic processes. Let us recall this important definition from [Barkat, 2005].

Theorem 3.5.5 (Wiener-Khinchin)**.** *If $x(t)$ is stationary in the wide-sense, the power spectral density $S_{xx}(f)$ can be expressed as the Fourier transform of the autocorrelation function $R_{xx}(\tau)$, that is*

$$S_{xx}(f) = \int_{\mathbb{R}} R_{xx}(\tau) e^{-j2\pi f\tau} d\tau$$

An extension of th.3.5.5 for cyclostationary signals was shown by W.A. Gardner in [Gardner, 1988b]. Hence, this property is still true, that way:

$$s_{xx}(t,f) = \int_{\mathbb{R}} r_{xx}(t,\tau) e^{-j2\pi f\tau} d\tau \tag{3.23}$$

As the power spectral density is periodic in time it admits a decomposition in Fourier series in eq.(3.24).

$$S_{xx}^{\alpha}(\tau) = \sum_{\alpha \in I_x} s_{xx}(t,\tau) e^{j2\pi\alpha t} \tag{3.24}$$

Coefficients $S_{xx}^{\alpha}(\tau)$ are called *Cyclic Spectrum Density Function (SCD)*, and exhibit same properties than their time domain counterparts. This link is determined thanks to the Cyclic Wiener Theorem and is simply expressed in eq.(3.25).

$$S_{xx}^{\alpha}(f) = \int_{\mathbb{R}} R_{xx}^{\alpha}(\tau) e^{-j2\pi f\tau} d\tau \tag{3.25}$$

For the particular value $\alpha = 0$, the SCD $S^0_{xx}(\tau)$ becomes simply the signal's Power Spectral Density (PSD).

Another interesting cyclostationarity property, besides not directly linked with the frequency domain development, is the linear filtering effect. The description of such an operation is easier in the frequency domain, since it could be simplified to a spectrum product. Indeed, as shown in [Gardner et al., 2006], for a filtered signal $y(t) = x(t) * h(t) = \int_{\mathbb{R}} h(u)x(t-u)du$, its SCD depends on the filter transfer function $H(\nu) = \int_{\mathbb{R}} h(t)e^{-j2\pi ft}dt$. Hence, its spectral correlation function could be defined as in eq.(3.26).

$$S^\alpha_{yy}(f) = H(f + \frac{\alpha}{2})H(f - \frac{\alpha}{2})S^\alpha_{xx}(f) \tag{3.26}$$

This property will be useful, in chapter 4 to determine the multi-path channel influence in our detection method.

3.5.2 Time Series Application

It turns out that the stochastic processes approach is only a mathematical point of view. In practice, we obviously have no access to a realization space Ω, and only one realization of the process is available. Hence, an alternative approach to the classical stochastic model was developed to determine cyclic properties of time-series. This framework is called *fraction-of-time* probability. In such a framework, probabilistic parameters are defined through infinite-time averages of a single time series rather than through expected values or ensemble averages of a stochastic process. More details on that theory may be obtained in [Gardner, 1994, Gardner et al., 2006]. But, the two theories may coexist thanks to the ergodic and latter, on cycloergodic properties of signals. Hence, in this part we link the continuous stochastic theory of cyclostationarity to time-series and discrete time processes.

In the large sense, a stochastic process is ergodic if all of its statistics can be determined from a sample function of the process. Equivalently, this process is ergodic if its ensemble average equals its time average with probability one. This condition is very restrictive, so several definitions of ergodicity are available depending on the needs (see [Barkat, 2005, Gardner, 1994]). Let us recall the wide-sense ergodicity definition in the mean:

Definition 3.5.6 (Ergodicity)**.** A random process $\{X_t\}$ is ergodic in the mean if the time-averaged mean value of a sample function x(t) is equal to the ensemble-averaged mean function value. That is,

$$E\left[\{X_t\}\right] = \langle x(t)\rangle_t$$

where $\langle . \rangle_t$ denotes a time average and is defined to be

$$\langle x(t)\rangle_t = \lim_{T\to\infty} \frac{1}{2T}\int_{-T}^{T} x(t)dt$$

This concept could be extended to cyclostationary processes, and its definition is called cycloergodicity. In [Boyles and Gardner, 1983], both wide-sense and strict-sense cycloergodicity are developed, but we just recall here the wide-sense definition.

Definition 3.5.7 (Cycloergodicity)**.** For any real number α, a random process X(t) is α-cycloergodic in the mean if

$$\lim_{N\to\infty} E\left[\left|\frac{1}{N}\sum_{k=0}^{N-1}\left(X(t_k) - E\left[X(t_k)\right]\right)e^{-\jmath 2\pi\alpha k}\right|^2\right] = 0$$

In other words, def.3.5.7 guarantees the equality of asymptotic sinusoidally weighted sample time averages with the corresponding time-averaged sinusoidally weighted probabilistic parameters, such as

$$\langle E\left[\{X_t\}\right] e^{-\jmath 2\pi\alpha t}\rangle_t \triangleq \lim_{N\to\infty}\frac{1}{N}\sum_{k=1}^{N} E\left[X(t)\right] e^{-\jmath 2\pi\alpha t} = \langle\left\{X(t)e^{-\jmath 2\pi\alpha t}\right\}\rangle_t \tag{3.27}$$

In the case of a cyclostationary cycloergodic process, this definition allows an interesting simplification of eq.(3.22), which becomes

$$R_{xx}^{\alpha}(\tau) = \langle x(t-\frac{\tau}{2})x^*(t+\frac{\tau}{2})e^{-\jmath 2\pi\alpha t}\rangle_t \tag{3.28}$$

Classically, to estimate the CAF, the expectation operator is replaced by a temporal average operator. Hence, eq.(3.27) is the link between continuous and discrete time, which leads to the estimate $\hat{R}_{x,N}^{\alpha}[l]$ of $R_x^{\alpha}[lT_s]$, with T_s the sampling period in eq.(3.29).

$$\hat{R}_{xx,N}^{\alpha}[l] = \frac{1}{N+1}\sum_{k=-N/2}^{N/2} x[k]\, x^*[k-l]\, e^{-\jmath 2\pi\alpha k} \tag{3.29}$$

When N tends to its asymptotic limit (i.e. infinity), eq.(3.29) meets the CAF definition in eq.(3.28).

Part I - Conclusions

In the first part of this document, we detailed the environment in which this study takes place. Tights FITNESS requirements of space and energy consumption impose a specific receiver architecture. However, to relax constraints on ADC, the received signal bandwidth was increased. That way, the useful signal and several adjacent channels go through the receiver. Interferer's presence may affect the useful signal quality due to a possible nonlinear regime of the receiver. Hence, a method based on interferer detection is required to make the receiver work in a linear way. Such a technique may allow a gain of almost 10 dB on ADC dynamic range.

To deal with the detection technique the received signal model was exposed. Assumptions due to FITNESS requirements were taken into account to fix a specific model. To make it clear, we detailed the detection theory basics and the most known method: the energy detector. Unfortunately, such a detection can't be performed in the FITNESS context. It requires noise and/or signal's power knowledge, or at least a noise power estimate. For those reasons, we choose the cyclostationary detection method.

However, several issues of detection were not tackled yet. Cyclostationary properties depend on received signal modulation. Some of FITNESS modulation schemes are in fact problematic as the chosen method does not allow a detection. This topic is developed in following chapters.

Part II

A Cognitive PMR Answer

CHAPTER 4

On-Carrier Phase Modulated Signal Cyclostationary Detector

4.1 Introduction

In the previous chapter, we developed theoretical tools to detect random signals. Now, we come to use them in the FITNESS project scope. We already underlined benefits to use cyclostationary properties of the received signal in our context. As we said earlier, our main constraint is the detection of phase modulated (i.e. O-QPSK and QAM) on carrier signals. Knowing the received signal particular cyclostationary pattern, it was shown in [Gardner, 1994] that a detection and even a classification is possible. It means that a prior knowledge of the studied signal is required, to look for a known cyclostationary pattern. A problem here is that our received signal is a mixture of several PMR channels. To deal with this issue, the detector must mandatory be able to detect a specific signal within the given set. The only parameter that is different for every signal in such a mixture is its carrier frequency. For this reason and as recommended in [Jouini et al., 2012], we assume the a priori knowledge of the carrier frequency set. So, in the following we focus on methods that are able to detect a particular frequency in the studied set. Nonetheless, another problem arise. It is well known that on-carrier phase modulated signals does not exhibit cyclic frequencies multiple of f_{ci}, which limits methods to perform a test. That's why classical detectors, such as the A.V. Dandawate and G.B. Giannakis in [Dandawate and Giannakis, 1994a] cyclic second order method, are not adapted.

Hence, we first present a higher order methods study in section 4.2. We analyze their benefits and drawbacks, to check their compliance to FITNESS context. As we will see, none of these methods perfectly fit our needs. The cyclostationary second order detection method is presented in section 4.3, in which we also point out a theoretical explanation of the QPSK detection issue. So, we propose a new algorithm to take advantage of the behavior difference between the Cyclic Autocorrelation Function (CAF) estimation and its theoretical expression. A mathematical solution, and an illustration of this concept is shown in section 4.4. At first, our theoretical results were obtained with following assumptions: neither multi-path, nor

carrier frequency shift. We also present detection results and performance metrics in this last part. These assumptions are finally released and an analysis of our criterion resilience is developed in this final section. For the following document the delay Δ_{t_1} in eq.(3.2) is considered zero, since it has no impact on the method and does not lead to a loss of generality. This demonstration is developed in Annexe A.

4.2 QPSK Detection - State of the Art

Several cyclostationary methods propose a joint presence detection and modulation classification of the received signal. For example, a second order cyclic-moments based approach is developed in [Kim et al., 2007] for modulation classification. But, this method uses the particularity that there is no cyclic frequency at $2f_{ci}$ for QPSK signals, to distinguish it from others modulations. In other words, the absence of cyclic frequency at $2f_{ci}$ discriminates the QPSK modulation in a set of several possible modulations. Nonetheless, this kind of approach can only be used for classification and not for detection. Classic methods are based on higher order statistics, or a nonlinear transformation to take advantage from the signal's specific properties. These methods are divided into two steps: a) measurement of a peak in signal's Cyclic Spectrum Density Function (SCD) or Cyclic Autocorrelation Function (CAF) at an existing cyclic frequency; b) estimation of its power and comparison to tabulated values to select the most likely modulation. Obviously, for a detection only, the processing can be stopped after the step a). Let develop this concept in following sections.

4.2.1 Higher Order Statistics

Higher order statistics are moments and cumulants higher than order two. They can be used to characterize the signal statistical properties when its mean and variance are not enough. In [Spooner, 2001] the n-th order moment function is defined as in eq.(4.1):

$$R_s(t,\tau;n,m) = E\left[\prod_{k=1}^{m} s^*(t+\tau_k)\prod_{k=m+1}^{n} s(t+\tau_k)\right] \tag{4.1}$$

Here m is the number of conjugated factors and $\tau = \{\tau_1,\ldots,\tau_n,\}$. $R_s(t,\tau;n,m)$ is linked to its cumulant counter part by eq.(4.2).

$$C_s(t,\tau;n,m) = \sum_{P_n}(-1)^{(p-1)}(p-1)!\prod_{k=1}^{p} R_{s_{\nu_k}}(t,\tau_{\nu_\mathbf{k}};n_k,m_k) \tag{4.2}$$

where $\{\nu_k\}_{k=1}^{p}$ are distinct partitions of the index $\{1,2,\ldots,n\}$, and P_n is the set of all partitions. This relation is fully explored in numerous papers, for example in [Gardner and Spooner, 1994] or [Gardner, 1994]. As an autocorrelation function combination, the cumulant function is periodic in time and admits a Fourier decomposition. Series coefficients are called *cyclic cumulants* and have cyclic frequencies.

In [Dandawate and Giannakis, 1994a], authors propose to use at least the third order cumulant to detect a on carrier M-PSK modulated signal. In such a case with I_s the set of

cyclic frequencies of $s(t)$, eq.(3.6) becomes:

$$\hat{C}_{3s}(\tau_1, \tau_2) = \frac{1}{N} \sum_{\alpha \in I_s} \sum_{t=0}^{N-1} s(t) s^*(t - \tau_1) s(t - \tau_2) e^{-\jmath 2\pi \alpha t} \tag{4.3}$$

The overall method is developed in section 4.3 at the order two. However, one major issue of this representation is its need of a covariance matrix estimation. Indeed, this matrix inverse is used to normalize the detection test, which may introduce instabilities in the algorithm. We also underline that this approach is limited by the estimated variance, which increases due to the additional product (compared to the order two) of delayed version $s(t - \tau_2)$. The only way to reduce that variance is to use a larger number of samples.

In [Spooner, 2001], it is also proposed to use higher order statistics to discriminate, and hence detect, a signal from a particular set. Forth and sixth order cumulants approaches are proposed and compared. The working assumption relies on a signal specific model, which is exposed in eq.(4.4).

$$x(t) = \sum_{i=1}^{M} \sum_{k=-\infty}^{\infty} a_{i,k} r(t - kT_i) e^{\jmath 2\pi f_{ci} t + \jmath \Phi_i} + w(t) \tag{4.4}$$

Here $w(t)$ is an AWGN noise, $a_{i,k}$ are complex symbols and $r(t)$ is a complex Fourier transformable pulse function of symbol rate $1/T_i$. Knowing the signal's carrier frequency f_{ci} gives its cyclic frequency knowledge, that allows to find the corresponding nonzero Fourier coefficient and solves the problem. The M signals case is tackled here, but a simplification where $M = 1$ is close to our formulation. This model is quite similar to our assumptions in eq.(4.17), with the notable difference that eq.(4.4) is baseband, with a carrier frequency residue. For the model eq.(4.4), C.M Spooner has shown that the cyclic cumulant function definition can be reduced to:

$$C_x^{\beta}(\tau; n, m) = \frac{C_{a,n,m}}{T} \int_{\mathbb{R}} \prod_{k=1}^{n} r^{(*)_k}(t + \tau_k) e^{-\jmath 2\pi \beta t} dt. \tag{4.5}$$

This relation is particularly interesting due to the factor $C_{a,n,m}$, which is the cumulant of random complex symbols $a_{i,k}$, of order n with m conjugation. Under the wide-sense cyclostationary hypothesis, we consider that a finite alphabet (i.e. a constellation) remains identical during a time T for each carrier. Hence, statistics of $s(t)$ keep same properties, and $C_{a,n,m}$ is constant. All values of $C_{a,n,m}$ are provided for QPSK, M-PSK, 8-256QAM and V29 constellations in [Spooner, 2001]. The remaining part of eq.(4.5) is deterministic. So, the coefficient $C_{a,n,m}$ alone allows to detect a modulation, as $C_x^{\beta}(\tau; n, m)$ differs only in the mean for each modulation.

This detection method efficiency is interesting and allows a good discrimination between the different modulations. Spooner's experimental results show that the P_d reaches quickly 1. However, that performance has to be balanced by an expensive computational cost as it requires a large number of symbols for detection (at least 1000). A better detection rate is achieved in most of presented cases when the number of symbols are greater than 3000. Hence, this is not compliant with FITNESS requirements. Moreover, the detection is performed at a SNR relatively high compared to the nonlinear transformation method that is presented in the next part.

4.2.2 Non-Linear Transformation

Another common detection technique is to apply a nonlinear transformation on the signal to create a DC component at a particular cyclic frequency. In [Hill and Bodie, 2001] a detector and a classifier are designed. However, the method relies on a filtering operation and an envelop detector, which is close to the energy detector that we discussed earlier. Hence, the technique developed by J. Reichert in [Reichert, 1992] is far more interesting. In this paper, the author developed a relation to maximize the SCD power. This is achieved when the original constellation is projected into a unique state different from zero. This concept is easier to understand on concrete examples. For a BPSK signal, the nonlinear transform $(.)^2$ projects the two symbols (± 1) onto $+1$. But, for the QPSK modulation case, two cases remains: ± 1, so the operation $(.)^4$ is considered. That way, a constant harmonic is created in the signal, equivalent to a line in its spectrum. The corresponding relation is developed in eq.(4.6) below.

$$S_{ss}^{\alpha}(\tau_0) = \frac{1}{T_1} \int_{\mathbb{R}} r_{ss}^{\alpha}(\tau_0) e^{-\jmath 2\pi\alpha\tau} d\tau \tag{4.6}$$

where, $r_{ss}^{\alpha}(\tau_0)$ is the averaged squared complex input signal autocorrelation such as:

$$r_{ss}^{\alpha}(\tau_0) = \frac{1}{T_1} \int_0^{T_1} E\left[s(t)s(t-\tau_0)s^*(t-\tau)s^*(t-\tau_0-\tau)\right] dt \tag{4.7}$$

In eq.(4.6), $S_{ss}^{\alpha}(\tau_0)$ is homogeneous to a SCD. This definition meets results in [Reichert, 1992] for the particular value of $\tau_0 = 0$. The delay τ_0 is introduced in eq.(4.6) and eq.(4.7) to be coherent with the J. E. Mazo notation in [Mazo, 1978]. Developing eq.(4.7) expectation leads to:

$$r_{ss}^{\alpha}(\tau_0) = \frac{1}{T_1} \int_0^{T_1} \sum_{i,j,k,l=-\infty}^{\infty} E\left[a_i a_j a_k^* a_l^*\right] h_i^0 h_j^{\tau_0} h_k^{*\tau} h_l^{*\tau+\tau_0} dt \tag{4.8}$$

where $h_k^x(t) = h(t - kT_1 + x)e^{\jmath 2\pi f_{c1}(t+x)}$, and $\sum_{i,j,k,l}$ is equivalent to four distinct summations over i, j, k, l. We clearly see that eq.(4.8) splits eq.(4.7) into a random and a deterministic part, in the same way that we discussed about Spooner's method. It was shown in [Mazo, 1978] that $E\left[a_i a_j a_k^* a_l^*\right]$ (the random part of eq.(4.8)) can be expressed as in eq.(4.9):

$$E\left[a_i a_j a_k^* a_l^*\right] = \delta_{ij}\delta_{kl} + \delta_{ik}\delta_{jl} + \mu_2^2\delta_{il}\delta_{jk} - (2 + \mu_2^2 - \mu_4^*)\delta_{ij}\delta_{ik}\delta_{il} \tag{4.9}$$

In eq.(4.9), the notation δ_{ij} stands for the Kronecker symbol, μ_2^2 is the second order moment and μ_4^* is the fourth order two-conjugated moment. So, $E\left[a_i a_j a_k^* a_l^*\right]$ is clearly the only part that depends on the modulation. The remaining part of eq.(4.8) is deterministic, with a unique value for each modulation (considering a integration over T_1). This is definitely different from [Dandawate and Giannakis, 1994a] or [Gardner and Spooner, 1992] approaches, which focus on the asymptotic behavior of their cyclostationary detectors. Here, eq.(4.7) is clearly a derivation of the CAF probabilistic behavior. In a similar manner to [Spooner, 2001], μ_4^* and μ_2 take specific values for each modulation. Second and forth order moments taken separately may be identical for two modulation. So, the couple has to be considered to choose the correct modulation. Then, a power detection of $S_s^{\alpha}(\tau_0)$ is performed in a classical way by the resolution of a Neyman-Pearson test.

This method allows a good detection and, knowing its statistics (i.e. $E\left[a_i a_j a_k^* a_l^*\right]$), also allows to classify the modulation. However, several modulations may have their low-order statistics identical, which implies to use higher order nonlinear function and perform the test for the two nonlinear functions (i.e. $(.)^2$ and $(.)^4$). Obviously, the detector becomes more sensitive to noise power due to higher orders. In a other hand, [Reichert, 1992] results shows that the QPSK classification rate is low when compared to other modulations. Indeed, a classification rate of 98% is obtained only for a SNR 8 dB higher than the classification rate obtained for a PAM modulation. We also notice that created spectral lines are located at $2f_{c1}$ and $4f_{c1}$. This implies that the sampling frequency f_s has to be greater than $8f_{c1}$ in order to avoid aliasing effects. In a general point of view this requirement seems reachable. But, in the FITNESS context the sampling rate $f_s = 4f_{c1}$. So, the anti-aliasing condition can't be respected.

4.3 Low-order Moment Detector

It is usually admitted that first order moment (mean) and second order moment (variance) are enough to characterize a stochastic process distribution. Moreover, the estimation of higher order moments consists in a mean delayed versions products of the original stochastic process. So, as the SNR decreases, it becomes harder to estimate the process high order moments with confidence. Furthermore, the algorithm computational complexity grows quickly as the order increases. For now, to limit the computational cost, let us first consider existing second order detection methods.

One approach to exploit a signal cyclostationary properties is to detect its cyclic frequencies, as described in [Gardner, 1988b]. The detection relies on the SCD estimation at a specific cycle frequency to measure the most powerful spectral line. Based on this idea, the complete work realized in [Gardner and Spooner, 1992], compares several detectors in terms of detection rate. However, as once again pointed out in this last document, there is no cyclic feature at the cycle frequency $2f_{c1}$ for a QPSK signal. Alternative methods to exploit cyclostationary properties of a signal also exist, as the work developed in [Ciblat et al., 2002]. The main idea is to consider cyclic frequencies as sinusoids embedded in noise. Nonetheless, it requires to make an assumption on the studied signal number of cyclic frequencies. Let now introduce the second order cyclic detector in order to become more familiar with the cyclostationarity detection concept.

4.3.1 A statistical Test Presence

Conveniently, the [Dandawate and Giannakis, 1994a] method allows a cycle detection presence without assuming any specific distribution of input data. A normal asymptotic test was developed, and recalled here for its lower order form. Both time and frequency test are tackled in the original paper, but let us use the time-domain only. This method allows to estimate the signal cyclic frequencies without prior input signal knowledge (i.e. unknown period symbol, carrier frequency, symbols distribution). It can be seen as a detection problem,

since it requires to estimate all CAF coefficients of eq.(3.22) to determine if they present some energy. If the energy is high enough, then the corresponding candidate cycle frequency is declared a cyclic frequency and the signal is detected. Let now develop the concept, keeping the detection problem in the line of sight. With the cycloergodic assumption, $s(t)$ (eq.(3.6)) estimated CAF (defined in eq.(3.29)) can be express in eq.(4.10).

$$\begin{aligned} \hat{R}^{\alpha}_{ss,N}(l) &\triangleq \frac{1}{N}\sum_{k=0}^{N-1} s(k)s^*(k-l)e^{-\jmath 2\pi\alpha k} && (4.10)\\ &= R^{\alpha}_{ss,N}(l) + \varepsilon^{\alpha}_{ss,N}(l) && (4.11) \end{aligned}$$

In eq.(4.11), $\varepsilon^{\alpha}_{ss,N}(l)$ is an estimation error and becomes asymptotically zero when N tends to infinity. In such a case, the estimate $\hat{R}^{\alpha}_{ss,N}(l)$ comes closer of its theoretical value $R^{\alpha}_{ss,N}(l)$. So, due to $\varepsilon^{\alpha}_{ss,N}(l)$ presence, the estimated CAF is never exactly zero. The remaining question is to decide when a *candidate* α is really a cyclic frequency (if $\alpha \in I_s = \left\{\frac{k}{T_1}, \frac{2m}{T_{c1}}, \frac{2m}{T_{c1}} \pm \frac{1}{T_1}, \{k,m\} \in \mathbb{Z}\right\}$). So, the following test is proposed:

$$H : \begin{cases} H_0 : \alpha \notin I_s,\ \forall\{l\}_{l=1,..,N} \rightarrow \hat{R}^{\alpha}_{ss,N}(l) = \varepsilon^{\alpha}_{ss,N}(l), \\ H_1 : \alpha \in I_s, \text{ for some } \{l\}_{l=1,..,N} \rightarrow \hat{R}^{\alpha}_{ss,N}(l) = R_{ss,N}(l) + \varepsilon^{\alpha}_{ss,N}(l). \end{cases} \tag{4.12}$$

All the power of this concept lies in eq.(4.12). It allows a cycle detection of a single input signal. Since $R_{ss,N}(l)$ is nonrandom, $\hat{R}^{\alpha}_{ss,N}(l)$ distributions under H_0 and H_1 differ only in the mean.

This test can be performed for a specific unique lag l or for several lags to improve the precision. For a set of lag $\{l\}_{l=1,..,N}$, let us define the $1 \times 2N$ row vector $\hat{\mathbf{R}}^{\alpha}_{\mathbf{ss,N}}$ by,

$$\begin{aligned} \hat{\mathbf{R}}^{\alpha}_{\mathbf{ss}}(\mathbf{l}) \triangleq \Big[&\Re\{\hat{R}^{\alpha}_{ss,N}(1)\}, \ldots, \Re\{\hat{R}^{\alpha}_{ss,N}(N)\}, \\ &\Im\{\hat{R}^{\alpha}_{ss,N}(1)\}, \ldots, \Im\{\hat{R}^{\alpha}_{ss,N}(N)\}\Big] \end{aligned} \tag{4.13}$$

In a simplified version, only one lag is necessary and $\hat{\mathbf{R}}^{\alpha}_{\mathbf{ss}}(\mathbf{l})$ becomes a 1×2 vector. As the input data distribution is unknown, the asymptotic properties of $\hat{R}^{\alpha}_{ss}(l)$ have to be derived to determine the asymptotic error distribution. With the assumption that samples of $s(k)$ are well separated in time and are independent, [Dandawate and Giannakis, 1994a] shows that the estimator in eq.(4.11) is consistent (i.e. $\lim_{N\rightarrow\infty} \hat{R}^{\alpha}_{ss,N}(l) = R^{\alpha}_{ss,N}(l)$). Another interesting result is the demonstration that $\sqrt{N}\varepsilon^{\alpha}_{ss,N}(l)$ follows asymptotically a complex normal distribution with covariance matrix Σ_{2c}, which estimated expression is provided in eq.(4.14).

$$\begin{aligned} \hat{\mathbf{\Sigma}}_{\mathbf{2c}} = \Big[&\Re\{\frac{\hat{Q}_2 + \hat{Q}_2^*}{2}\}, \Im\{\frac{\hat{Q}_2 - \hat{Q}_2^*}{2}\}, \\ &\Im\{\frac{\hat{Q}_2 + \hat{Q}_2^*}{2}\}, \Re\{\frac{\hat{Q}_2 + \hat{Q}_2^*}{2}\}\Big] \end{aligned} \tag{4.14}$$

where $\hat{Q}_2$ and $\hat{Q}_2^*$ are homogeneous to periodograms of $s(k)s(k+l)$ such as,

$$\begin{aligned}\hat{Q}_2 = \hat{S}_2(2\alpha,\alpha) &= \frac{1}{NL}\sum_{i=-(L-1)/2}^{(L-1)/2} W(i)F_T(\alpha-\frac{2\pi i}{N})F_T(\alpha+\frac{2\pi i}{N}),\\ \hat{Q}_2^* = \hat{S}_2(0,-\alpha) &= \frac{1}{NL}\sum_{i=-(L-1)/2}^{(L-1)/2} W(i)F_T(\alpha+\frac{2\pi i}{N})F_T^*(\alpha+\frac{2\pi i}{N})\end{aligned} \tag{4.15}$$

with $W(i)$ a spectral window of length L and $F_T(s) = \sum_{k=0}^{N-1} s(k)s(k+l)e^{-\jmath 2\pi ik}$ the Fourier transform of $s(k)s(k+l)$. This knowledge leads to normalize the test eq.(4.12) by its covariance to get a generalized maximum-likelihood function. Its asymptotic distribution turns out to be expressed as in eq.(4.16).

$$H:\begin{cases} H_0 : \tau_{2c} \sim \mathcal{N}(0, 4\hat{\mathbf{R}}_{\mathbf{ss}}^{\alpha}\hat{\mathbf{\Sigma}}_{\mathbf{2c}}^{-1}\hat{\mathbf{R}}_{\mathbf{ss}}^{\alpha\prime}),\\ H_1 : \tau_{2c} \sim \mathcal{N}(N\hat{\mathbf{R}}_{\mathbf{ss}}^{\alpha}\hat{\mathbf{\Sigma}}_{\mathbf{2c}}^{-1}\hat{\mathbf{R}}_{\mathbf{ss}}^{\alpha\prime}, 4N\hat{\mathbf{R}}_{\mathbf{ss}}^{\alpha}\hat{\mathbf{\Sigma}}_{\mathbf{2c}}^{-1}\hat{\mathbf{R}}_{\mathbf{ss}}^{\alpha\prime}).\end{cases} \tag{4.16}$$

where, $\hat{\mathbf{\Sigma}}_{\mathbf{2c}}$ is the $\hat{\mathbf{R}}_{\mathbf{ss}}^{\alpha}$ covariance matrix and $(.)'$ is the vector transpose operation. The 2×2 matrix $\hat{\mathbf{\Sigma}}_{\mathbf{2c}}$ is obtained using the relation eq.(4.14). A theoretical threshold is then obtained thanks to the $\mathcal{Q}$ function (reciprocal normal distribution).

Hence, this method seems particularly well adapted to look for cyclic frequencies of a communication signal. The proposed test is simple, with a simple detection metric. However, a few remarks could be made. The first one concerns the funding assumption of that work, which implies that input samples are well separated in time and independent. If this condition is not restrictive for stable linear processes, it is a real problem for communication signals. Indeed, due to the shaping filter and oversampling, samples could not be considered independent. This is all the more true when the symbol period is long compared to the sampling period.

A second limitation is the need of the estimated covariance matrix. For a single lag, the matrix $\hat{\mathbf{\Sigma}}_{\mathbf{2c}}$ is small (2×2). So, the inversion process is not an expensive calculation time. But, due to inversion it may introduce instabilities in the process, if the inverse matrix is ill-conditioned. Finally, as a second order method it does not allow a detection of QPSK signals on carrier, since by definition for a QPSK signal $\alpha = 2f_{c1}$ corresponds to the H_0 hypothesis in eq.(4.12).

Let us give an example with signal $y_1(t)$ for which $z_1(t)$ are BPSK symbols. In that case, eq.(3.2) could be simplified into eq.(4.17) which is a real signal ($z_{1_I}(t) = 0$). That way $s(t) = y_{1_R}(t) + w(t)$, and one can show that $R_{ss}^{\alpha}(\tau) = R_{yy}^{\alpha}(\tau)$.

$$y_1(t) = \sum_{k=0}^{N} a_k h(t-kT)\cos(2\pi f_{c1}t) \equiv z_{1_R}(t)\cos(2\pi f_{c1}t) \tag{4.17}$$

The quadratic form $y_1(t)y_1(t-\tau)$, which complete expression is detailed in eq.(4.18), allows

to determine $y_1(t)$ cyclic frequencies.

$$\begin{aligned} y_1(t)y_1(t-\tau) &= \frac{1}{4}(z_{1_R}(t)z_{1_R}(t-\tau)e^{\jmath 2\pi f_{c1}\tau}) \\ &+\frac{1}{4}(z_{1_R}(t)z_{1_R}(t-\tau)e^{-\jmath 2\pi f_{c1}\tau}) \\ &+\frac{1}{4}(z_{1_R}(t)z_{1_R}(t-\tau)e^{\jmath 2\pi f_{c1}(2t-\tau)}) \\ &+\frac{1}{4}(z_{1_R}(t)z_{1_R}(t-\tau)e^{-\jmath 2\pi f_{c1}(2t-\tau)}) \end{aligned} \tag{4.18}$$

As we see, this quadratic form clearly exhibits temporal sine-wave components for $\alpha \pm 2f_{c1}$. However, the analysis is not that obvious for the two first terms of eq.(4.18). Let us make a focus on the first right hand-side term. Thanks eq.(3.21), its autocorrelation is:

$$\begin{aligned} R_{zz}(t,\tau) &= \frac{1}{4}E\left[z_{1_R}(t)z_{1_R}(t-\tau)e^{-\jmath 2\pi\alpha t}\right]e^{\jmath 2\pi f_{c1}\tau} \\ &= e^{\jmath 2\pi f_{c1}\tau}\sum_{u=-\infty}^{\infty}\sum_{v=-\infty}^{\infty}E\left[a_u a_v^*\right]h(t-uT_1)h(t-\tau-vT_1) \end{aligned} \tag{4.19}$$

The variable change $t = t + T_1$ leads to eq.(4.20).

$$R_{zz}(t+T_1,\tau) = e^{\jmath 2\pi f_{c1}\tau}\sum_{u=-\infty}^{\infty}\sum_{v=-\infty}^{\infty}E\left[a_u a_v^*\right]h(t+T_1-uT_1)h(t-\tau-vT_1+T_1) \equiv R_{zz}(t,\tau) \tag{4.20}$$

So, the $z_{1_R}(t)$ autocorrelation has a periodic behavior in $\pm T_1$, which produces cyclic frequencies $\alpha = \pm\frac{1}{T_1}$. Hence, the theoretical CAF of eq.(4.18), with a set $I_{y_1} =$

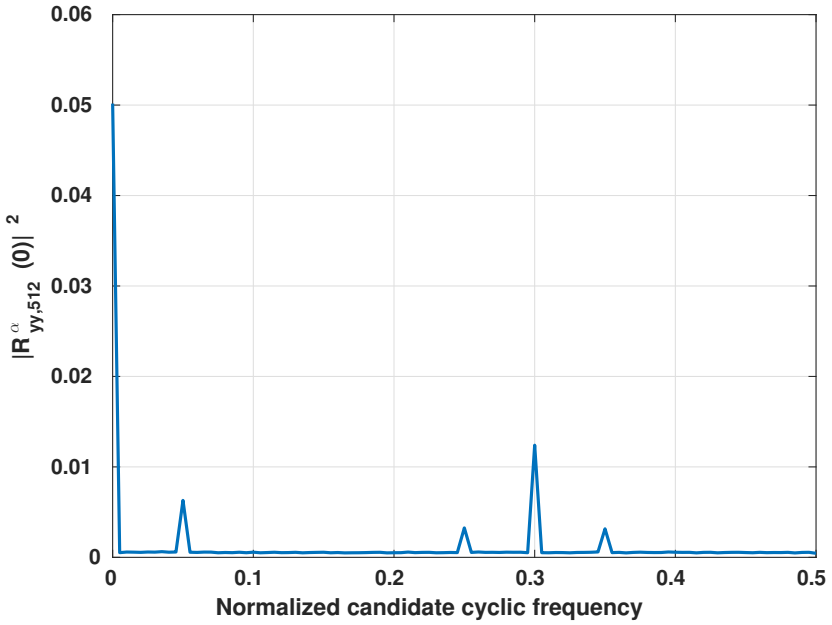

Figure 4.1: CAF magnitude for a BPSK signal, at SNR of 0dB, 512 symbols, averaged over 100 independent run

$\{0, \pm\frac{1}{T_1}, \pm 2f_{c1}, \pm 2f_{c1} \pm \frac{1}{T_1}\}$ is

$$\begin{aligned} R^{\alpha}_{yy}(\tau) &= \frac{1}{4}E\left[z_{1_R}(t)z_{1_R}(t-\tau)e^{-\jmath 2\pi\alpha t}\right]e^{\jmath 2\pi f_{c1}\tau} \\ &+\frac{1}{4}E\left[z_{1_R}(t)z_{1_R}(t-\tau)e^{-\jmath 2\pi\alpha t}\right]e^{-\jmath 2\pi f_{c1}\tau} \\ &+\frac{1}{4}E\left[z_{1_R}(t)z_{1_R}(t-\tau)e^{\jmath 2\pi(2f_{c1}-\alpha)t}\right]e^{-\jmath 2\pi f_{c1}\tau} \\ &+\frac{1}{4}E\left[z_{1_R}(t)z_{1_R}(t-\tau)e^{-\jmath 2\pi(2f_{c1}+\alpha)t}\right]e^{\jmath 2\pi f_{c1}\tau} \end{aligned} \tag{4.21}$$

Or for more convenience,

$$R^{\alpha}_{yy}(\tau) = \begin{cases} \frac{1}{2}cos(2\pi f_{c1}\tau)R^{\alpha}_{zz}(\tau) & \text{if } \alpha = 0 \text{ or } \pm\frac{1}{T_1}, \\ \frac{1}{4}e^{\pm j2\pi f_{c1}\tau}R^{\alpha}_{zz}(\tau) & \text{if } \alpha = \pm 2f_{c1} \text{ or } \pm 2f_{c1} \pm \frac{1}{T_1}, \\ 0 & \text{otherwise.} \end{cases} \tag{4.22}$$

Fig.4.1 represents $|R^{\alpha}_{ss}(\tau)|^2$ (i.e. the $s(t)$ CAF energy) versus α. As expected, the energy is different from zero only for α in $I_s \equiv I_{y_1}$. This representation was obtained for $\tau = 0$, $N_s = 512$ symbols, a SNR of 0 dB, a symbol period $T_1 = 1$ ($T_{ech} = 1/20$) and a normalized carrier frequency $f_{c1} = 0.15$ over 100 independent realizations. We clearly see the classic autocorrelation range in the main peak at $\alpha = 0$. There is also a peak at $\alpha = 0.05$, which corresponds to the symbol period. An important peak shows the carrier frequency influence at $\alpha = 2f_{c1} = 0.3$ with smaller responses at each side due to the symbol period. Moreover, when the candidate cyclic frequency does not belong to I_s, the CAF energy tends to be zero but not seldom zero, as expected.

4.3.2 The Carrier QPSK Signal Cyclostationary Detection Issue

However, if the same example with an input signal QPSK modulated is done, no cyclic frequency at $\alpha = 2f_{c1}$ can be found. An illustration of this result is proposed in fig.4.2, which was realized with same parameters as for fig.4.1. We clearly see that there is no energy close to $\alpha = 2f_{c1}$.

Let us now derive the cyclostationary analysis for the signal $y_1(t)$ in this case. We need first to complete the notation introduced in chapter 3.

$$y_{1_R}(t) = \Re\left[z_1(t)\right]cos(2\pi f_{c1}t) \text{ and } y_{1_I}(t) = \Im\left[z_1(t)\right]sin(2\pi f_{c1}t) \tag{4.23}$$

That way $s(t) = y_{1_R}(t) - y_{1_I}(t) + w(t)$. Using eq.(3.22), one can easily show the following relation:

$$R^{\alpha}_{ss}(\tau) = R^{\alpha}_{y_{1_R}}(\tau) + R^{\alpha}_{y_{1_I}}(\tau). \tag{4.24}$$

So, eq.(4.24) is the sum of the CAF of $y_{1_R}(t)$ and $y_{1_I}(t)$. The theoretical CAF of $y_{1_R}(t)$ is given by:

$$R^{\alpha}_{y_{1_R}y_{1_R}}(\tau) = \begin{cases} \frac{1}{2}cos(2\pi f_{c1}\tau)R^{\alpha}_{z_{1_R}z_{1_R}}(\tau) & \text{if } \alpha = 0 \text{ or } \pm\frac{1}{T_1}, \\ \frac{1}{4}e^{\pm j2\pi f_{c1}\tau}R^{\alpha}_{z_{1_R}z_{1_R}}(\tau) & \text{if } \alpha = \pm 2f_{c1} \text{ or } \pm 2f_{c1} \pm \frac{1}{T_1}, \\ 0 & \text{otherwise.} \end{cases} \tag{4.25}$$

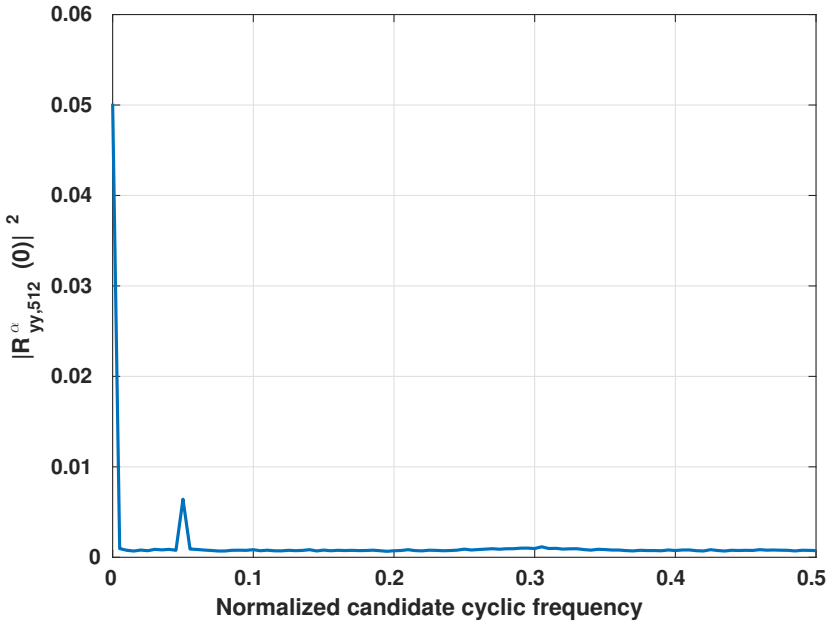

Figure 4.2: CAF magnitude for a QPSK signal, at SNR of 0dB, 512 symbols, averaged over 100 independent run

With $I_{y_{1_R}} = \left\{ \{ \frac{k}{T_1}, 2kf_{c1}, 2kf_{c1} \pm \frac{k}{T_1} \}, k \in \mathbb{Z} \right\}$ the set of cyclic frequencies of $y_{1_R}(t)$, which is defined in eq.(4.23). As $I_{y_{1_R}}$ contains elements that are not multiple to each other, the signal $y_{1_R}(t)$ is poly-cyclostationary (see section 3.5 for more details).

Note that the CAF expression of $y_{1_I}(t)$ is detailed in eq.(4.26).

$$R^{\alpha}_{y_{1_I} y_{1_I}}(\tau) = \begin{cases} \frac{1}{2} cos(2\pi f_{c1}\tau) R^{\alpha}_{z_{1_I} z_{1_I}}(\tau) & \text{if } \alpha = 0 \text{ or } \pm\frac{1}{T_1}, \\ -\frac{1}{4} e^{\pm j2\pi f_{c1}\tau} R^{\alpha}_{z_{1_I} z_{1_I}}(\tau) & \text{if } \alpha = \pm 2f_{c1} \text{ or } \pm 2f_{c1} \pm \frac{1}{T_1}, \\ 0 & \text{otherwise.} \end{cases} \tag{4.26}$$

With $I_{y_{1_I}} = \left\{ \{ \frac{k}{T_1}, 2kf_{c1}, 2kf_{c1} \pm \frac{k}{T_1} \}, k \in \mathbb{Z} \right\}$ the set of cyclic frequencies of $y_{1_I}(t)$ defined in eq.(4.21). We underline that cyclic frequencies multiple of f_{c1} exist in eq.(4.25) and eq.(4.22). Indeed, for baseband QPSK signals, the constellation projection in the complex or real plan is consistent to BPSK modulation. Consequently, real and imaginary parts of baseband QPSK have cyclic frequencies multiple of the carrier frequency. Noticing that $R^{\pm 2f_{c1}}_{y_{1_R} y_{1_R}}(\tau) = -R^{\pm 2f_{c1}}_{y_{1_I} y_{1_I}}(\tau)$, and replacing eq.(4.25) and eq.(4.22) in eq.(4.24) leads to the following expression for $\alpha \in I_s$:

$$R^{\alpha}_{ss}(\tau) = \frac{1}{2} cos(2\pi f_{c1}\tau) R^{\alpha}_{z_{1_R} z_{1_R}}(\tau) + \frac{1}{2} cos(2\pi f_{c1}\tau) R^{\alpha}_{z_{1_I} z_{1_I}}(\tau). \tag{4.27}$$

In eq.(4.27), $s(t)$ is cyclostationary with $I_s = \{ \frac{k}{T_1}, k \in \mathbb{Z} \}$. We notice that I_s does not have any cyclic frequency depending on f_{c1}, in agreement with state of the art analysis.

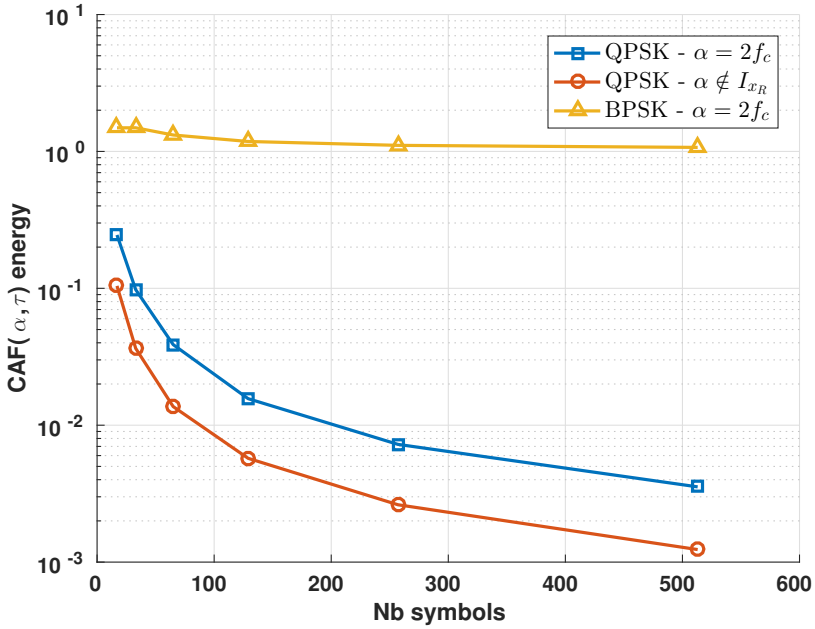

Figure 4.3: CAF energy versus the observation duration (number of samples) for different modulation schemes (i.e. QPSK, BPSK) and for different α

4.4 New Detection Feature Analysis

As we saw, the basic method of second order cyclic-moments is unable to detect any CAF energy linked to the signal carrier for phase modulated signals. Based on this analysis, we propose a new method to perform the detection thanks to second order cyclostationarity theory. This method exploits the convergence speed of the cyclic autocorrelation function estimator. We also develop a statistical test and derive the asymptotic probability density function of the criterion to propose a detection threshold. Detection performance simulation results are then evaluated by Monte Carlo simulations and compared to the fourth order nonlinear transformation method.

4.4.1 New Detector Definition

We saw that QPSK signal's CAF converges to zero, but not in the same way if the cyclic frequency is a multiple of the carrier frequency or not. Let us develop this concept graphically. The fig.4.3 illustrates the CAF speed convergence for different values of cyclic frequencies if $\alpha \in I_s$ or if $\alpha \notin I_{y_{1_R}}$. Experimental conditions are detailed in the next section. In fig.4.3 when $\alpha \in I_{y_{1_R}}$, the CAF estimator applied to a BSPK signal (i.e. to $y_{1_R}(t)$ or $y_{1_I}(t)$) converges quickly through a non zero constant value (triangle yellow curve). In the same way, when $\alpha \notin I_s$, the estimator decreases in $1/N$ and tends to zero (red circled curve). For a QPSK signal, when $\alpha = 2f_{c1}$, the estimated speed convergence is similar but with a different leading coefficient. However, there is a gap between the curves $\alpha = 2f_{c1}$ and $\alpha \notin I_s$, which gives an

indication on the idea that we develop in this section.

Let now develop our detection method expression. As shown in subsection 4.3.2, for any $\alpha \notin I_s$, $R_{ss}^{\alpha}(\tau) = 0$. This is also true for particular values of $\alpha = \pm 2f_{c1}$. But we also notice that $R_{y_{1_R} y_{1_R}}^{\pm 2f_{c1}}(\tau) = -R_{y_{1_I} y_{1_I}}^{\pm 2f_{c1}}(\tau) \neq 0$ which leads to:

$$R_{ss}^{\pm 2f_{c1}}(\tau) = R_{y_{1_R}}^{\pm 2f_{c1}}(\tau) + R_{y_{1_I}}^{\pm 2f_{c1}}(\tau) = 0. \tag{4.28}$$

This is the property we harness to develop our criterion: we expect that the estimation of $\hat{R}_{ss}^{\alpha}$ will not converge in the same way to zero if $\alpha = \pm 2f_{c1}$ and $\alpha \notin I_{y_{1_R}}$ as shown in fig.4.3. By definition, for a given $\alpha \notin I_s$, $\hat{R}_{ss}^{\alpha}(l) \triangleq 0$ since α is not a cyclic frequency. Using eq.(3.29), if we invoke the cycloergodic character of $y_1(t)$, it comes that eq.(4.28) leads to 0 only when N tends to infinity since $\lim_{N\to\infty} \hat{R}_{y_{1_R}}^{\pm 2f_{c1}}(l) = \lim_{N\to\infty} \hat{R}_{y_{1_I}}^{\pm 2f_{c1}}(l) \neq 0$. Consequently, with finite number of samples, the behavior of the CAF estimator is different between the $\alpha = \pm 2f_{c1}$ and all the other non-cyclic frequency. Hence, we propose to take advantage of the variance difference between the two cases.

Our criterion $\hat{J}_{L,N}(\alpha)$ is defined as follows:

$$\hat{J}_{L,N}(2f_{c1}) = \frac{\hat{C}_N^{2f_{c1}}(L)}{\hat{C}_N^{\beta}(L)}, \tag{4.29}$$

where $\beta \notin I_s$ and:

$$\hat{C}_N^{\alpha}(L) = \frac{1}{L+1} \sum_{l=0}^{L} |\hat{R}_{ss,N}^{\alpha}(l)|^2. \tag{4.30}$$

L is the number of lags of the autocorrelation function considered, and $|.|$ is the modulus operator. As the precision of the estimated CAF in eq.(3.29) depends on N, so does eq.(4.30). This criterion can be interpreted as a reciprocal correlation coefficient (see [Gardner, 1994]). Indeed, it makes a comparison between the estimated CAF at two α that are not cyclic frequencies. Our criterion can also be used for MPSK or MQAM modulations with $M >= 2$. The only constraint is that $z_{1_R}(t)$ and $z_{1_I}(t)$ of eq.(3.1) have to be independent. Our criterion exploits the property of quasi-constant energy shift within the two curves at $\alpha = 2f_{c_1}$ in fig.4.3.

This idea is similar to several applications in cognitive radio, as [Muraoka et al., 2008] where a method called *Maximum Cyclic Autocorrelation Selection (MCAS)* is proposed for the first time. The idea is to compare the peaks and non peaks values of CAF to decide whether a signal/user is present or not. In other words, the idea is to decide the presence if $R_{ss}^{\alpha}(\tau) \geq R_{ss}^{\varepsilon}(\tau)$, with $\alpha \in I_s$ and $\varepsilon \notin I_s$. This method could also be refined using several ε_i, to decrease the estimation variance. Still in the context of CR, another interesting idea was proposed in [Narieda and Hada, 2017]. Using the MCAS method, in this work $|R_{ss}^{\alpha}(\tau)|^2$ is assumed to be a signal component and $R_{ss}^{\varepsilon}(\tau)$ a noise component. The ratio in eq.(4.31) is proposed as a "CAF SNR".

$$\text{CAF SNR} = \frac{|R_{ss}^{\alpha}(\tau)|^2}{|R_{ss}^{\varepsilon}(\tau)|^2}. \tag{4.31}$$

Although very interesting, these methods cannot be applied directly in our context since the $R_{ss}^{2f_{c1}}(\tau)$ tends to zero, i.e. there is no cyclic energy to measure. Hence, our criteria is completely new.

4.4.2 Binary Test

As we defined the criterion to test, let now realize its theoretical analysis. To find a threshold, statistical distributions of $\hat{J}_{L,N}(\alpha)$ under both assumptions have to be considered. Using the Neyman-Pearson approach [Kay, 2009], a threshold Γ is determined with a constrained Probability of False alarm $P_{fa} = P[\hat{J}_{L,N}(2f_{c1}) \geqslant \Gamma | H_0]$. The following statistical hypothesis test is defined below:

$$H : \begin{cases} H_0 \rightarrow s(t) = w(t), \\ H_1 \rightarrow s(t) = y_1(t) + w(t). \end{cases} \tag{4.32}$$

Here H_0 denotes the absence of signal and H_1 denotes its presence.

When no signal is present, the criterion distribution is obtained more easily. So, to define Γ, let us consider the H_0 hypothesis, where the numerator and the denominator of eq.(4.29) have same statistical properties. It was shown in [Dandawate and Giannakis, 1994b], that the CAF estimator is unbiased and that the estimation error is asymptotically complex normal. Using eq.(3.29) as the sum of a real and imaginary part leads to:

$$\hat{R}^{\alpha}_{ss,N}(l) = \Re[\hat{R}^{\alpha}_{ss,N}(l)] + \jmath\Im[\hat{R}^{\alpha}_{ss,N}(l)], \tag{4.33}$$

where both real and complex terms follow asymptotically complex independent normal distributions for each l. The mean power expression in eq.(4.30) is consequently a sum of normal values, not reduced and non-centered. Under H_0, one can write the modulus expression of eq.(4.33):

$$|\hat{R}^{\alpha}_{ss,N}(l)|^2 = \Re[\hat{R}^{\alpha}_{ss,N}(l)]^2 + \Im[\hat{R}^{\alpha}_{ss,N}(l)]^2. \tag{4.34}$$

From eq.(4.30) and eq.(4.34) we obtain:

$$(L+1)\hat{C}^{2f_{c1}}_{N}(L) = \sum_{l=0}^{L} \Re[\hat{R}^{2f_{c1}}_{ss}(l)]^2 + \sum_{l=0}^{L} \Im[\hat{R}^{2f_{c1}}_{ss}(l)]^2. \tag{4.35}$$

Real and imaginary parts are independents and have same mean and variance.

Let now show that $\hat{J}_{L,N}(2f_{c1})$ follows a doubly non-central Fisher distribution. Thanks to [Kay, 2009], we noticed that eq.(4.35) is quite similar to a non-central chi-square distribution $\chi^2_{\nu}(\lambda)$, defined as:

$$\chi^2_{\nu}(\lambda) \sim \sum_{i=0}^{\nu} \frac{X_i^2}{\sigma_i^2}. \tag{4.36}$$

Where $\lambda = \sum \mu_i^2$ is the non-centrality parameter, $\nu = 2(L+1)$ is the number of degrees of freedom and X_i's are independent and $X_i \sim \mathcal{N}(\mu_i, 1)$. However, eq.(4.35) is not a sum of reduced Normal distributions. We also notice that the doubly non-central Fisher distribution is the ratio of two independent chi-2 distributions. Using eq.(4.36), $F''_{\nu_1,\nu_2}(\lambda, \delta)$ is denoted as:

$$F''_{\nu_1,\nu_2}(\lambda, \delta) \sim \frac{\sum_{l=0}^{\nu_1} \frac{X_l^2}{\sigma_l^2}}{\sum_{k=0}^{\nu_2} \frac{Y_k^2}{\sigma_k^2}}. \tag{4.37}$$

With our considered criterion, we have $\sigma_l^2 = \sigma_k^2$ since we use eq.(4.30) to estimate $\hat{J}_{L,N}(2f_c)$. Consequently we proved that $\hat{J}_{L,N}(\alpha) \sim F''_{\nu_1,\nu_2}(\lambda,\delta)$.

Non-centrality parameters λ and δ tend to zero asymptotically, and the degrees of freedom $\nu_1 = \nu_2 = 2(L+1)$. As eq.(4.29) is a ratio of random laws of similar moments, there is no need to determine λ and δ since the ratio tends to 1. At the asymptotic (N is large) both $\hat{C}_N^{2f_{c1}}(L)$ and $\hat{C}_N^{\varepsilon}(L)$ tend to zero. Non-centrality parameters become then $\lambda = \delta = 0$. In that case eq.(4.29) follows a central Fisher law $F(\nu_1,\nu_2)$. This approximation works well in practice even for N small.

In the other hand, when H_1 is considered, the nominator and denominator variances of eq.(4.37) are different (i.e. $\sigma_k^2 \neq \sigma_l^2$). It was shown in [Dandawate and Giannakis, 1994a] that $var\left[\hat{R}_{ss}^{\alpha}(l)\right]$ does not depends on lags l, which is also verified in simulations. It means that eq.(4.37) could be written as:

$$F''_{\nu_1,\nu_2}(\lambda,\delta) \sim \left(\frac{\sigma_Y^2}{\sigma_X^2}\right)\frac{\sum_{l=0}^{\nu_1} X_l^2}{\sum_{k=0}^{\nu_2} Y_k^2}. \tag{4.38}$$

It comes that way that $\hat{J}_{L,N}(\alpha) \sim (\frac{\sigma_X^2}{\sigma_Y^2})F''_{\nu_1,\nu_2}(\lambda,\delta)$ since $\hat{J}_{L,N}(\alpha)$ is not reduced. σ_X^2 and σ_Y^2 correspond to the criterion nominator and denominator variances respectively (i.e. CAF energy at $2f_{c1}$ and at ε). It was shown in [Gouldieff et al., 2018] that σ_X^2 is related to $y_1(t)$ power, and that σ_Y^2 is related $w(t)$ power. Hence, $\frac{\sigma_X^2}{\sigma_Y^2}$ is equivalent to the SNR. This is particularly interesting for a coarse analysis of $\hat{J}_{L,N}(\alpha)$ under H_1. As we said, $\hat{J}_{L,N}(\alpha) \sim (SNR)F''_{\nu_1,\nu_2}(\lambda,\delta)$. So, $E\left[\hat{J}_{L,N}(\alpha)\right] = (SNR)E\left[\hat{J}_{L,N}(\alpha)\right]$. Consequently, the criterion mean is directly proportional to the SNR. As the SNR decreases, the criterion distribution under H_1 comes closer to its distribution under H_0. Another effect due to this factor is the distribution scaling. Indeed, $var\left[\hat{J}_{L,N}(\alpha)\right] = (SNR)^2 var\left[\hat{J}_{L,N}(\alpha)\right]$, which implies the distribution enlargement.

Finally, to determine a threshold value to choose between H_0 and H_1, we simply have to refer to $\hat{J}_{L,N}(\alpha)$ under H_0 since its distributions is simply a central Fisher law with known freedom degrees. So, to fix Γ, the inverse function of $F(\nu_1,\nu_2)$ is required. A simple close form of $F(\nu_1,\nu_2)$ is detailed in [Johnson and Kotz, 1972]. However, it implies to use the inverse incomplete beta function, for which no close form expression exists. The usual method consists then in realizing an approximation. Thanks to the Newton algorithm and to the theoretical quantile function of central Fisher law, it becomes possible to determine a threshold Γ. So, let choose Γ for a given false alarm probability such as $P_{fa} = P[F_{2(L+1),2(L+1)} \geqslant \Gamma | H_0]$. Then, the same threshold will be applied for any SNR level.

4.4.3 Obtained Results

Experimental conditions

In this part, we propose several simulations to show our criterion accuracy and usefulness. We set a sampling rate $f_s = 10f_{c_1}$, in order to make a comparison with a high order moment

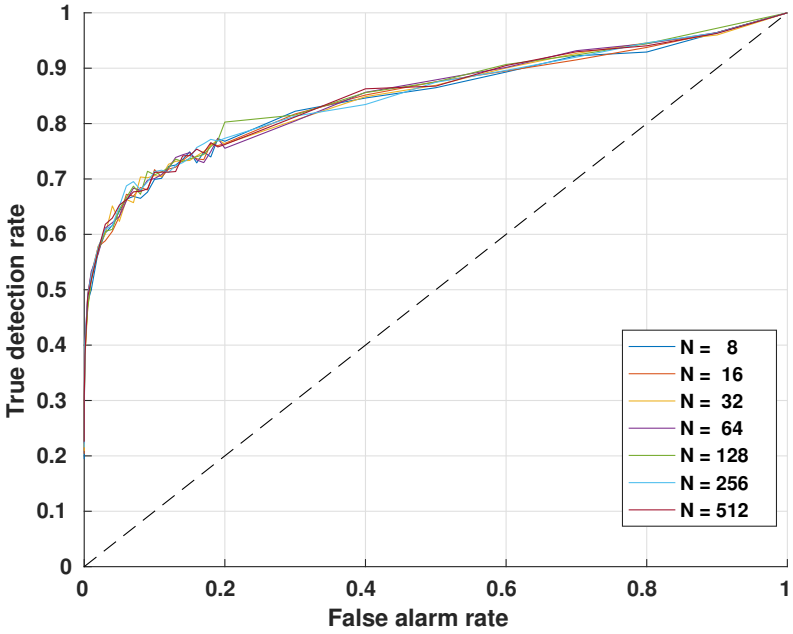

Figure 4.4: ROC curves at fixed SNR = 0dB, 2048 Monte-Carlo run, performance evolution for $N = 8$ to $N = 512$ symbols used

detection method. In our context f_{c_1} is the signal carrier frequency after down conversion. A square-root raised cosine filter of bandwidth $T = 2.5T_1$, is used as shaping filter with roll-of at 0.8 and span at 6 symbols. For first results, as discussed in subsection 3.2.2, channel's impulse response is considered as a dirac function. We also consider a perfect synchronization, but when these assumptions are relaxed, the limits are indicated. The SNR level is fixed at 0 dB, except when its values are given. Monte Carlo simulations were run, in which we considered 2048 realizations to determine the *false alarm probability* (H_0) and the *power of the test* (H_1).

Simulations - part 1

We first analyze our criterion detection rate in function of the number of symbols used to estimate it. Overall parameters are: a fixed SNR level of 0 dB, the maximum number of delays L is fixed at 20, and we plot ROC curves for $N = 8$ to $N = 512$. As we can see in fig.4.4, our algorithm provides similar detection probability for each N. Also, we notice that the detector gives about 65% of good detection for a false alarm rate of 5%. The strong point is that even with a small number of symbols, we are able to differentiate the presence or absence of the signal to detect. This is an advantage, because the number of samples is dramatically decreased compared to state of the art methods (e.g over 3000 symbols are required in [Spooner, 2001]). On the other hand, our algorithm is inconsistent since increasing N also doesn't improve the detection rate. This behavior is due to the constant ratio of our criterion nominator and denominator. It was highlighted in fig.4.3 by the constant gap between $\alpha = 2f_{c1}$ and $\alpha \notin I_s$. Besides increasing N doesn't improve the detection rate, an

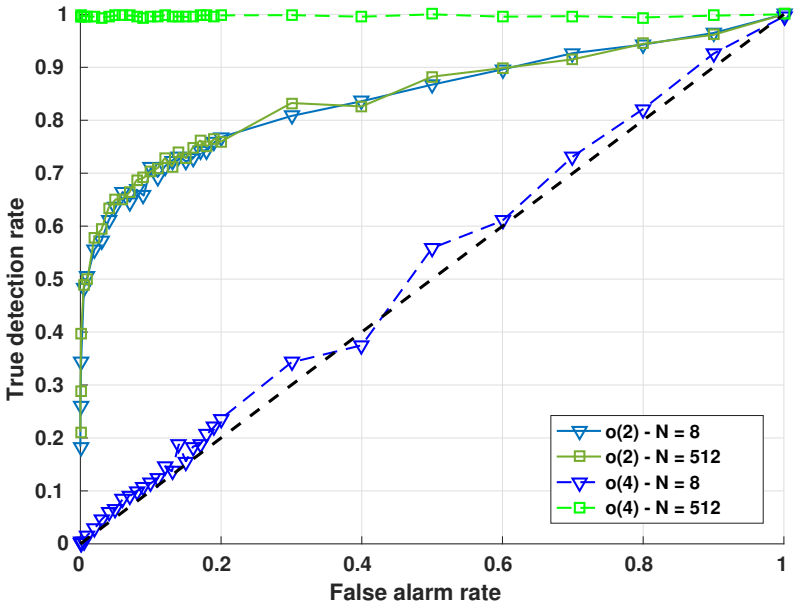

Figure 4.5: ROC curves at fixed SNR = 0dB, 2048 Monte-Carlo run, performance evolution for $N = 8$ or $N = 512$ symbols used. Comparison with fourth order moment method in [Reichert, 1992]

improvement could be obtained by adjusting the parameter L. This study is realized further.

As shown in fig.4.4, eq.(4.29) is independent of N. Let compare our detection rate with the fourth order moment method (dashed lines) described in [Reichert, 1992] in fig.4.5. It is clear that this method outperforms our algorithm for $N = 512$. But, we also noticed that for $N = 8$, the probability of detection provided by the fourth order moment method dropped. This point is particularly interesting, since using our algorithm could significantly decreases the number of operations and consequently allows a quick decision.

Let us now illustrate the influence of the parameter L on detection rate, with N set at 8 symbols. We plot ROC curves for several numbers of delay in fig.4.6. Considering only $L = 5$ leads to poor detection performances. There is an improvement around 20% of true detection rate for the rise of L from 5 to 20 delays. Then, increasing by 2.5 times the number of delays leads to another 20% rise of true detection rate. Consequently, better detection rates are achieved by increasing the number of delay used in the criterion estimation. The most important result is that increasing L provides a better rate of true detection. However, a trade-off between complexity and performance has to be made.

The eq.(4.38) showed that our criterion statistics are linked to the SNR. So, another important aspect to tackle is our statistical test reliability with respect to the SNR. That is why we present ROC curves for several SNR levels (from 0 dB to 10 dB) in fig.4.7. We set N equals 8 symbols and L equals 20 delays. We can see a noticeable evolution depending on SNR level. At SNR = 5dB, the detection probability reaches around 90% for a given 5% P_{fa}. The 10dB SNR obviously outperforms previous performance with more than 98% true

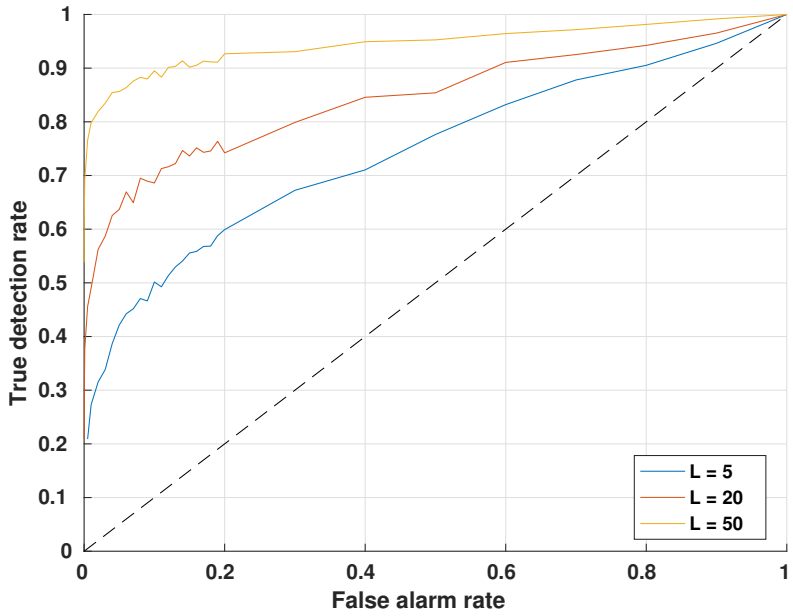

Figure 4.6: ROC curves at fixed SNR = 0dB, 2048 Monte-Carlo run, fixed number of samples (64 symbols), performance evolution with several delays L

detection at same false alarm probability.

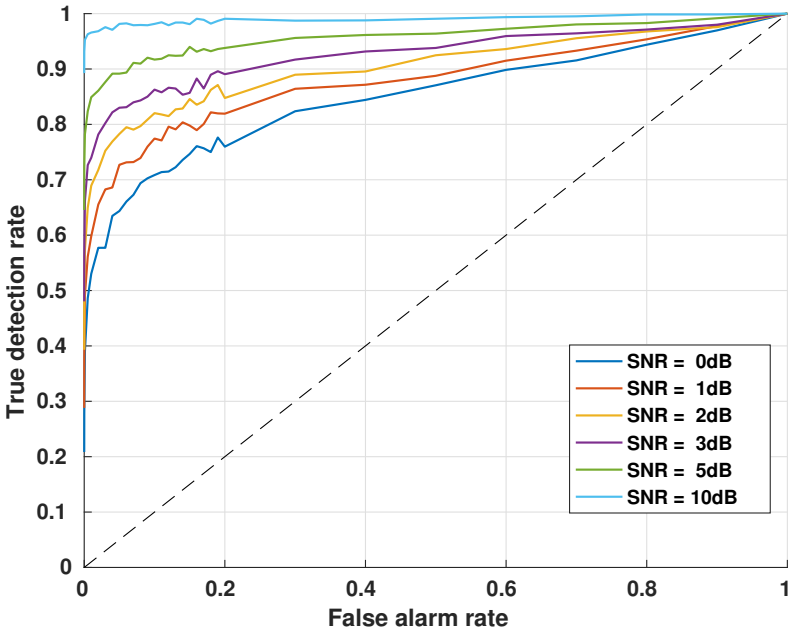

Figure 4.7: ROC curves evolution for several SNR level at fixed $N = 64$ symbols, 2048 Monte-Carlo run

Fig.4.8 illustrates benefits to measure $\hat{J}_{L,N}(\alpha)$ with a large L versus the SNR level, which vary in -12 dB to 6 dB. A threshold at 5% P_{fa} is set for several delays for each curves (20 and 1000). As we can see, the two curves decrease with the SNR level, to finally reach the $P_d = 5\%$. This is in fact the 5% false alarm rate that we defined as a parameter. If we consider a $P_d = 70\%$ at SNR = 0dB and $L = 20$ as a reference, this value is obtained at a SNR around -8dB for $L = 1000$. We notice a detection rate improvement about 8 dB. We also see that a 100% detection rate is achieved for SNR = -5dB. For any SNR smaller than -5dB, when L is large, the P_d decreases also quickly. In fact, as L increases, the Fisher distribution tends to normality (see [Kay, 2009]). So, $\hat{J}_{L,N}(\alpha)$ distribution could be approximated by a Normal distribution. This approximation explains why the curve for $L = 1000$ decreases more quickly than the other one: the Fisher distribution have a positive skewness when the Normal distribution is symmetric.

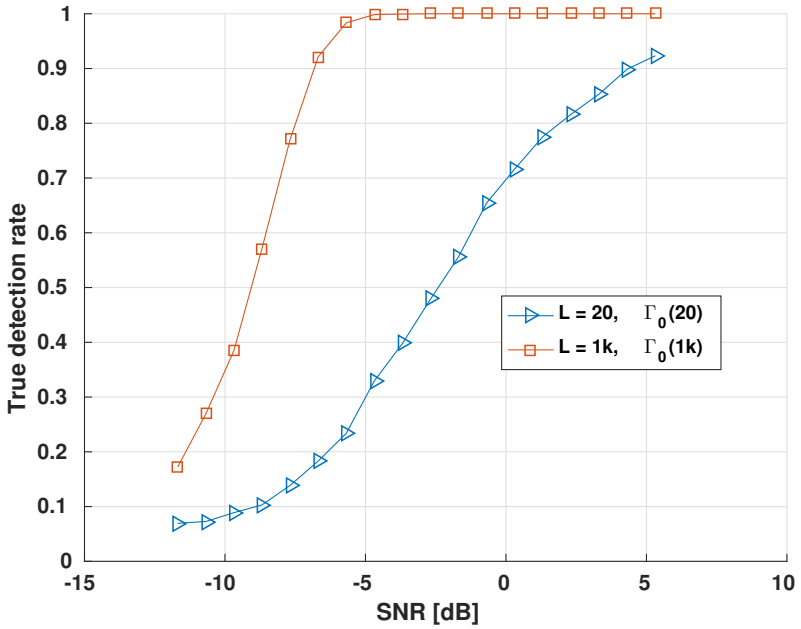

Figure 4.8: Comparison of true detection rate for several delays L, with threshold Γ defined set for a SNR = 0dB

Simulations - part 2

Let now relax the assumption of an ideal impulse channel, and consider a static multi-path channel. As discussed in subsection 3.2.2, the channel impulse response model is different depending on the signal's propagation path. In fig.4.9, we considered the Porat channel influence on detection probability under H_1. This simulation was realized considering that the behavior of $\hat{J}_{L,N}(\alpha)$ may be different under a multi-path channel assumption. Several ROC curves were obtained for different number of symbols from $N = 8$ to $N = 512$. We clearly see that all curves have a similar detection rate. It illustrates that this particular channel has no influence

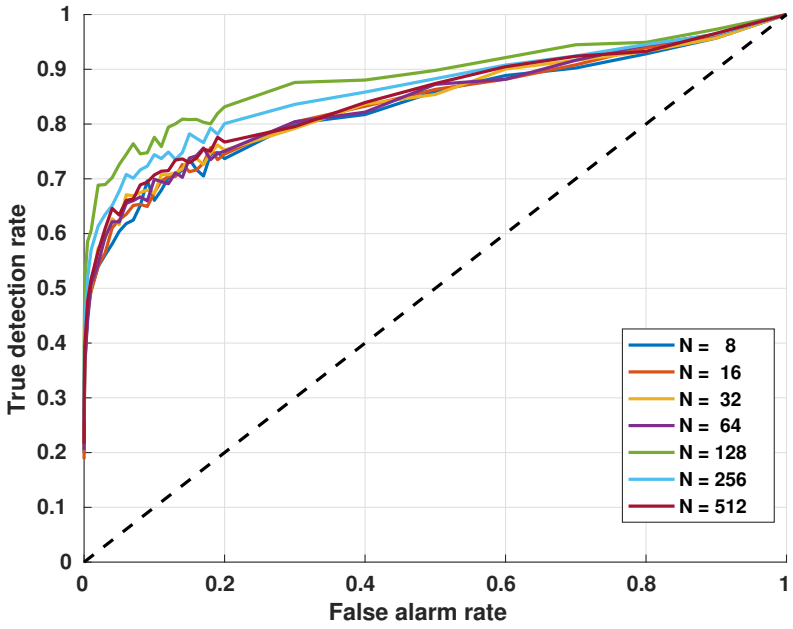

Figure 4.9: Comparison of true detection rate under the influence of Porat Channel in function of N, with threshold Γ defined at SNR fixed at 0dB

neither on the overall criterion behavior nor on the detection probability. Moreover, we can see in fig.4.10 the Porat channel influence, as the probability of detection is similar to the case when $g(t,\tau) = \delta_0$. In fig.4.10 other channel models were considered. We clearly see that all curves are superimposed. It seems that none of considered channels has any influence on the detection probability. Indeed, as introduced in section 3.5, $S^{\alpha}_{ss}(f)$ is a product of shifted versions of the channel $G(f)$, which is the channel Fourier transform. Starting from eq.(4.30), let us consider a limit case where L tends to infinity, to make $\lim_{N\to\infty} \hat{C}^{\alpha}_{N}(L) = S^{\alpha}_{ss}(0)$. That way, from eq.(3.6) and eq.(3.26) one can write the relation in eq.(4.39) below.

$$S^{\alpha}_{ss}(0) = G(+\frac{\alpha}{2})G^{*}(-\frac{\alpha}{2})S^{\alpha}_{xx}(0) + S^{\alpha}_{ww}(0) \tag{4.39}$$

As the channel Fourier transform is not flat, the product $G(\frac{\alpha}{2})G^{*}(-\frac{\alpha}{2})$ becomes a constant factor, that is simplified by the ratio in eq.(4.29). Hence, the independent character of $\hat{J}_{L,N}(\alpha)$ for a multi-path channel influence is demonstrated. This result is of a major interest, since it comforts us in the utility of our method and its usefulness in real use cases in the FITNESS project context.

However, the channel is not the only assumption we made: we also assume a perfect synchronization. So, it is also interesting to evaluate our approach robustness to a frequency shift of the received signal. On carrier signal definition in eq.(3.2) could be adapted to become:

$$y_1(t) = \Re[z_1(t)e^{j2\pi(f_{c1}+\Delta_f)t}]. \tag{4.40}$$

In a first approach, a BPSK modulation is used to gives an answer when the CAF power at $2f_{c1}$ is different from zero. We have to introduce that $y_1(t)$ in eq.(4.23) could be written

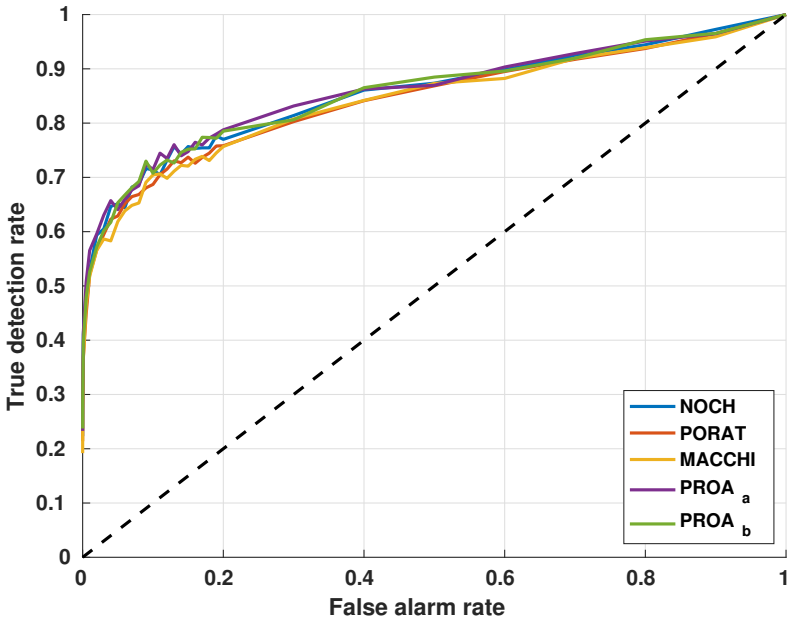

Figure 4.10: Comparison of true detection rate under different channels influence, for $N = 8$ symbols and threshold Γ defined at SNR fixed at 0dB

as a product of the useful signal and a temporal rectangular window. Such an operation is commonly considered to take the implicit temporal windowing into account. That way, for a signal of length T, eq.(4.23) becomes:

$$s_W(t) = s(t)\Pi_{[0,T]} \tag{4.41}$$

In [Gardner, 1994], a temporal multiplication of two time series leads to a resulting CAF which expression is the discrete circular convolution in the cycle frequency domain of these signals. Applying a Fourier transform on the corresponding equation leads to the expression in eq.(4.42), which is more convenient:

$$S_{s_W s_W}(f) = \int_{-\frac{1}{2}}^{\frac{1}{2}} \sum_{\beta \in \left(-\frac{1}{2}, \frac{1}{2}\right]} S_{ss}^{\beta}(\nu) S_{\Pi_{[0,T]}}^{\alpha-\beta}(f-\nu) d\nu \tag{4.42}$$

for which $S_{\Pi_{[0,T]}}(f) = |\mathcal{F}_{/t}\left\{\Pi_{[0,T]}\right\}(f)|^2$, where $\mathcal{F}_{/t}\{.\}(f)$ stands for the Fourier transform with respect of time. It means that $S_{\Pi_{[0,T]}}(f)$ is a squared cardinal sine function.

$$S_{\Pi_{[0,T]}}^{\alpha}(f) = \begin{cases} S_{\Pi_{[0,T]}}(f) & \text{for } \alpha = 0, \\ 0 & \text{otherwise.} \end{cases} \tag{4.43}$$

As presented in fig.4.11, around $2f_{c1}$ a squared cardinal sine shape indeed appears. When T increases in the CAF estimate, the energy peak comes sharper. This is the normal effect of windowing $s(t)$, due to the cardinal sine function, which bandwidth is $\frac{2}{T}$. A larger lobe could be obtained for a shorter observation duration. As we can see, the main lobe bandwidth is

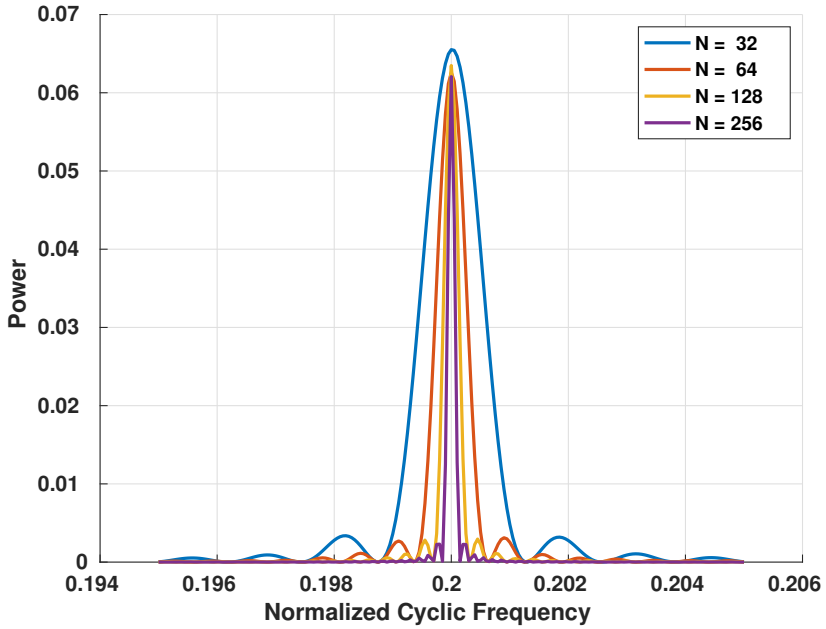

Figure 4.11: Comparison of CAF power measure at cyclic frequency $\alpha = 2f_{c1}$, for a BPSK signal of size $N = 32$ to $N = 256$

multiplied by a factor two for a proportional decrease of T. In [Houcke, 2002], this idea was exploited to coarsely search for the received signal cyclic frequencies. Back to our frequency shift problem, it means that if the shift is small enough, the CAF detector may still be useful. More precisely, the detection could be performed with success if $\Delta_f < \frac{1}{T}$. At an existing cyclic frequency, this topic was analyzed in [Rebeiz et al., 2012], which results confirm our analysis. A numeric application with FITNESS parameters for a signal length of 32 symbols (with F_{ech} =18 MHz and a channel of 12.5 kHz bandwidth) would lead to $\Delta_f = 39.06$ Hz (or $\Delta_f = 156.24$ Hz for a signal length of 8 symbols). These values are small compared to the RX sampling frequency. Nonetheless, it answers FITNESS project requirements. The worst Doppler shift is obtained only for the higher PMR communication band (i.e. around 900 MHz). So, with $\Delta_f = 156.24$ Hz the corresponding relative speed limit to make the detection unable to work is 187.7 km/h, which is a comfortable speed margin.

But, our detector was mainly designed to detect phase modulated signals: no peak can be used to perform the detection. It was shown in [Gouldieff et al., 2018] that the CAF variance is different if $\alpha \in \left[-\frac{1}{T_1}, \frac{1}{T_1}\right]$. So, our detector gives a maximized detection at $\alpha = 2f_{c_1}$, and degraded values are obtained if the tested cyclic frequency is in $\left[2f_{c_1} - \frac{1}{T_1}, 2f_{c_1} + \frac{1}{T_1}\right]$. Outside this interval, only false alarms occurs. This is precisely what can be observed in fig.4.12. The detection probability meet the value obtained in fig.4.4 for $\alpha = 2f_{c_1} = 0.2$. At each side of $\alpha = 2f_{c_1}$, we see a detection rate degradation until bounds $2f_{c_1} \pm \frac{1}{T_1}$ are reached. With our detector, the detection could be performed with success if $\Delta_f < \frac{1}{T_1}$, which is even more interesting than using a classic cyclostationary detector where $\Delta_f < \frac{1}{T}$.

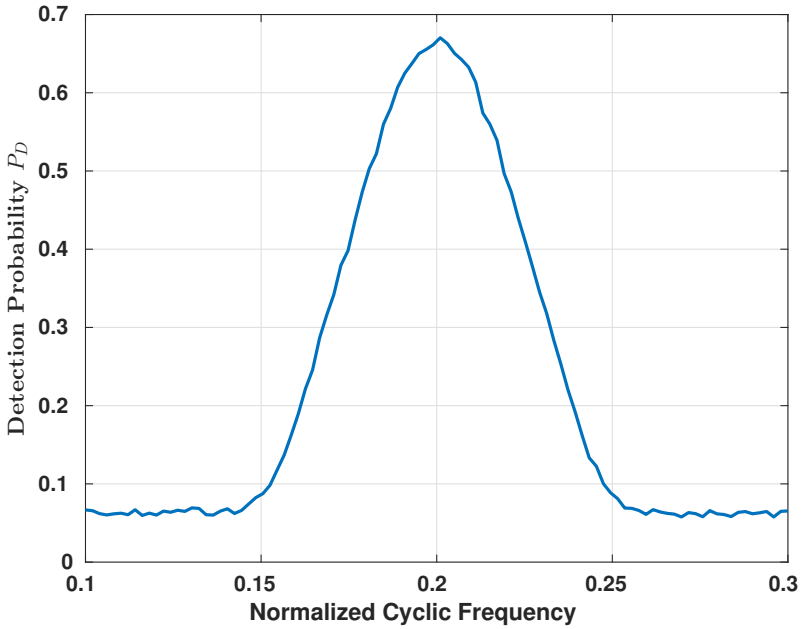

Figure 4.12: P_d resilience against a carrier frequency shift for a given $P_{fa} = 5\%$

4.5 Conclusion & Perspectives

In this chapter, we realized a review of cyclostationary methods that allow to detect a phase modulated signal on carrier. As we saw, low order moments methods are not adapted because some PMR modulations has no energy at multiple of their cyclic frequency. Hence, higher order statistics have to be used, or a nonlinear transformation method. But, theses methods (which have very similar points) require a large amount of samples as main drawback. That is why, we proposed a novel algorithm to detect phase modulated signals using a low order moments method.

We showed that it is possible to detect a signal presence at a cyclic frequency where there is theoretically no energy. Through simulations, we explored different characteristics of that criterion. A major benefit of this method is that the detector performs well for only 8 symbols, which is particularly few. As a comparison, we realized a detection test with the nonlinear transformation method. Our detection results are far more interesting when the input signal size is small, but are clearly overcome when the number of symbols comes high. Besides, our criterion is also tunable thanks to the parameter L. The number of delays taken into account influences the detection probability, and allows a detection rate improvement. A better detection rate is nevertheless obtained at the cost of a computational time increase. Often, detection state of the art methods are performed in ideal conditions (i.e no channel). In the last part of this chapter, we tried to answer issues of multi-path channel and bad synchronization. We showed that with our method, the channel influence is negligible. A short analysis on this topic showed that the method is also robust to Doppler shift. Hence, our detector turns out to have several advantages that may justify an integration in the

FITNESS receiver prototype. Moreover, results obtained with the QPSK modulation are easily extended to phase modulated MPSK or MQAM (with $M > 2$) signals.

Besides no study of the emission filter excess band was done in this document, the influence of such a parameter is known: an excess bandwidth the closer to 1 produces the better detection. As an example, the work in [Houcke, 2002] is complete on this topic and the adaptation to our context doesn't have a great interest. Furthermore, we only analyzed our criterion detection rates in the case of phase modulated signal. But, there is no reasons for our method to perform in a different way when there is a non zero energy at the monitored cyclic frequency. In such a case, state of the art methods could be used and might be more efficient than our method. But, using our algorithm allows to perform a detection without the noise power knowledge.

This work raises several perspectives:

1. In the present work, we only defined our criterion theoretical expression in the absence of useful signal. However, the same work have to be done considering its presence. If the theoretical probability distribution knowing H_1 could be obtained, one could link it with the signal power (or the SNR at least). An estimation of the signal power might be useful, as we develop in following chapters.

2. As a prospective work to improve our criterion, we propose to modify its definition in eq.(4.29). The denominator would become a mean of k values for a set of $\{\varepsilon_1, \cdots, \varepsilon_{M-1}\}$ such as in eq.(4.44).

$$\hat{K}_{L,N}(2f_{c1}) = M \frac{\sum_{l=0}^{L} |\hat{R}^{2f_{c1}}_{ss,N}(l)|^2}{\sum_{m=0}^{M-1} \sum_{l=0}^{L} |\hat{R}^{\varepsilon_m}_{ss,N}(l)|^2} \tag{4.44}$$

   Here, ε_m are not in the set of $s(t)$ cyclic frequencies. That way, the CAF power due to noise variance would be averaged, which could improve the detection rate.

3. Another idea, similar to eq.(4.44) concerns the resilience against frequency shift. A test on several values close to the cyclic frequency could be realized as developed in eq.(4.45),

$$\widetilde{K}_{L,N}(2f_{c1}) = \frac{M}{J} \frac{\sum_{j=0}^{J-1} \sum_{l=0}^{L} |\hat{R}^{\beta_j}_{ss,N}(l)|^2}{\sum_{m=0}^{M-1} \sum_{l=0}^{L} |\hat{R}^{\varepsilon_m}_{ss,N}(l)|^2}, \tag{4.45}$$

   where $\beta_m \in [2f_{c1} \pm m/T_s]$. Thanks to this process, a detection could be maximized to limit the issues due to Doppler shift.

CHAPTER 5

Enhanced Spectrally Aware RF front end Receiver under Non-linearity

5.1 Introduction

The chapter 2 was devoted to the new PMR receiver and its constraints description. As we saw, the convergence of several norms into one device makes ADC's specifications difficult to achieve. This is due to unwanted signals presence at ADC input, which limits its dynamic range. Hence, a method to detect such signals has to be identified, which justifies this study. Signal model and basic detection methods were developed in chapter 3. With considered assumptions, the most appropriated detection method is the cyclostationary approach. However, as we saw in chapter 4, some PMR modulations can't be detected in a simple manner. So, in order to address the on carrier phase modulated signals detection problematic, we developed a new method.

In this chapter, we propose to use this new tool to detect unwanted signals in the FITNESS context. As seen in chapter 2, due its internal analog components, the receiver is not perfectly linear and is modeled as a polynomial. In presence of at least two signals (i.e. the useful signal and an interferer) additional harmonics appear due to saturation. Hence, to answer FITNESS requirements, we have to determine when ADCs come to saturate according to the mechanism described in fig.2.7. Two scenarios are considered:

a) useful signal only (sensitivity scenario);

b) useful signal plus an interferer signal (linearity scenario).

In case a), if SOI's power is high enough, it may introduce a saturation and creation of harmonics at frequencies that are multiple of SOI's carrier. In case b), two situations are possible:

b.i) interferer's power is small enough. It implies that unwanted harmonics power are also

small, which left the SOI unharmed;

b.ii) interferer's power is high enough to create powerful unwanted harmonics.

In this chapter, we propose a method to distinguish these three cases. Our goal is to realize several successive detections thanks to our cyclostationary sensing method. The first step is to decide if an interferer is present or not, monitoring our new criterion at $2f_{c2}$ (where f_{c2} is the interferer's carrier frequency). The second step, consists in identifying if the nonlinear behavior is due to a powerful interferer's presence, or to a powerful SOI. Monitoring specific harmonics created by the nonlinear function at $4f_{c1}$ and $4f_{c2}$ allows the scenario identification.

Our founding assumptions are tackled in section 5.2. We realize a theoretical analysis to show mechanisms that damage the SOI in linearity or sensitivity scenarios. Method principles are developed there, as well as the detection theoretical analysis in the nonlinear distortion context. The section 5.3 is devoted to present our results and to show the compliance to FITNESS requirements. Thanks to simulations, we then show that this method is reliable and allows a nonlinearity detection 16dB below the compression point.

5.2 Nonlinear Sensing Mechanism

5.2.1 Nonlinear Model

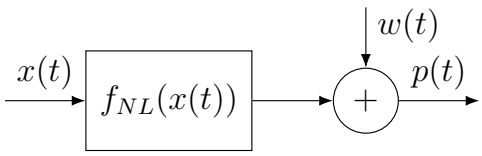

Figure 5.1: nonlinear received signal model

According to fig.5.1, the nonlinear RX which input is $x(t)$ defined in eq.(3.5), is expressed as a polynomial of order three:

$$p(t) = \alpha_1 x(t) + \alpha_2 x(t)^2 + \alpha_3 x(t)^3 + w(t) \tag{5.1}$$

Where $\alpha_k, k \in \{1,2,3\}$ are characteristics of the RX front-end, $x(t) = \sum_{i=1}^{2} y_i(t)$ with $y_i(t)$ on-carrier signals defined in eq.(3.1), eq.(3.3) and $w(t)$ is AWGN. Let us recall from eq.(3.2) that $y_i(t) = \Re\left[z_i(t)e^{j2\pi f_{ci}}\right]$, with f_{ci} signals carrier frequencies and $z_i(t)$ from eq.(3.1) signals baseband representations. Let also define by β_1 (respectively β_2) the squared-root power of signal $z_1(t)$ (respectively $z_2(t)$). There is a significant difference between eq.(5.1) and the model defined in eq.(3.6) and represented in fig.3.1. Here, the noise is added after that $x(t)$ goes through the nonlinear function. This assumptions is commonly admitted as in [Valkama et al., 2006, Zou et al., 2009, Keehr and Hajimiri, 2008], and simplifies the following study. However, it does not represent the real receiver behavior with confidence.

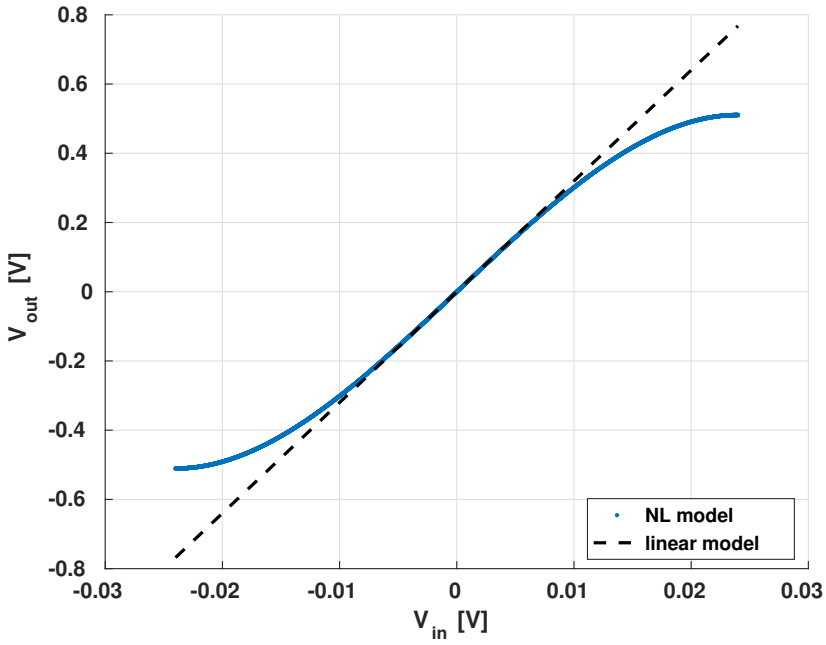

Figure 5.2: V_{in}/V_{out} representation of a PMR receiver nonlinear model

We consider here that the α_2 coefficient equals 0, since harmonics created by even coefficients are located at twice the input signal carrier frequency. Such contributions are suppressed by a low-pass filter and a differential architecture before digitization. Thus, there is no harmonic leaks in SOI bandwidth due to IMD2, or in other words no harmful effects for the useful signal. As in [Rebeiz et al., 2015], α_3 is obtained thanks to the relation eq.(5.2):

$$\alpha_3 = -\frac{4}{3}\frac{\alpha_1}{V_{IIP3}^2} \tag{5.2}$$

where V_{IIP3} is the RX Input Interception Point of third order (IIP3). Here, $p(t)$ coefficients are extracted from practical measurements on the PMR receiver demonstrator developed in CEA lab. The input-output representation of $p(t)$ with those parameters is displayed in fig.5.2. Let us define V_{sat}^{in} as the minimum input that makes the nonlinear RX saturate. In this example, V_{sat}^{in} is about 25 mV, for a saturated output V_{sat}^{out} about 550 mV.

In this part, the whole RX is modeled as a nonlinear system to address the combination of several nonlinear stages. This assumption holds, thanks to the nonlinear Friis formula counterpart(see [Razavi, 2011]). For now on, as a simplification α_k coefficients are assumed constant. Indeed, in a classic receiver the systems analog parameters are fixed by design.

The substitution of eq.(3.5) into eq.(5.1) leads to the complete formula of harmonic creation for the nonlinear model. All terms are listed in [Zou et al., 2009], but α_2 is not considered here. We focus on the received signal baseband representation in a given sub-band of interest.

The SOI in this sub-band is given by:

$$\begin{aligned} p(t) &= \Re\Big\{(\alpha_1 z_1(t) + \frac{3\alpha_3}{2} z_1(t)|z_1(t)^2| \\ &\quad + 3\alpha_3 z_1(t)|z_2(t)|^2) e^{j2\pi f_{c1} t}\Big\} + w(t) \end{aligned} \tag{5.3}$$

In the linearity scenario context (fig.2.7), we consider that the SOI is much smaller than the blocker, so the term in $z_1(t)|z_1(t)^2|$ can be neglected. The term proportional to $|z_2(t)^2|$ becomes dominating as blocker's power comes high, and may affect the SOI. In the other hand, in the sensitivity scenario (in absence of interferer), the term in $z_1(t)|z_1(t)^2|$ becomes harmful if SOI's power is high enough.

5.2.2 Nonlinear Harmonics Cyclostationary Detection

Let now develop the cyclostationary analysis of $p(t)$ after digitization. Considering the linearity scenario, we assume that a powerful interferer $y_2(t)$ is present. Using the criterion eq.(4.29), allows us to track the interferer presence at $2f_{c2}$. To determine if the RX works in a nonlinear mode, we propose to realize a short cyclostationary analysis. Hence, we need to understand how nonlinear harmonics impact received signal's cyclostationarity properties.

Due to the $(.)^3$ operation, eq.(5.1) is in fact a sum of 9 harmonics, that are detailed in [Zou et al., 2009]. So, a theoretical search of cyclic frequencies (using eq.(3.29) and eq.(5.1)) leads to a 81 terms expression, which are useless to detail. We focus only on nonlinear terms that are

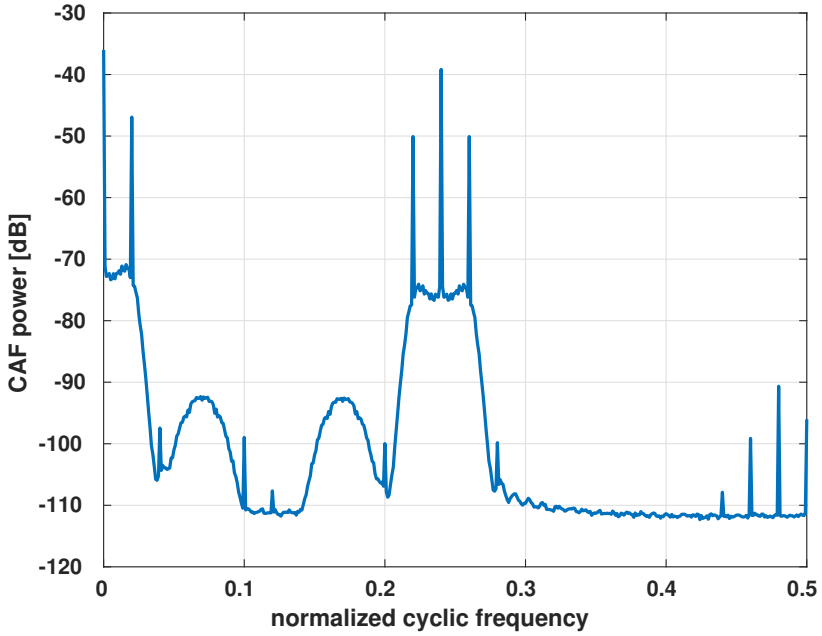

Figure 5.3: CAF energy in the cyclic frequency domain averaged over 100 realizations, in SOI ($f_{c1} = 0.05$) and interferer ($f_{c2} = 0.12$) presence for a SIR $= -30$ dB, SNR $= 0$ dB, in a weakly nonlinear circuit.

the most powerful, as it seems reasonable that their detection is easier. Developing eq.(5.1), we have eq.(5.4):

$$p(t) = \alpha_1\Big(y_1(t) + y_2(t)\Big) + \alpha_3\Big(y_1^3(t) + y_2^3(t) + 3y_1^2(t)y_2(t) + 3y_2^2(t)y_1(t)\Big) \tag{5.4}$$

An analysis of a single BPSK signal, developed in Annexe B, shows the presence of powerful CAFs at cyclic frequencies $4f_{c1}$ and $4f_{c2}$. One can notice that, CAF expressions are homogeneous to high order moments due to the nonlinear transformation, which produce peaks of significant power, as illustrated in fig.5.3. The most important peak is located at $\alpha = 2f_{c2}$, which corresponds to the interferer's presence. Peaks located at $\alpha = 2f_{c2} \pm \frac{1}{T_2}$ corresponds to it's symbol period. We also see additional peaks located at $4f_{c2}$, as discussed earlier. In this example, the SOI contribution is completely overpowered by the interferer's cyclic harmonics.

Hence, we focus on cyclic harmonics that are created by the nonlinear process: we propose to monitor the criterion set $\mathcal{M} = \{\hat{J}_{L,N}(2f_{c2}), \hat{J}_{L,N}(4f_{c1}), \hat{J}_{L,N}(4f_{c2})\}$ (with $\hat{J}_{L,N}(\alpha)$ defined in eq.(4.29)). That information is enough to select the corresponding linearity or sensitivity scenario described in fig.2.7. We choose to use our criterion to monitor the cyclic frequencies $4f_{c1}$ and $4f_{c2}$, in spite of the fact these cyclic harmonics are created by the $(.)^3$ operation. Indeed, evident peaks are created at cyclic frequencies $4f_{c1}$ and $4f_{c2}$, which indicates that a classic second order method could be used. Nonetheless, using our criterion allows to perform a detection without neither the noise power knowledge nor a covariance matrix estimation.

5.2.3 Binary Hypothesis Testing

Each element $\mathcal{M}_k$ of $\mathcal{M}$ is tested accordingly to a Neyman-Pearson approach [Kay, 2009]. A constant false alarm threshold Γ, is set to satisfy $P_{fa} = P[\mathcal{M}_k \geq \Gamma | H_0]$, where H_0 represents the absence of harmonic corresponding to $\mathcal{M}_k$, the k-th element of $\mathcal{M}$ (with $k \in \{1, 2, 3\}$). But, as $\mathcal{M}$ is a set of three criterion, three tests have to be defined. Whatever the scenario, and for any input signal, $p(t)$ is a nonlinear function with fixed parameters. So, reasons for the system to work in a nonlinear regime are the signals power β_1 and β_2.

For the test formulation, we defined intervals $I_{lin} = [0, \gamma]$ where no detectable saturation occurs, and $I_{nl} =]\gamma, C_{sat}]$ its counterpart. Let $\gamma > 0$ be a power, such as replacing $\beta_i = \gamma$ in eq.(3.1) (respectively eq.(3.3)) leads to $p(t)$ in eq.(5.1) at the limit of saturation such as $P[\mathcal{M}_2 \leq \Gamma | H_1]$ (respectively $P[\mathcal{M}_3 \leq \Gamma | H_1]$). In other words, γ is the limit power for which an existing nonlinear cyclic harmonic is not detected. At this state, we have no idea of the γ real value with our method. So, let us define $\gamma = C_{-1dB}$, where C_{-1dB} is the input level for which the nonlinear output is decreased by 1 dB in comparison with a linear output. C_{-1dB} is usually called the compression point: it allows to compare analog circuits linearity. The γ value is adjusted in the end of this chapter, in the light of our method detection results in a nonlinear environment.

The first test to be conducted is the interferer's test presence with:

$$\mathcal{H}_1 : \begin{cases} H_0 \rightarrow p(t) = \alpha_1 y_1(t) + \alpha_3 y_1(t)^3 + w(t) \text{ with } \beta_1 \in I_{lin} \cup I_{nl} \text{ and } \beta_2 = 0 \\ H_1 \rightarrow p(t) = \alpha_1 x(t) + \alpha_3 x(t)^3 + w(t) \text{ with } \beta_i \in I_{lin} \cup I_{nl}, i \in \{1, 2\} \end{cases} \tag{5.5}$$

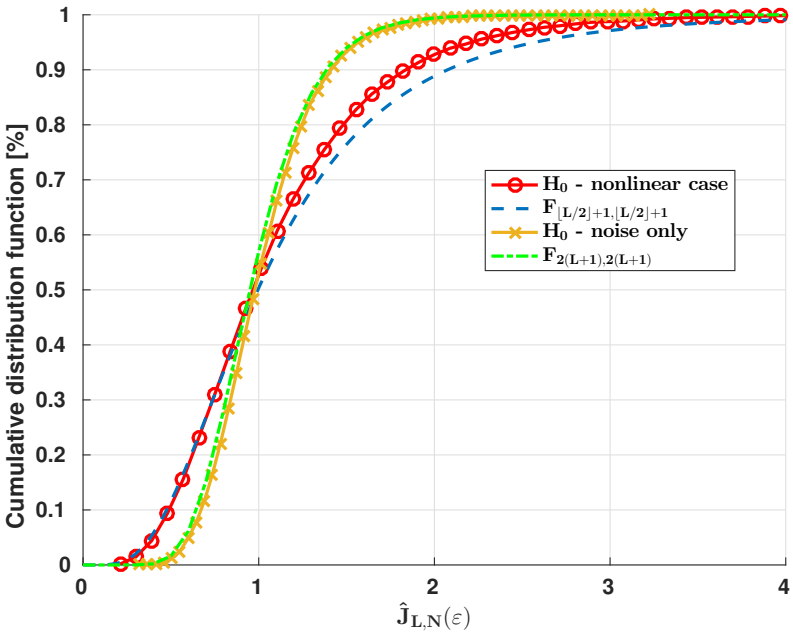

Figure 5.4: Cumulative distribution functions of $P\left[\hat{J}_{L,N}(\alpha) \geq \Gamma | H_0, \{\alpha \notin I_p, \beta_1 = 0, \beta_2 = 0\}\right]$ and $P\left[\mathcal{H}_1 | H_0\right]$ with their corresponding theoretical Fisher cumulative distribution, where $L = 20$, SNR $= 0$ dB and averaged over 2048 realizations.

If no interferer is detected (i.e. $\mathcal{H}_1|H_0$), a sub-test to determine if the SOI power causes a saturation is done thanks to the test $\mathcal{H}_2$ in eq.(5.6):

$$\mathcal{H}_2 : \begin{cases} H_0 \rightarrow p(t) = \alpha_1 y_1(t) + \alpha_3 y_1(t)^3 + w(t) \text{ with } \beta_1 \in I_{lin} \text{ and } \beta_2 = 0 \\ H_1 \rightarrow p(t) = \alpha_1 y_1(t) + \alpha_3 y_1(t)^3 + w(t) \text{ with } \beta_1 \in I_{nl} \text{ and } \beta_2 = 0 \end{cases} \tag{5.6}$$

Nonetheless, if an interferer is detected (i.e. $\mathcal{H}_1|H_1$), we have to test if it degrades the SOI thanks to test $\mathcal{H}_3$ in eq.(5.7):

$$\mathcal{H}_3 : \begin{cases} H_0 \rightarrow p(t) = \alpha_1 x(t) + \alpha_3 x(t)^3 + w(t) \text{ with } \beta_1 \in I_{lin} \cup I_{nl} \text{ and } \beta_2 \in I_{lin} \\ H_1 \rightarrow p(t) = \alpha_1 x(t) + \alpha_3 x(t)^3 + w(t) \text{ with } \beta_1 \in I_{lin} \cup I_{nl} \text{ and } \beta_2 \in I_{nl} \end{cases} \tag{5.7}$$

We underline that for each test, the H_0 hypothesis corresponds at least to the SOI presence through the RX plus noise, instead of noise only as assumed in the previous chapter.

Such a difference causes a significant change in our method, as underlined in fig.5.4. We clearly see a loss of freedom degrees of $P\left[\mathcal{H}_1 \geq \Gamma | H_0\right]$ in the nonlinear case. It leads to a higher positive skewness of the false alarm probability. Indeed, the experimental cumulative distribution function is closer to a $F_{\lfloor L/2\rfloor+1,\lfloor L/2\rfloor+1}$ distribution, which nevertheless does not fit perfectly to experimental data. We showed analytically in chapter 4, that $P\left[\hat{J}_{L,N}(2fci), \{\beta_i = 0, i \in \{1,2\}\}\right]$ follows a doubly non central Fisher law of $2(L+1)$ freedom degrees. However, these results are different from the detection probability obtained in chapter 5 (linear signal presence plus noise). In other words : $P\left[\mathcal{H}_j | H_0, j \in \{1,2,3\}\right] \neq$

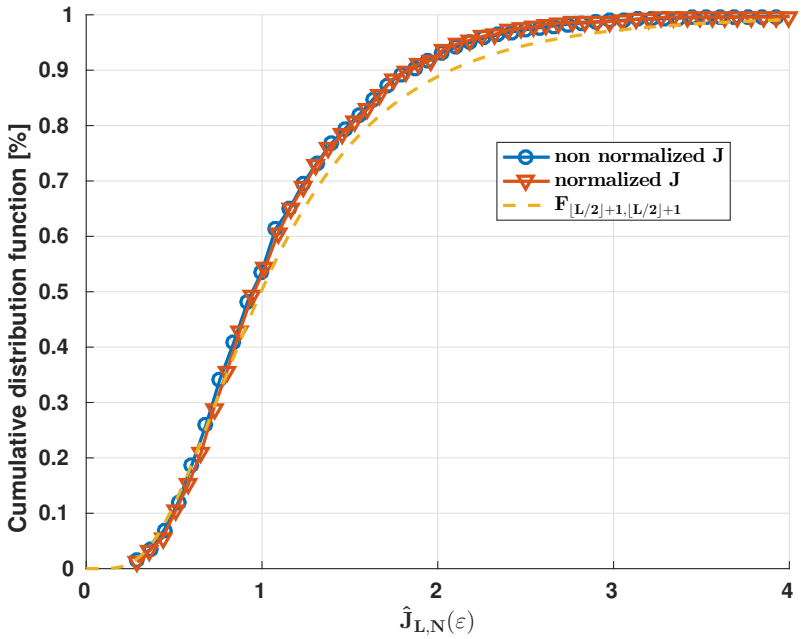

Figure 5.5: Cumulative distribution functions of $P\left[\mathcal{H}_1 \geq \Gamma | H_0\right]$ with and without normalized coefficients, where $L = 25$, SNR $= 0\,$dB and averaged over 2048 realizations.

$P\left[\hat{J}_{L,N}(2f_{ci})|H_1\{\beta_i \in I_{lin}, \beta_2 = 0\}\right]$. Let us develop further this analysis, in order to explain this behavior difference. We investigated two possibilities that could explain this difference:

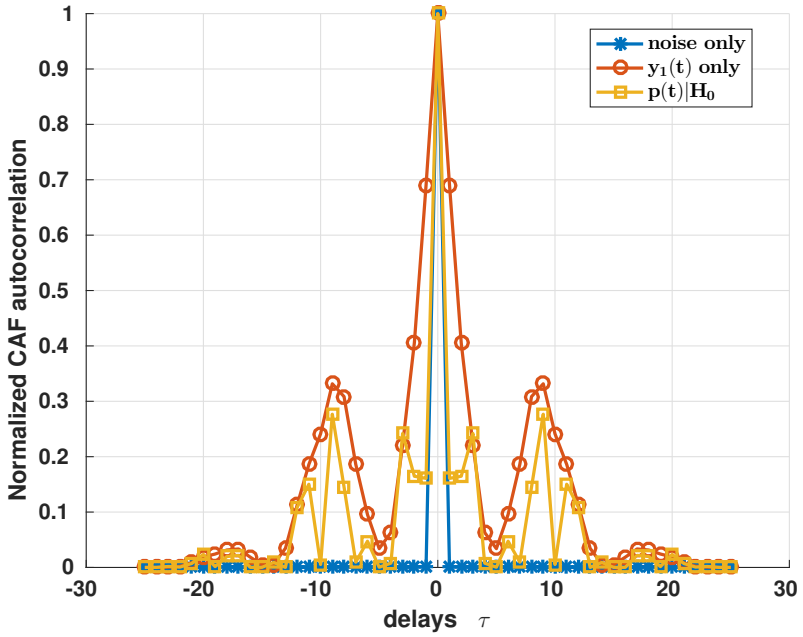

Figure 5.6: Normalized Autocorrelation of CAF delays for noise only, undistorted signal only and nonlinear signal, where $L = 25$, and averaged over 1000 Monte-Carlo realizations.

1. $\hat{J}_{L,N}(\alpha)$ is the ratio of the CAF energy at α over the CAF energy at ε. Denominator and numerator are not normalized. It means the scaling factor absence changes the distribution variance, as discussed for criterion analysis under H_1 hypothesis in section 4.4. We said that the CAF distributions for each delay are Normal due to central limit theorem. So, the CAF energy mandatory follows a chi-square distribution if each component is scaled by its standard deviation. Nevertheless, none of our criterion values (defined in eq.(4.29)) $\hat{R}^{\alpha}_{pp,N}(l), \forall l \in \{0, \dots, L\}$ are normalized. Hence, if each element $\hat{R}^{\alpha}_{pp,N}(l)$ has a different variance, then the CAF energy doesn't follow a chi-square distribution. To check this assumption, a simulation was conducted where each $\hat{C}^{\alpha}_{N}(L)$ coefficient was normalized. As shown in fig.5.5, there is no obvious difference due to normalization. It means that the drop of freedom degrees is not a consequence of to a bad scaling.

2. The second possibility concerns the independence between each variables. The most likely explanation would be that real and complex parts of the CAFs $\hat{R}^{\varepsilon}_{pp,N}(l)$ are not independent. It is also plausible that a correlation between samples exists when the oversampling factor is important. So, the search for a particular periodic pattern between the different delays in CAF was considered. Fig.5.6 highlights this work. Considering the noise only, the CAF autocorrelation tends to be a dirac, which is coherent due to samples perfect independence. For the two remaining curves, a similar pattern appears, which suggest a correlation between some $\hat{R}^{\varepsilon}_{pp,N}(l)$. However, for $y_1(t)$ only (linear model) we obtained the same kind of CAF correlation than when $p(t)$ is the input signal (nonlinear signals model).

The only explanation is that the loss of freedom degrees is due to the nonlinear model. For now, this problem is still open: a link has to be found between the nonlinear model and the loss of degrees of freedom. So in the following study, we assume that for $\mathcal{H}_j|H_0, j \in \{1, 2, 3\}$ the criterion distribution could be approximated by a $F_{\lfloor L/2 \rfloor+1, \lfloor L/2 \rfloor+1}$ law. But, with correct parameters the detection rate may probably be improved in a certain extent.

5.3 Main Results

In this section, we develop our simulation results, and we show that we are able to identify precisely in which scenario the RX is. We also show thanks to simulations, that the proposed detection method answers the problematics of rapidity, sensibility and reliability defined in chapter 2.

5.3.1 Experimental Conditions

To make sure that there is no cyclic frequency overlap, we set a sampling rate $f_s = 10 f_{c1}$. The shaping filter $h(t)$ is defined as a square-root raised cosine of period $T = 2.5T_1$, a roll-off at 0.8 and span at 6 symbols. As detailed in section 5.2, nonlinear model coefficients are set thanks to measurements on an experimental RX. The RX gain is fixed at $32dB$, when the input interception point of order 3 V_{IIP3} is set to 3.6 dBm. Blocker and useful signals

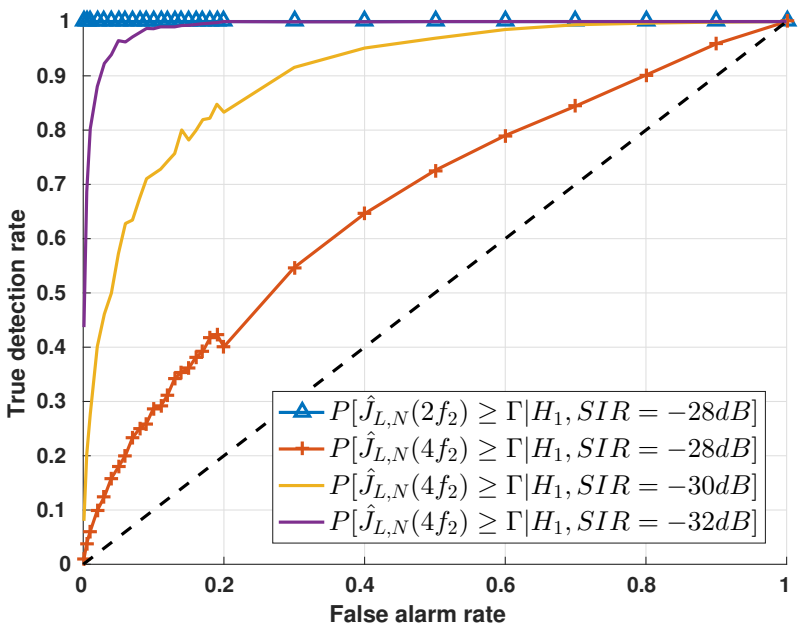

Figure 5.7: ROC curves at fixed SNR = 2 dB, SIR = −30 dB, power of test for monitored CAFs of set $\mathcal{M}$

are in adjacent channels, and the blocker carrier frequency is defined as $T_2 = T_1/2.4$. Both SOI and blocker are 4QAM symbols, independent and identically distributed. N the number of symbols is set to 32, which is small, as discussed in the previous chapter. We set L, the number of delays used in the $\hat{J}_{L,N}(\alpha)$ estimation at 25, in order to limit the calculation cost. We defined the SOI power β_1 to −106.0 dBm, and the Signal-to-Interference-Ratio (SIR) is defined as β_1/β_2. 2048 Monte Carlo runs are performed to estimate our method's performance.

5.3.2 Simulations

We begin this section with the power of the test analysis, for each element $\mathcal{M}_k$ of $\mathcal{M}$, with consideration of the corresponding test $\mathcal{H}_k, k \in \{1, 2, 3\}$. We provide results only for tests $\mathcal{H}_1$ and $\mathcal{H}_3$, since the $P[\mathcal{M}_2 \geq \Gamma|\mathcal{H}_2]$ and $P[\mathcal{M}_3 \geq \Gamma|\mathcal{H}_3]$ have same distributions. To answer the nonlinear sensibility issue, we designed a simulation that corresponds to the linearity scenario (i.e. fig.2.7c) to analyze the impact of nonlinear cyclic harmonics of different power. The Signal to Noise Ratio (SNR) is set to 2 dB and the SIR is defined as summed up in tab.5.1.

In fig.5.7, we draw the power of the test using criteria $\mathcal{M}_1$ and $\mathcal{M}_3$ (i.e. $\hat{J}_{L,N}(2f_{c2})$ and $\hat{J}_{L,N}(4f_{c2})$) for tests $\mathcal{H}_1$ and $\mathcal{H}_3$ respectively. These curves represent the receiver operating characteristic (ROC) for the two criteria. For each SIR, the criterion $\mathcal{M}_1$ allows us to reach 100% of good detection. Hence, the $P[\mathcal{M}_1 \geq \Gamma|H_1, \mathcal{H}_1]$ ROC for a SIR set to −28 dB, is the only one represented for convenience. With those simulation parameters the blocker presence could be determined with high confidence. As the RX is weakly nonlinear, the $4f_{c2}$ cyclic

SIR [dB]	Blocker Range [mV_{pp}]	$P_D(4f_{c2})$ [%]
-28	4.0	23
-30	4.5	65
-32	5.0	95

Table 5.1: SIR values and corresponding detection probability, for a $P_{fa} = 5\%$

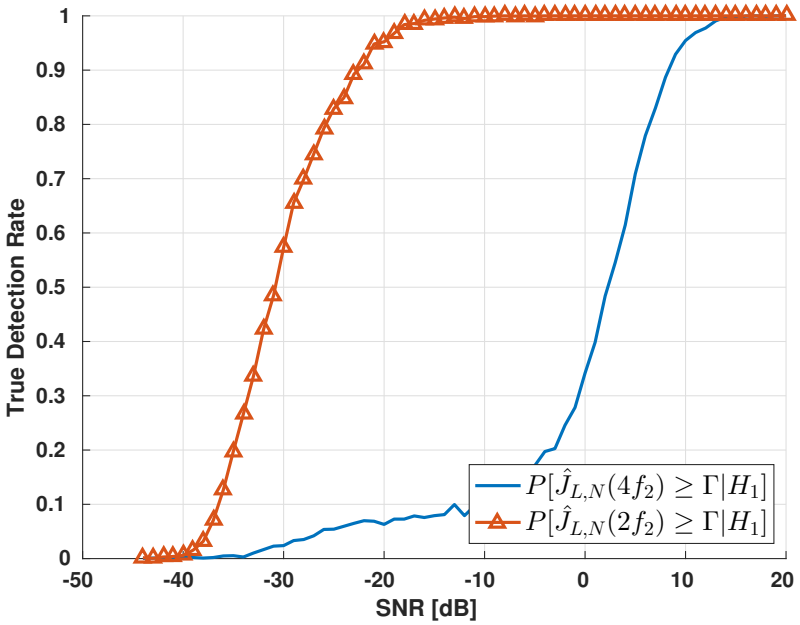

Figure 5.8: criterion probability of true detection in function of SNR level, with a fixed threshold $P_{fa} = 5\%$ and SIR $= -30\,\text{dB}$

harmonic is too small to be detected. But, we can see in fig.5.7 and in table 5.1, that a higher SIR (in absolute value) allows a better nonlinear cyclic harmonic detection.

To answer to the nonlinear cyclic harmonic detection reliability against noise, we defined the P_{fa} to 5%. The SIR is defined to $-30\,\text{dB}$, to remain slightly nonlinear. We measure the detection probability for several values of SNR, which is illustrated through fig.5.8. As we can see, the blocker detection is perfect if the SNR is greater than $-15\,\text{dB}$. Indeed, the blocker is much more powerful than the nonlinear cyclic harmonics, and so, could be detected with a higher confidence. As the RX works in a weakly nonlinear mode, the $4f_{c2}$ harmonic is small in comparison to the noise floor. Hence, if the SNR increases, the detection probability increases to reach 95% of good detection for a SNR of 10 dB.

Fig.5.9 is dedicated to illustrates the sensibility of our detector. This detection curve was obtained for a SNR of 2 dB and the $P_{fa} = 5\%$. The true detection rate grows quickly when the SIR comes lower than $-27\,\text{dB}$, which is consistent with remarks on fig.5.8. As V_{IIP3} =3.6 dBm, the corresponding compression point is V_{C1dB} =-6 dBm. A perfect detection is obtained for a SIR set at $-32\,\text{dB}$, which corresponds to an input power of $-22\,\text{dBm}$. Hence, the detection

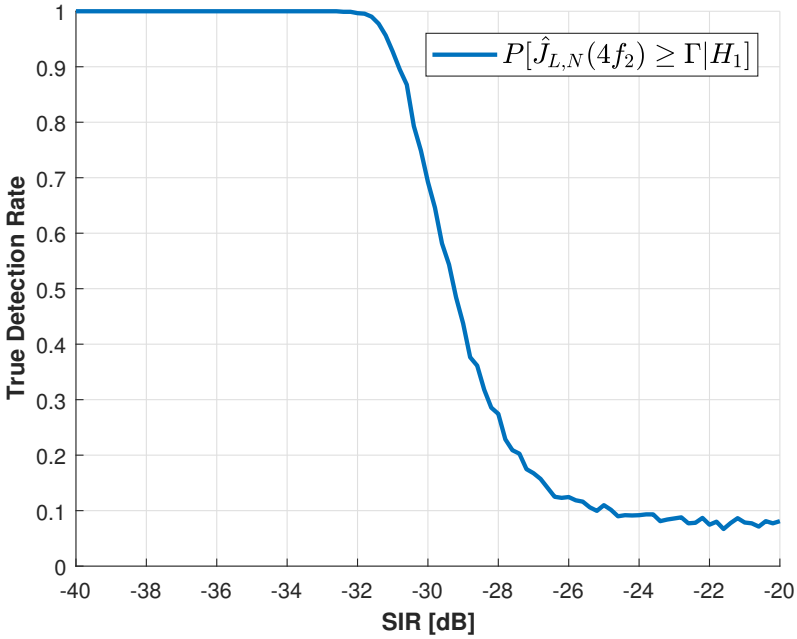

Figure 5.9: Criterion probability of true detection in function of SIR level, with a fixed threshold $P_{fa} = 5\%$ and SNR $= 2\,\text{dB}$

is performed 16 dB before the V_{C1dB}. Our detector allows a detection before the system comes in a strong nonlinear region. So, our method could be used to adjust accordingly the RX dynamic range, before the degradation of its performance. Also, we can now redefine precisely γ of eq.(5.5), with its current value of $-22\,\text{dBm}$ instead of the compression point (which value is $-6\,\text{dBm}$) as we first set it.

5.4 Conclusion & Perspectives

In this chapter, we applied our new detector defined in chapter 4, in the FITNESS context. We first recall the two scenarios (presence/absence) of interference and conditions that makes the RX works in a nonlinear regime. We go on with the nonlinear system model and the adaptation of our detection algorithm. To determine if an interferer is present and if the receiver works in a nonlinear regime we proposed three statistical tests. But, we only defined their probability density functions in the absence of signal to detect, in the nonlinear context. We point out differences between a single signal detection and a signal detection in a mixture of several signals. Finally, we showed through simulations that using our criterion, we are able to choose between the linearity or sensibility scenarios. As an additional benefit, this method is also able to determine the reason for the system to work in a harmful nonlinear regime. These two information fulfill the section 2.4 FITNESS requirements.

As main benefits, our method bypasses the nonlinear model identification. Indeed, the proposed scheme in section 5.2 is only necessary to run simulations. In practice, no prior

knowledge on model parameters is required (i.e. polynomial order, α_k coefficients). A detection could be performed without any knowledge and gives a reliable result. Also, the detection performance metrics proves the sensibility and reliability of the chosen approach. As the detection method is fast and sensitive, we consider that it could be used to implement a feedback loop. In such a scheme, the gain is the parameter to modify, with consideration of the receiver working scenario. The design and analysis of a feedback loop has to be carried out according to fig.2.8. With the scenario knowledge, the RX parameters could be adjusted, which is considered in chapter 6.

Nonetheless, the method also suffers from significant limitations. This work raised several perspectives that are developed below.

1. Our detector implementation improvement points:

   (a) To be detected blockers have to be digitized with respect of Shannon's condition. Hence, to monitor the interferer cyclic harmonics, the system sampling frequency has to be at least four times higher than interferer's carrier. Each higher cyclic harmonic will alias in the cyclic domain. It is likely that our method allows to monitor such cyclic harmonics. But, additional tests have to be conducted to confirm this assumption.

   (b) Another point that is still unclear is the probability distribution parameters if a nonlinear signal is considered. As we saw, the chosen approximate distribution does not fit perfectly the experimental probability density function. So, a significant improvement could be obtained deriving its theoretical expression.

   (c) We only considered a memoryless nonlinear model, which could be a restrictive assumption in some application (such as satellite communication). Some time could be allocated to develop the same analysis using another nonlinear model such as Saleh's model or Volterra series.

2. A global questionable point concerns the signal's model composed of a signal through a nonlinear function plus a white Gaussian noise. This is a widely accepted assumption and used amongst other in [Valkama et al., 2006, Keehr and Hajimiri, 2008, Zou et al., 2009, Rebeiz et al., 2015]. Nevertheless, in a real use case the noise may not be white, due to its transition into the nonlinear receiver. In that case, it questions all these studies and our method. Moreover, for those ones that use one or several LMS algorithms, it also implies to take the slower convergence speed into account. The speed decrease is unavoidable and is due to impulse noise and correlated samples. So, an analysis to take the correlated noise effect into account may be appropriate and valuable.

CHAPTER 6

Variable Gain Enhancement of a Nonlinear PMR Receiver

6.1 Introduction

Our main goal in this chapter is to propose a method to relax constrains that lay at ADC level. In chapter 5, we showed that we are able to detect if the receiver is working in its nonlinear region. However, we only evaluated the interference detection mechanism. It means that no feedback of this information was realized. So, we continue in this way to make our RX aware of its spectral environment (chapter 5), and able to adapt its parameters to it (chapter 6).

We recall that in the new FITNESS receiver many constraints lay at ADC level, due to the backward compliance of several PMR norms. The digital sensing mechanism is meant to decrease these constraints, while keeping constant the energy consumption. Furthermore, the additional requirement for a small size terminal implies an analog front-end size as small as possible, which limits analog options. Amongst other reasons, as our receiver is all-integrated and reconfigurable, the use of SAW filters (i.e. external devices) is not possible. Most advanced nonlinearities equalization methods rely on modeled intermodulation terms and subtraction mechanisms to overcome the issue. Besides such techniques seem powerful, as detailed in this chapter, their characteristics doesn't meet FITNESS specifications. So, we propose a proof of concept for a novel technique to limit nonlinearities harmful effects. According to the spectral enhancement method that was proposed in chapter 5, the circuit gain could be decreased if the receiver works in a nonlinear regime. In the other hand, the gain could be increased if no interferer and no saturation are detected. We propose to use a feedback loop as a gain adaptation mechanism that has to work as quick as possible. Modifying the gain also changes the circuit Input Interception Point of order 3 (IIP3) value, as described by the Friis formula nonlinear counterpart [Razavi, 2011]. The proposed mechanism was coarsely defined in chapter 2.

In section 6.2 we present several state of the art solutions, which main topics are nonlinearities cancellation. Without to much details, this part shows differences between our

concept and such methods. Besides, their cancellation results are very interesting, a fair comparison between them is difficult since each one has its own performance metric. Then, the section 6.3 is devoted to the adaptive mechanism description. Principles of the gain adaptation are described, and a formulation of an adaptive gain based on a proportional relation is proposed. We begin a discussion on this method. Finally, the method results are presented in section 6.4. Benefits in term of bit error rate are studied and we show that our method allows a significant improvement.

6.2 Nonlinearity Cancellation - State of the Art

The nonlinearity cancellation is a vast topic that is generally addressed in an analog way. This is usually a well-known designer problem. Indeed, devices such as Power Amplifier (PA) or mixers are meant to realize an analog operation (e.g. amplification or multiplication), without input signal alteration. But, due to their basics components imperfect nature, input signal gain and phase may be affected. A clever design [Cripps, 2006,Razavi, 2011,Kenington, 2000] limits such effects under specific bounds. Devices specifications could be adjusted by proper analog design to maximize one or several criteria amongst power efficiency, linearity, PAPR or adjacent channel power ratio. We propose the analysis in [Brandon et al., 2014] as an example of such techniques.

6.2.1 Analog Canceler

An extensive literature is available on the "PA linearization" topic, for which [Raab et al., 2002] is a good introduction. The linearization consists in improving the device linearity to allow more efficiency at the cost of less linear operations. Main methods are: feedback, feedforward and predistortion. The feedback method consists in forcing the output to follow the input, thanks to a fed back and subtraction of output signal, without detection or down-conversion. It can be applied directly on the RF PA output or indirectly on signal's modulation (envelope, phase, I or Q components) thanks to envelop, polar or Cartesian method. But, such techniques could be applied only with a known input to correct the PA

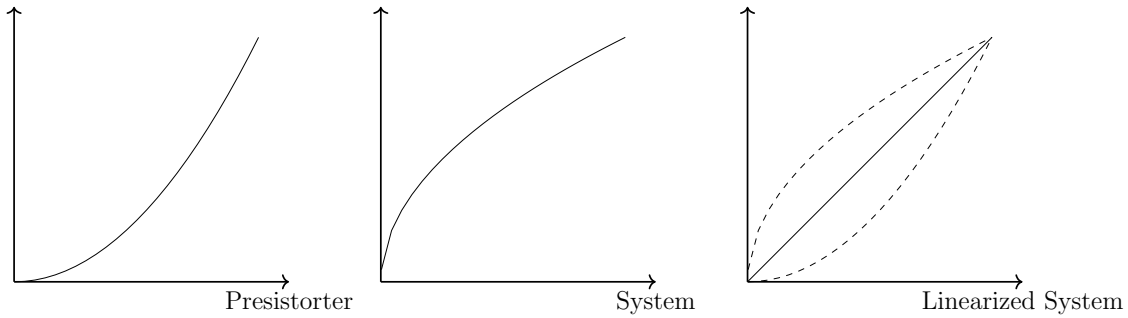

Figure 6.1: Predistortion Principles.

output. Another popular technique is the predistortion (see [Kenington, 2000]), which main idea is to compensate for nonlinearities before their occurrence so that the system becomes linear. The device is then assimilated to a mathematical model with more or less fine-tuning (phase effects, memory, etc. consideration). A nonlinear model synthesis was done in [Jung, 2013] and benefits/drawbacks for polynomial, Saleh and Volterra series are also discussed in chapter 3. The model can be realized with analog circuits or look-up tables and a DSP. A look-up table implementation requires a large chip area (DSP and memory). But, it avoids calculations needs, which leads to a larger power consumption.

The feedforward method is more interesting and may be applied at RX level. As shown in fig.6.2, its principle is to split the input signal in two different paths. A main path is sent through the nonlinear device, and the second one is left distortion free. Then, with a gain, phase and delay adjustment mechanism the secondary path is subtracted from main path to only obtain nonlinear components. With a final scaling, nonlinear harmonics are subtracted from the PA output, to obtain a linear PA output. The overall effectiveness depends on gain and phase adjustments precision.

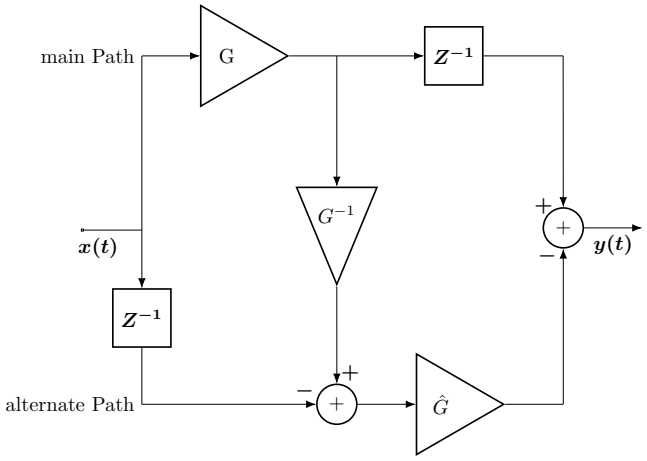

Figure 6.2: Feedforward Principles

In spite of their obvious benefits (e.g. linearity improvement, spurious suppression, etc.), these approaches are more adapted to transceivers, which input signal characteristics can be controlled. In the other hand, they are meant to be used on a single analog component, and could hardly be adapted to a complete RX front-end for energy and size consumption. So, in the following section, we develop several state of the art methods that are inspired by analog cancellation techniques. The former are applied to the whole receiver, when the latter are applied to a single analog component.

6.2.2 Digital Methods

In this section, three methods based on the feedforward approach are briefly developed. As we will see, each one has its own strategy and deserves a particular interest. Such a summary

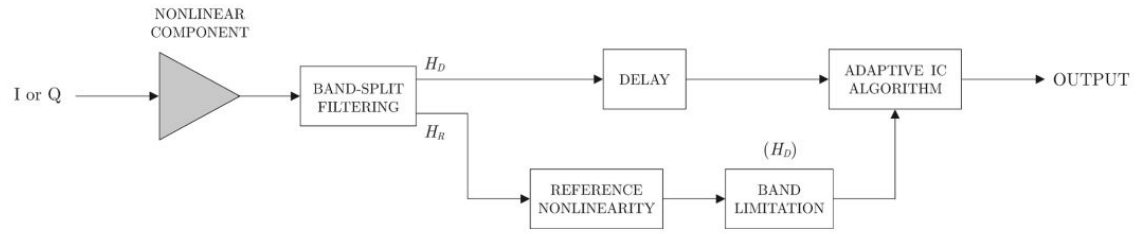

Figure 6.3: [Valkama et al., 2006] ©2006 IEEE - Post Distortion Compensation Concept

allows to check their compliance with FITNESS requirements, and to compare our method to existing ones. To our best knowledge the digital IMD3 compensation was first addressed by [Valkama et al., 2006] in the broadband signals context. In previous works [Faulkner, 2002] the compensation was limited to IMD2, but with a similar technique. As shown in fig.6.3, it consists in a post distortion compensation thanks to an advanced digital processing. This approach is applied directly after digitization, at intermediate frequency level. Thanks to a very selective band-split filtering, the whole SOI bandwidth (H_D path) is split from the remaining bandwidth (H_R path), which may contain several unwanted signals. The H_R path is fed to a nonlinear model to reproduce the component behavior and harmonics that lay into SOI bandwidth. Then, an adaptive scaling mechanism, such as a least mean square (LMS) algorithm, scales their amplitude and phase to subtract it from the main desired path (H_D).

This correction leads to a 25 dB carrier to interference ratio improvement. It also allows in-band nonlinearities compensation, that could be performed in blind mode. A H_R path power measure could be considered in our context, but does not perfectly fit our needs. Indeed, it does not allow to choose the correct scenario for the circuit to work in its nonlinear region. Nonetheless, this method also suffers from several drawbacks that must be considered. A better speed convergence could be achieved modifying the algorithm step-size, but at degraded effectiveness cost. This drawback is balanced observing that circuits nonlinear characteristic can be considered constant, which is a restrictive assumption. However, the method major drawback is the following one: ADCs sampling rate has to be high enough to respect Shannon's condition for all interfering signals. This last requirement is very stringent if we consider a large bandwidth, and also puts additional requirements on ADCs. For these reasons such a method is not adapted to FITNESS needs.

Another strategy was chosen by [Zou et al., 2009], which relaxes the [Valkama et al., 2006] constant nonlinear characteristic assumption. Moreover, another strong aspect is a SAW filter absence, which makes the whole system on-chip integrable and reconfigurable. Hence, that makes it close to FITNESS requirements. The concept is shown in fig.6.4. One path is used to acquire the signal in the desired band and a second one to acquire a blocker signal. A noticeable difference with the previous method is that both SOI and blocker are down-converted to baseband before processing. These two signals are then fed to the baseband post-processing block, which works in two steps. The first step is very innovative: it exploits the pilot sequence in the desired signal, which is present at the beginning of each packet,

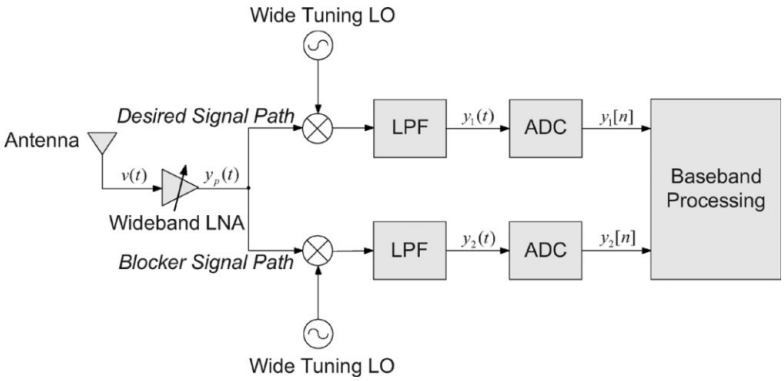

Figure 6.4: [Zou et al., 2009] ©2009 IEEE - Software Define Radio Processing Block Diagram

to jointly estimates the channel response and nonlinear model parameters. With this known sequence, channel and nonlinear parameters estimation are reduced to a least-square problem formulated in eq.(6.1).

$$\min_{\mathbf{h}} ||\mathbf{y} - \mathbf{AXh}||^2 \tag{6.1}$$

Here, $\mathbf{y}$ is the discrete-time baseband SOI column vector, $\mathbf{h}$ is the discrete-time channel impulse response column vector, $\mathbf{X}$ is the nonlinear parameters diagonal matrix and $\mathbf{A}$ is the pilots observation matrix. Starting from eq.(6.1), a one dimensional search has to be conducted to find the optimal nonlinear parameter matrix, which is then used to determine the optimal $\mathbf{h}$. This is all the more interesting after few iterations, when the RX has information on channel response statistics. In that case, [Zou et al., 2009] shows that eq.(6.1) could be solved using in a Minimum-Mean-Square-Error (MMSE) approach. A comparison with the theoretical Cramer-Rao bound shows that even with powerful blockers, the compensation works well for high SNR. However, the method is less interesting for low SNR (i.e. smaller than 5 dB in this application), since simulations show very few differences between the corrected and uncorrected signals. Furthermore, the method is based on a baseband processing that we try to avoid in FITNESS. The data flow interpretation to use this training approach may also be not affordable in a real-time application.

As a final digital method, the recent work of [Rebeiz et al., 2015] is quite different and opens new possibilities from the two previous methods. The principle is to estimate the IMD3 terms that lay into the SOI bandwidth thanks to a cyclostationary sensing mechanism. Blocker's power is then estimated and fed to the model, which allows the detection. As in previous methods, the next step is to split the received signal in several parts to obtain blockers complex baseband and then subtracts it from SOI samples thanks to an adaptive algorithm. But, here IMD3 terms are obtained from a measure and no longer thanks to a model as in other approaches. Theoretical IMD probability distributions are also developed, which is another strong aspect of this work. Nevertheless, the method requires two successive adaptive minimization to obtain: 1) blockers power; 2) a nonlinearities compensation. Another assumption limits greatly the method's impact: the order three nonlinear parameter (α_3 in

eq.(2.1)) is assumed to be known. It's hard to believe that in a industrial context, every single device could be subjected to a two-tone test to determine its nonlinear parameters. This issue could be solved thanks to an alternative approach using SOI training sequences to estimate it. But, it requires an access to network level, which is time consuming. The proposed analysis on this topic is not enough to allow a use of such a method in the FITNESS context.

As a brief sum-up, these methods allow to deal with reconfigurable circuits while almost suppressing unwanted harmonics in the SOI band. On the other hand, each one require a complex digital processing and often an access to particular data that are unknown in our application.

6.2.3 Mixed Analog & Digital Solution

In [Keehr and Hajimiri, 2008], the chosen strategy uses a joint analog and digital linearization method. The main principle is close to the feedforward mechanism presented in subsection 6.2.1. Its graphical description is provided in fig.6.5. Every operation before low-pass filter blocs (included) are realized in the analog domain. A down conversion to a low frequency is done before the digitization. In the parallel alternate path, after a SOI heavy attenuation, unwanted signals are fed to an analog cubic generator to create same IMD3 harmonics that occur in the main path. The digital equalization is then realized thanks to an adaptive filter, which minimizes the subtraction of main and alternate paths. This method achieves a sensitivity increase around 25 dB, compared with the blocking situation.

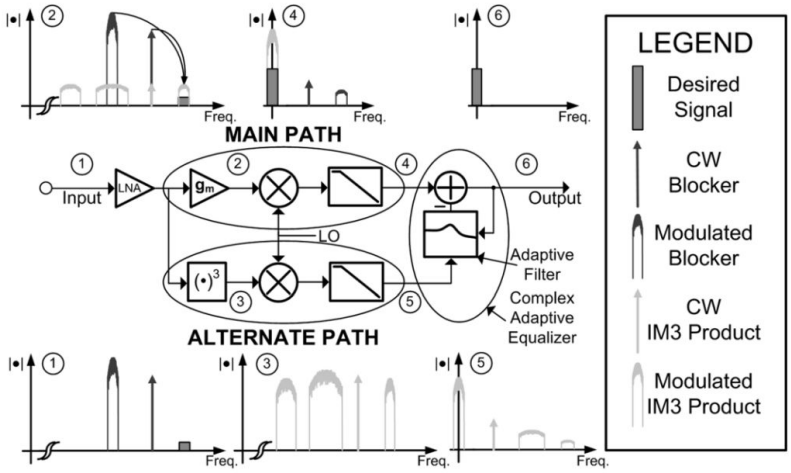

Figure 6.5: [Keehr and Hajimiri, 2008] ©2008 IEEE - Adaptive Feedforward error cancellation concept applied to RF receiver IMD3

This clever electronic circuit solves the problem of high ADCs sampling rate to respect Nyquist condition for blocking signals, which is a major issue in [Valkama et al., 2006]. Indeed, there is no more need to digitize the full bandwidth to have access to original jammers. As this technique is realized for an integrated receiver, there is no external SAW filters, which is very interesting in our context. One could say that such a method is more power expensive

due to additional circuitry. But, a total IMD3 power measure on the alternate path allows to turn it off when the energy comes under a threshold, to decrease the power consumption. However, as the RX was frozen by FITNESS preliminary work, our analog RX architecture can't be modified in proportions required in [Keehr and Hajimiri, 2008]. This solution also requires additional analog components and thus probably consumes more size and power than a simpler architecture, even when the alternate path is turned off. Furthermore, the main path processing is similar to a classic receiver, so ADCs constraints are unchanged.

So, this architecture is not able to tackle the problem of circuit saturation due to a powerful SOI. Finally, on the contrary to our detection method, this mixed analog/digital strategy gives no knowledge for the reasons why the RX works in its nonlinear region.

6.2.4 Discussion on Prior Art Limits

All papers summarized in section 6.2 show that it is possible to almost completely remove IMD3 terms at the cost of complex operations in analog and/or digital domain. But, none of them allow to relax significantly ADCs requirements compared to a classic RX architecture. Another point identified in each study is that IMD3 terms complete suppression is not possible due to nonlinear parameters estimation error. Finally, the more restrictive assumption is often a nonlinear model with constant parameters, which is not the case in the FITNESS receiver. We believe that with the proposed following method, these issues could be overcome. So, we based our analysis on a simple assessment: each of these studies left aside the fact that powerful IMD3 harmonics are created when interferers power are stronger than SOI's power and/or close to the RX maximum dynamic. It is important to understand that a classic receiver works usually in its nonlinear mode for a small fraction of time. However, with the considered RX, such an assumption may not be true in a general scenario due to multiple unattenuated blockers presence in adjacent channels. The usual solution consists to set a large PAPR margin and limits the RX gain. But, it is done at the cost of a great decrease of the available dynamic range.

That is why, our goal is now to propose a method to identify in which regime the RX works, and design a feedback loop to adapt its parameters. We propose to adjust the gain to change the RX regime and relax ADC margins according to the scenario (linearity or sensitivity) described in fig.2.7. This method should not be considered as a new linearization method, since it is not a compensation of unwanted harmonics. Moreover, on the contrary of Automatic Gain Control (AGC) devices, the proposed feedback loop will not maintain constant the output level. In addition, we made several assumptions that fit FITNESS needs, and that can eventually be released in future works. We assume a perfect synchronization between emitter and receiver in phase and frequency. We also consider the case of a nonlinear RX front-end able to deal with narrowband PMR signals. We consider a model of third order with no even coefficient, since even-order harmonics lay far from SOI carrier frequency and thus can be discarded by a filtering operation and a differential architecture. This simplification holds as higher odd-order harmonics are far less powerful than third-order harmonics. The SOI selection and amplification are performed before digitization, as shown in fig.2.8.

6.3 Proposed Concept

For now on, let develop the idea that makes a feedback loop possible. The feedback loop design is tackled in a second time. The method we propose in following sections is completely new and relies on a feedback loop concept. To our best knowledge, this idea has not been explored yet. This work will lead to several scientific publications.

6.3.1 PMR Receiver Enhancement

Overall Principles

We rely on the work realized in chapter 5 to detect when the RX works in a nonlinear regime, which allows us to decide if the gain has to be adapted. From chapter 5, we recall that the whole receiver is modeled as a polynomial expressed as:

$$p(t) = \alpha_1 x(t) + \alpha_2 x(t)^2 + \alpha_3 x(t)^3 + w(t) \tag{6.2}$$

Where $\alpha_k, k \in \{1,2,3\}$ are characteristics of the RX front-end, $x(t) = \sum_{i=1}^{2} y_i(t)$ with $y_i(t)$ on-carrier signals defined in eq.(3.1), eq.(3.3) and $w(t)$ is AWGN. Let us recall from eq.(3.2) that $y_i(t) = \Re\left[z_i(t)e^{\jmath 2\pi f_{ci}}\right]$, with f_{ci} signals carrier frequencies and $z_i(t)$ from eq.(3.1) signals baseband representations. Let define by β_1 (respectively β_2) the squared-root power of signal $z_1(t)$ (respectively $z_2(t)$). In the following chapter, α_2 is assumed zero and α_3 is obtained thanks to eq.(5.2).

The main idea that we develop in chapter 6 consists in adjusting the receiver gain automatically. Indeed, for a given input power, decreasing the gain allows the receiver to work in a more linear regime. This concept is illustrated in fig.6.6. We clearly see that, for a constant input a high gain (i.e. 32 dB in that example) saturates the output. However, when the gain is adjusted (i.e. here we proposed the value 18 dB) the system output is much more linear. On the other hand, when the input signal range is small, the gain could be increased. We want our receiver to have this behavior in an automatic way.

For several cascaded nonlinear stages, the circuit nonlinearity can be estimated thanks to a relation equivalent to the well known Friis formula. This equation analysis explains the basic concept that we propose to exploit. From [Razavi, 2011], we have:

$$\frac{1}{V_{IIP3,tot}^2} \approx \frac{1}{V_{IIP3,1}^2} + \frac{\alpha_{1,1}^2}{V_{IIP3,2}^2} + \ldots + \frac{\prod_{k=1}^{n-1}\alpha_{1,k}^2}{V_{IIP3,n}^2} \tag{6.3}$$

The eq.(6.3) is the general expression for n cascaded nonlinear stages. Let define $\alpha_{1,i}$ the linear gain of stage i and and $V_{IIP3,i}$ their corresponding Input Interception Point of order 3 (IIP3), with $i \in \{1,2,3\}$. From chapter 5, we recall that $V_{IIP3,i}$ coefficients are linked to eq.(6.2) by the nonlinear gain α_3 such as:

$$\alpha_{3,i} = -\frac{4}{3}\frac{\alpha_{1,i}}{V_{IIP3,i}^2} \tag{6.4}$$

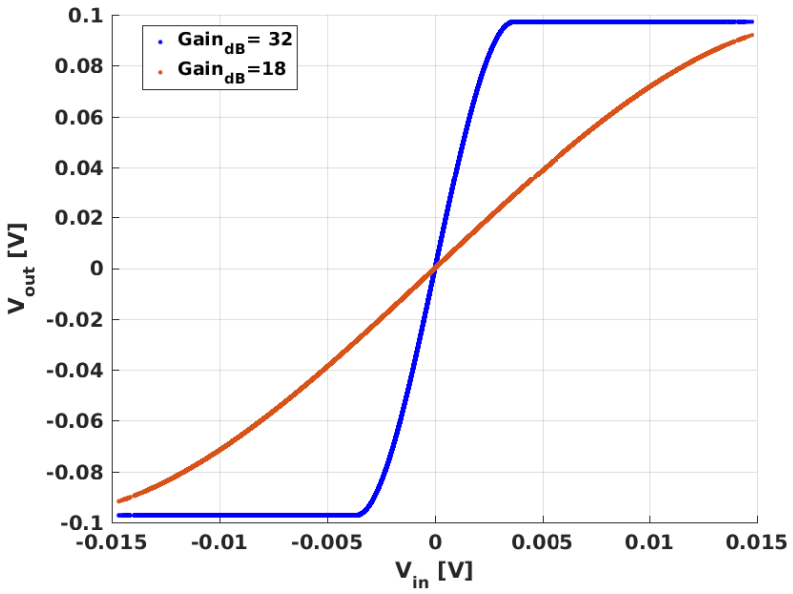

Figure 6.6: V_{in}/V_{out} representation for two nonlinear model of different α_1

Eq.(6.4) is a relation that can be applied indifferently for each stage i or for the overall cascaded stage. Hence, any modification on a particular analog component impacts the whole following RX chain.

In particular, if we consider the linearity scenario: the linear gain has to be decreased. A short analysis of eq.(6.3) shows that when coefficients $\alpha_{1,i}$ decrease, so do the quantity $1/V^2_{IIP3,tot}$. In eq.(6.4), when V_{IIP3_i} increases the nonlinear gain $\alpha_{3,i}$ decreases. So, increasing $V_{IIP3,tot}$ makes the circuit more linear, which is the searched effect in the linearity scenario. However, the maximum gain decrease is limited by the overall noise floor than can be obtained thanks to the Friis formula in eq.(6.5). For m stages, from [Razavi, 2011] we have:

$$NF_{tot} = 1 + (NF_1 - 1) + \frac{NF_2 - 1}{\alpha_{1,1}} + \ldots + \frac{NF_m - 1}{\prod_{k=1}^{m-1} \alpha_{1,k}} \tag{6.5}$$

Hence, a gain decrease makes the noise floor increases proportionally. In practice the gain can be decreased until the noise floor comes too high.

So, by a clever RX linear gain decrease the circuit could becomes more linear. The inverse effect can be obtained increasing the linear gain, which is the sensing scenario goal. Now, our aim is clearer: the gain of one analog device (at least) has to be modified according to the corresponding scenario. Let now tackle the practical method to realize such an operation.

Actual System Operating Mode

As we saw in fig.2.4, that the CEA experimental PMR platform is composed of several nonlinear stages. It means that the number of tunable components is limited: only N-path filters parameters are adjustable. This restriction implies that the analog feedback may only be

able to combine few possibilities. So, the number of possible linear gain values is also reduced, as represented in fig.6.7. In practice, modifying one stage parameters changes automatically the nonlinear gain $\alpha_{3,tot}$. One can remark that in eq.(6.3) and eq.(6.5), a gain variation early in the RX front-end has more influence than in following analog components. For now on,

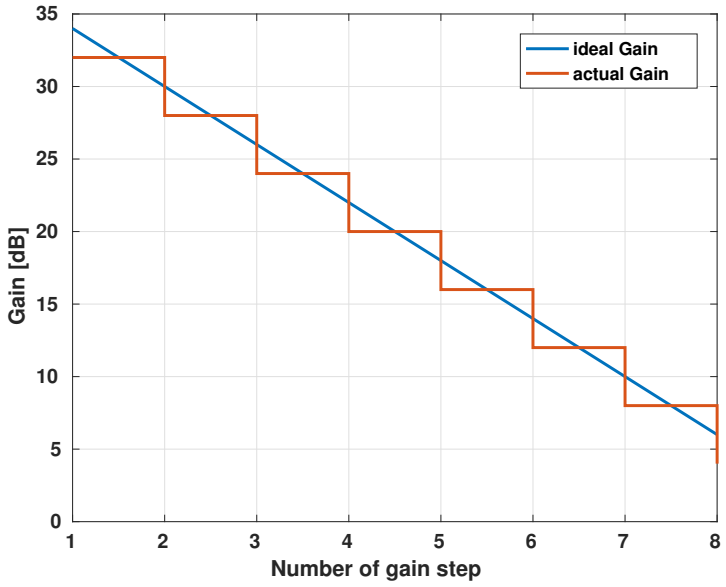

Figure 6.7: Example of a more realistic system gain against simulated gain

we consider a computer simulation to characterize our concept. Hence, we assume that $\alpha_{1,tot}$ and $\alpha_{3,tot}$ are continuous and are continuously modifiable. In a real use case, the linear gain could be approximated the closer of the theoretical function as represented in fig.6.7. As the number of values is small, the feedback may be realized with a single low-cost digital-to-analog converter with few bits (e.g. 3bits).

However, to realize computer simulations, a relation between $\alpha_{3,tot}$ and $\alpha_{1,tot}$ has to be modeled. In the aim to change the linear gain parameter, one has to change accordingly the $V_{IIP3,tot}$ value. As seen in chapter 5, one value $V_{IIP3,tot}$ can be measured for a given $\alpha_{1,tot}$. This is done thanks to a two-tone test on the CEA experimental PMR circuit. During an experiment in the CEA lab, we tested several linear gain values and performed a two-tone test for each one. That way, we obtained an experimental relation between $\alpha_{1,tot}$ and $V_{IIP3,tot}$. For this particular receiver, this relation is proposed in eq.(6.6):

$$(V_{IIP3,tot})_{|dB} = -((\alpha_{1,tot})_{|dB} + 10.7) \tag{6.6}$$

We notice the convenient linear behavior of eq.(6.6) in logarithmic scale (dB). So, when the linear gain $\alpha_{1,tot}$ decreases, so does the nonlinear gain $\alpha_{3,tot}$ as described by eq.(6.4).

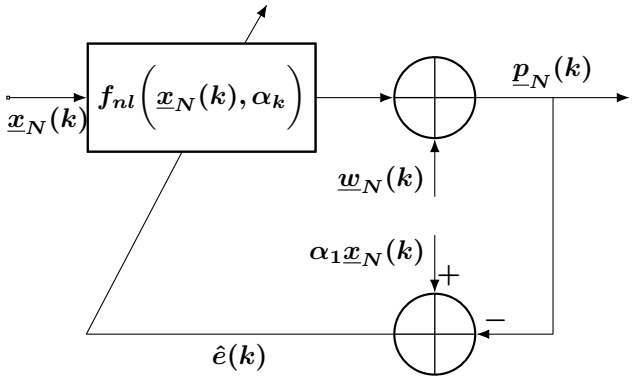

Figure 6.8: Classic Optimal Feedback Loop Scheme

6.3.2 Feedback Loop Design

To present the method, we consider that an interferer detection (of cyclic frequency $2f_{c2}$) was performed with success. So, the RX is at least weakly nonlinear, which corresponds to the linearity scenario of fig.2.7. To relax constraints, coefficients $\alpha_k, k \in \{1, 3\}$ have to be modified to overcome the blocker influence. Hence, the chapter 5 assumption of constants α_k is released. We first present the optimal gain mechanism, then we develop our solution to point out differences between the two approaches.

Wiener Optimal Approach

Our goal is to find a linear gain value such as any nonlinear cyclic harmonic can be detected. To achieve it, the classic method consist of an adaptive filter mechanism. The classic Wiener optimization method is represented in fig.6.8. Let define the input signal vector $\underline{\boldsymbol{x}}_{\boldsymbol{N}}(\boldsymbol{k})$ as a N samples vector such as $\underline{\boldsymbol{x}}_{\boldsymbol{N}}(\boldsymbol{k}) = [x(k), \ldots, x(k+N-1)]$. N is considered large enough to allow the iterative process to converge to its optimal value. Let also define $\underline{\boldsymbol{\Phi}}_{\boldsymbol{N}}(\boldsymbol{k}) = [\underline{\boldsymbol{x}}_{\boldsymbol{N}}(\boldsymbol{k}); \underline{\boldsymbol{x}}^{\boldsymbol{3}}_{\boldsymbol{N}}(\boldsymbol{k})]$ a $2 \times N$ matrix, $\boldsymbol{W} = [\alpha_1, \alpha_3]$ a vector of gain and $\underline{\boldsymbol{w}}_{\boldsymbol{N}}(\boldsymbol{k}) = [w(k), \ldots, w(k+N-1)]$ a $1 \times N$ complex AGWN samples vector such as $\underline{\boldsymbol{p}}_{\boldsymbol{N}}(\boldsymbol{k})$ is defined as in eq.(6.7).

$$\underline{\boldsymbol{p}}_{\boldsymbol{N}}(\boldsymbol{k}) = \boldsymbol{W}\underline{\boldsymbol{\Phi}}_{\boldsymbol{N}}(\boldsymbol{k}) + \underline{\boldsymbol{w}}_{\boldsymbol{N}}(\boldsymbol{k}) \tag{6.7}$$

Let $\hat{\boldsymbol{e}}(\boldsymbol{k})$ be the error vector such as:

$$\hat{\boldsymbol{e}}(\boldsymbol{k}) = \boldsymbol{\alpha_1}\underline{\boldsymbol{x}}_{\boldsymbol{N}}(\boldsymbol{k}) - \underline{\boldsymbol{p}}_{\boldsymbol{N}}(\boldsymbol{k}) \tag{6.8}$$

where $\boldsymbol{\alpha_1}\underline{\boldsymbol{x}}_{\boldsymbol{N}}(\boldsymbol{k})$ is the ideally amplified output vector. Following S. Haykin method in [Haykin, 1996b], knowing $\underline{\boldsymbol{x}}_{\boldsymbol{N}}(\boldsymbol{k})$ theoretical expression is essential. The idea is to obtain the gradient of $\hat{\boldsymbol{e}}(\boldsymbol{k})^{\boldsymbol{2}}$ with respect to polynomial coefficients α_1 and α_3. This is the Minimum Mean Square Error (MMSE) method, that allows to tend to an optimal solution to modify the gain weights vector $\boldsymbol{W}$. Nonetheless, we can't use this method because in our receiver, since we have no access to $\underline{\boldsymbol{x}}_{\boldsymbol{N}}(\boldsymbol{k})$ without important architecture modification.

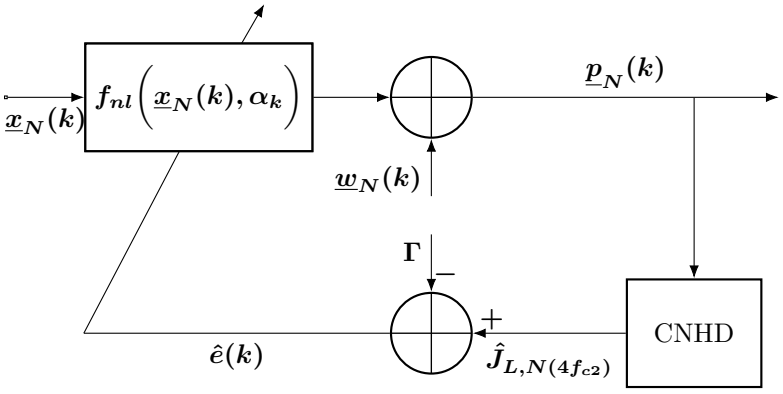

Figure 6.9: Adaptive Feedback Loop with a Cyclostationary Nonlinear Harmonics Detector (CNHD)

Experimental Approach

So, we propose a different scheme to take advantage of the nonlinear cyclic harmonic detection that we performed earlier. Let now develop our feedback loop concept, that is represented in fig.6.9. In this figure, the bloc CNHD stands for Cyclostationary Nonlinear Harmonics Detector, which is the method developed and adapted in chapter 4 and chapter 5. Following definitions are different from the Wiener method. Here, we process blocks instead of samples. Let us define the input signal vector $\underline{\boldsymbol{x}}_{\boldsymbol{N}}(\boldsymbol{k})$ as the k-th block of N samples such as $\underline{\boldsymbol{x}}_{\boldsymbol{N}}(\boldsymbol{k}) = [x(kN), \ldots, x(kN+N-1)]$. N is considered large enough to perform the detection with confidence (i.e. higher than 8 symbols). Let also define $\underline{\boldsymbol{\Phi}}_{\boldsymbol{N}}(\boldsymbol{k}) = [\underline{\boldsymbol{x}}_{\boldsymbol{N}}(\boldsymbol{k}); \underline{\boldsymbol{x}}^{\boldsymbol{3}}_{\boldsymbol{N}}(\boldsymbol{k})]$ a $2 \times N$ matrix, $\boldsymbol{W} = [\alpha_1, \alpha_3]$ a vector of gain and $\underline{\boldsymbol{w}}_{\boldsymbol{N}}(\boldsymbol{k}) = [w(kN), \ldots, w(kN+N-1)]$ a $1 \times N$ complex AGWN samples vector such as $\underline{\boldsymbol{p}}_{\boldsymbol{N}}(\boldsymbol{k})$ is defined as in eq.(6.7).

For each input vector of N samples the CNHD block estimates $\hat{J}_{N,L}(4f_{c2})$ the criterion output value. If $\hat{J}_{N,L}(4f_{c2})$ is greater than Γ (the detection threshold), then we decide the presence of unwanted harmonics. So, the distance of $\hat{J}_{N,L}(4f_{c2})$ to the threshold gives us an indication on the power of this unwanted harmonic. We want to keep it as close as possible to the detection limit Γ. Let define the estimated error $\hat{e}(k)$ for the block k in eq.(6.9).

$$\hat{e}(k) = \hat{J}_{N,L}(4f_{c2}) - \Gamma \tag{6.9}$$

This formulation is equivalent to maintaining the RX at the limit of detectable harmful harmonics. It allows to take advantage of the largest affordable gain while decreasing the power of unwanted components. However, one can notice that contrary to the Wiener formulation, eq.(6.9) is not a function of the polynomial coefficients. So, it provides no information on the optimal gain value.

The best way to adjust the gain value is to realize a gradient descent minimizing the quadratic error $\hat{e}(k)^2$. It requires to assume that $\hat{e}(k)^2$ is convex, which implies that $\hat{J}_{N,L}(4f_{c2})$

depends on α_1 and is monotone. The ideal gradient descent updating relation is:

$$\hat{\alpha}_1(k+1)_{|dB} = \hat{\alpha}_1(k)_{|dB} - \mu \frac{\partial \hat{e}(k)^2}{\partial \alpha_1} \tag{6.10}$$

Here μ is a step size chosen in function of the algorithm complexity. Indeed, it can be constant, function of k or optimal depending on the needs. Nonetheless, eq.(6.10) implies mandatory the $\hat{J}_{N,L}(4f_{c2})$ theoretical expression, in function of $\alpha_{1,tot}$. For now, we don't have such an expression that have to be obtain for future developments.

Hence, we chose to focus on a method able to decrease or cancel unwanted harmonics of order 3. This topic has been tackled in details in chapter 5. As noticed, a cyclostationary analysis at the order two shows that the $4f_{c2}$ cyclic harmonic exists. So, using our detector $\hat{J}_{N,L}(4f_{c2})$ is not mandatory to realize the feedback. It could also be easier to replace $\hat{J}_{N,L}(4f_{c2})$ by the estimated CAF energy $\sum_{l=0}^{L} |\hat{R}_{pp}^{4f_{c2}}(l)|^2$. Such an operation could simplify the eq.(6.9) expression.

As the FITNESS project is close to its end, we propose an experimental solution. We propose to use eq.(6.9), as it represents the distance to the ideal gain value, to adjust the amplification of the whole circuit. This approach is valid since the value of $\hat{J}_{N,L}(4f_{c2})$ is linked to the gain thanks to eq.(6.4). So, we propose an approximated solution that takes into account the value of $\hat{e}(k)$ in eq.(6.11).

$$\hat{\alpha}_1(k+1)_{|dB} = \hat{\alpha}_1(k)_{|dB} - \mu(k) sgn(\hat{e}(k)) \log_{10}\Big(sgn(\hat{e}(k))\hat{e}(k) + 1\Big) \tag{6.11}$$

Here, $sgn(.)$ stands for the sign function and $\mu(k) = 10/k$ is a variable step size that allows a convergence to a fixed value. In eq.(6.12), the V_{IIP3} value is also updated with the new linear gain value $\hat{\alpha}_1(k+1)_{|dB}$ following the relation eq.(6.6).

$$\hat{V}_{IIP3}(k+1)_{|dB} = -(\hat{\alpha}_1(k+1)_{|dB} + 10.7) \tag{6.12}$$

In the following sections, we develop an analysis of this function speed convergence. Nonetheless, the obtained values of $\hat{\alpha}_1(k+1)_{|dB}$ and $\hat{V}_{IIP3}(k+1)_{|dB}$ can't be called "optimal". There is no guaranty that final values of our algorithm minimize the MMSE problem in eq.(6.8). So, an objective optimality criterion is required to make sure that for a k large enough, $\hat{\alpha}_1(k+1)_{|dB}$ is an acceptable solution. After an analysis of the algorithm convergence, we propose a metric that answers this issue. Indeed, the choice of this updating function is empirical, but the function converges through gain values that minimize the BER. Obtained values are in coherence with a theoretical analysis of a new metric that is developed below. Hence, the updating relation were chosen accordingly to simulations and a theoretical analysis.

Finally, this approach was developed in the linearity scenario in line of sight, but the same method can be used in the sensing scenario. In the two cases, the gain is only limited by the range of its possible values. The minimum affordable gain is the one that makes the noise floor too important, and the maximum amplification makes the circuit too nonlinear.

6.4 Simulations

In this part, we first evaluate updating relations eq.(6.11) and eq.(6.12). The convergence speed and the solution stability are studied for the gain, but are also valid for V_{IIP3}. Then, we go on with a presentation of the feedback loop benefits in terms of Bit Error Rate (BER). It allows us, to address the algorithm tuning.

6.4.1 Experimental Conditions

To respect the Shannon's condition for the interferer signal, we set a sampling rate $f_s = 10f_{c1}$. The shaping filter $h(t)$ is defined as a square-root raised cosine of period $T = 2.5T_1$, a roll-off at 0.8 and span at 6 symbols. Blocker and useful signal are in adjacent channels, and the blocker carrier frequency is defined as $T_2 = T_1/2.4$. Both SOI and blocker are 4QAM symbols, independent and identically distributed. As discussed in chapter 4, we assume that 8 symbols are enough to perform a detection of such signals, with the CNHD method. We set L, the number of delays used in the $\hat{J}_{L,N}(\alpha)$ estimation at 25, in order to limit the calculation cost. We defined the SOI power β_1 to $-106.0\,\text{dBm}$, and the Signal to Interference Ratio (SIR) is defined as the ratio β_1/β_2 (SOI power over interferer power). The RX gain is initialized at $\alpha_1(1) = 32dB$, when the corresponding $V_{IIP3}(1) = -42.7dB$. Nonlinear model coefficients are then adapted thanks to relations eq.(6.11) and eq.(6.12).

6.4.2 Results

First results concern the gain evolution over the time. This study is realized in noiseless conditions with a the SIR set to $-30\,\text{dB}$. In our gain estimation algorithm, the parameter that has the most influence is the detection threshold Γ, that depends on the chosen false alarm probability. So, we represent several evolutions of $\hat{\alpha}_1(k+1)_{|dB}$, changing the P_{fa} of each curve in fig.6.10. As we can see, for each curve there is a first transition phase that last about 20 blocs to be processed. Then, there is a stabilized part. We notice that the lowest P_{fa} (i.e. 0.1%) gives the highest gain. Indeed, a low false alarm probability implies that the detection threshold Γ is high. When the gain is low enough, the probability mass functions of $\hat{J}_{L,N}(4f_{c2})$ under H_0 and H_1 are almost superimposed. In such a case, a high Γ implies that even under H_1 a detection is less likely than in a small Γ case (the mean value of $P\left[\hat{J}_{L,N}(4f_{c2})|H_1\right]$ has to be higher than Γ). On the contrary, a high P_{fa} implies a low Γ. Hence, even in the absence of the $4f_{c2}$ cyclic harmonic a signal is more likely to be detected and the estimated gain is decreased more often. Another interesting result is the fast algorithm convergence: around 20 (i.e. 160 symbol period) are needed to obtain a final stable value. This solution allows a quick adjustment of the nonlinear model parameters.

However, we saw in chapter 4 that our method detection rate depends on SNR level. So, we realized the same study with the same SIR value, but with several noise powers. The convergence behavior is similar to the fig.6.10 case. In tab.6.1 we sum up the gain values after 40 blocs processing. For a given P_{fa}, we clearly see that when the noise level increases

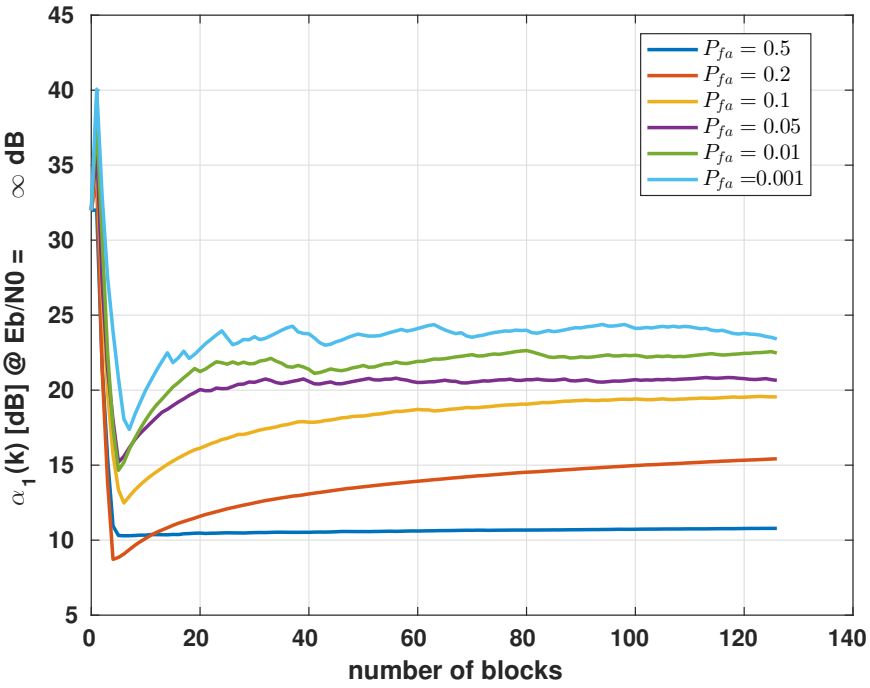

Figure 6.10: Gain convergence representation for several P_{fa} values, for $E_b/N_0 = \infty$ and SIR $= -30\,\text{dB}$

the final gain value is much higher than in the noiseless case. Indeed, due to the noise level our detection algorithm detection rates are lower (see subsection 4.4.3). It implies that the estimated gain is decreased less often. This behavior might be a problem. In noisy conditions the gain value could be far from its value in noiseless condition. For all P_{fa} values, the gain increases in a range of 6.5 dB to 7.5 dB between the case E_b/N_0 equals 20 dB and E_b/N_0 equals 0 dB. So, in noisy conditions, the estimated gain would be misfitted.

$\boldsymbol{\alpha_1(\infty)}$ [dB]		$\boldsymbol{P_{fa}}$ [%]					
		50	**20**	**10**	**5**	**1**	**0.1**
$\boldsymbol{E_b/N_0}$ [dB]	**0**	18.1	24.7	26.1	27.0	28.9	30.2
	5	16.2	21.3	22.8	24.6	26.7	27.9
	10	12.3	16.9	21.7	22.9	24.4	26.5
	20	11.0	17.3	19.4	20.8	22.5	23.7
	∞	12.6	17.2	20.0	21.0	22.2	23.9

Table 6.1: Summary of Gain values after algorithm convergence for several E_b/N_0 and false alarm probability for a SIR $= -30\,\text{dB}$

Before studying the effect of a too large gain value, let analyze the SIR influence on the final gain value. Indeed, as we can see in fig.6.11, the gain value depends on the SIR level. In this figure, the gain mean value is represented and that was obtained over 100 realizations

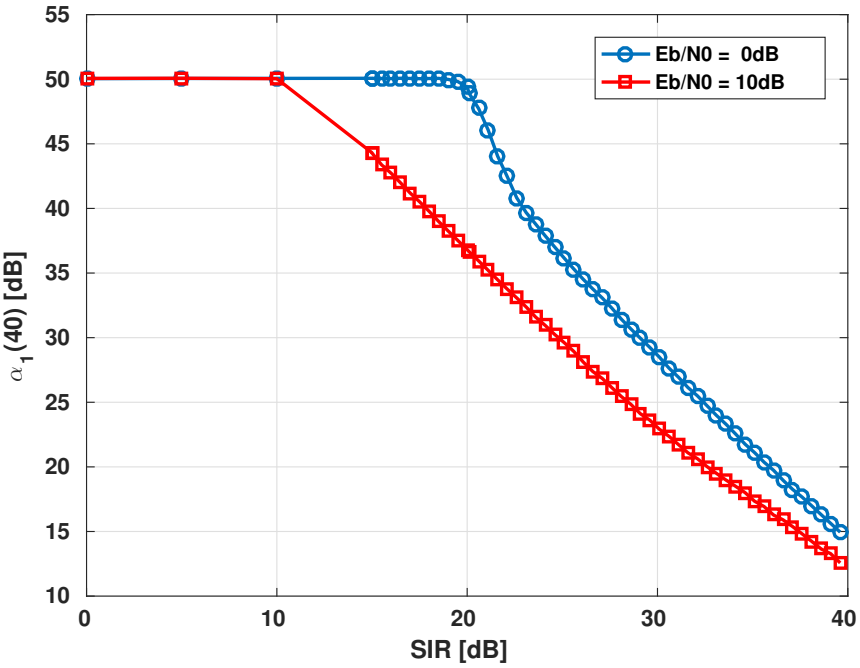

Figure 6.11: Gain evolution in function of interferer's power, for $E_b/N_0 = 0\,\text{dB}$ and $10\,\text{dB}$ at fixed $P_{fa} = 0.01$, averaged over 100 realizations

for each SIR level. We defined the noise power such as E_b/N_0 equals 0 dB, the maximum gain at 50 dB and the $P_{fa} = 0.01$. It is clear that when the SIR comes too high, the circuit linear gain decreases. This is the behavior we seek. When no nonlinear harmonic is detected, the gain is increased (i.e. sensitivity scenario). In this example, there was no mechanism to monitor nonlinear harmonics due to the SOI. So, the gain reached its maximum value defined for the simulation. We notice that close to SIR equals $-20\,\text{dB}$ a detection occurs and the gain is decreased, which is coherent with the linearity scenario. Indeed, in this case the nonlinear harmonic detection is easier. After a short quick decrease (3 dB), the curve evolution shows a smaller leading coefficient. We remark that at SIR equals $-30\,\text{dB}$, the gain equals 28.5 dB, which is the final value in tab.6.1 for a P_{fa} equals 1%. This value is also in coherence with tab.5.1. One can notice that for a higher E_b/N_0, the gain has an equivalent behavior but is adapted for a lower SIR.

Let now determine if the obtained gain value is adapted and allows better system performance in terms of BER. To realize this study, we propose to link the system performance with the power of the nonlinear terms that lays in the SOI bandwidth. We saw in eq.(5.3) that the theoretical expression of this unwanted harmonic, denoted as $s(t)$, is: $s(t) = 3\alpha_3 z_1(t)|z_2(t)|^2$. From this relation, $s(t)$ theoretical power is developed in eq.(6.13).

$$P_s = E\left[|s(t)|^2\right] = \left(3\alpha_3\beta_1\beta_2^2\right)^2 \tag{6.13}$$

Let also introduce a new comparison metric between the power of $s(t)$ and the power of

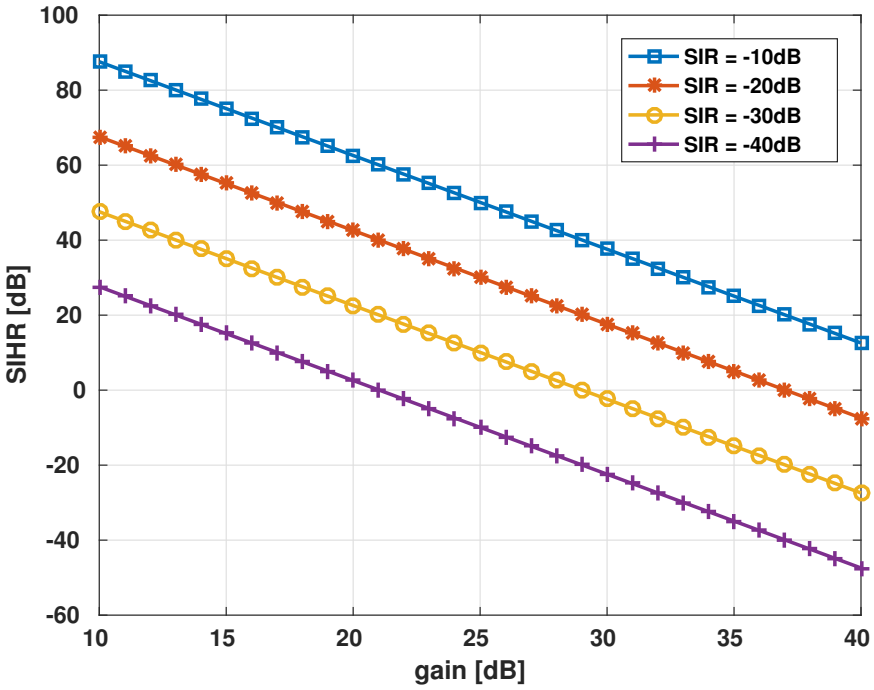

Figure 6.12: Comparison of theoretical power of in-band components for several SIR values in function of the RX gain

$\alpha_1 y_1(t)$ (the ideally amplified SOI): the Signal to In-band Harmonic Ratio (SIHR).

$$SIHR = \frac{P_{\alpha_1 y_1}}{P_s} \tag{6.14}$$

This relation is represented graphically in fig.6.12, in function of the gain for several SIR values. The first noticeable point is the linear relation between the SIHR and the gain value in logarithmic scale. Let study the $-30\,\text{dB}$ SIR curve as an example. For the initial $32\,\text{dB}$ gain value, the SIHR is $-11.4\,\text{dB}$. It means that the in-band harmonic power is much higher than the SOI power. Hence, a gain decrease is necessary. Let now see if we can answer how much the value has to be decreased. To make sure that P_s is smaller than SOI's power, we provide the fig.6.13. For several noise level, we measured the influence of the SIHR value. We see that for each E_b/N_0 level, a low SIHR implies a higher BER, as expected. When the SIHR increases, the BER value decreases to get closer of its theoretical value. One can see that the BER decreases quickly to a stable value when the SIHR increases. Then, as the SIHR increases its influence on the BER is much smaller. We assume that a SIHR close to $20\,\text{dB}$ is enough to reduce the BER significantly. Hence, the SIHR is a reliable criterion to measure the unwanted harmonic power in the SOI bandwidth. In other words, it means that past this particular value, even a large gain decrease may not lead to a significant BER improvement. This behavior is verified in following simulations. So, one can use the fig.6.12 to choose the correct value of α_1 for other SIR values. That way, for a $-30\,\text{dB}$ SIR the optimal gain value is located in the range of $18\,\text{dB}$ to $21\,\text{dB}$, which is coherent with fig.6.11 analysis and tab.6.1 for

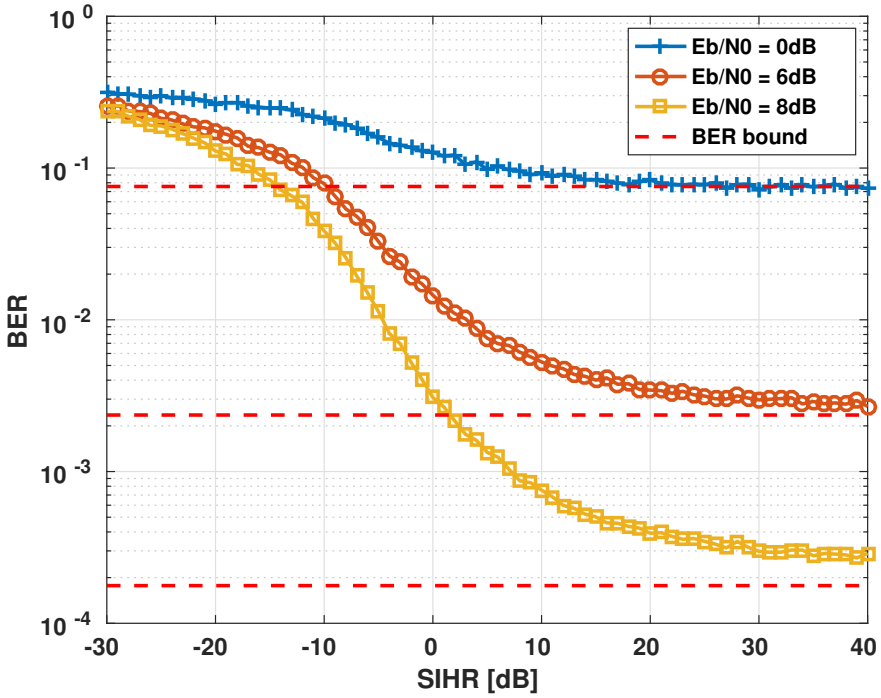

Figure 6.13: Influence of SIHR on the BER for several E_b/N_0 values at fixed SIR $= -30$ dB

the 1% and 5% P_{fa}. Knowing the nonlinear gain, signal and interferers powers, this method gives the ideal gain value without any adaptive algorithm.

Let now tackle the effect of the gain adaptation through a BER analysis. In fig.6.14, we defined a SIR such as the RX is faintly nonlinear (i.e. -30 dB). As it can be seen, the uncorrected BER is severely degraded: for a -10^3 BER value, there is a 5 dB E_b/N_0 gap when compared to BER values in absence of blocker. Nonetheless, the RX is still able to decode a part of the received signal as the curve decreases when the E_b/N_0 ratio increases. It means that the unwanted harmonic in the SOI band is powerful but not dominating. However, our gain adjustment mechanism allows a significant BER improvement. We represent several BER curves for which α_1 is different. In compliance with the SIHR analysis, the more the gain is decreased, the more the simulated BER is improved. For a BER of 10^{-4}, the improvement is close to the theoretical BER value. We analyzed previously that a 21 dB is enough to meet the best results. Indeed, such a gain still provides a BER improvement compared to a 25 dB for which the SIHR is still too high. There is also a small difference between the 21 dB and the 5 dB BER curves. Nonetheless, the BER improvement is too limited to decrease the gain below 21 dB. All the more, this difference is negligible at low E_b/N_0 but becomes more important as the E_b/N_0 increases. If we compare now the 21 dB BER curve with the theoretical limit, for a 10^{-7} BER the improvement margin is about 0.85 dB, which is small. Finally, there is still a small gap between the ideal value and algorithm output. This behavior is normal as the interferer influence may not be completely removed by the RX adapted filter.

Finally, let us assume a SIR equals -40 dB such as the RX works in a highly nonlinear

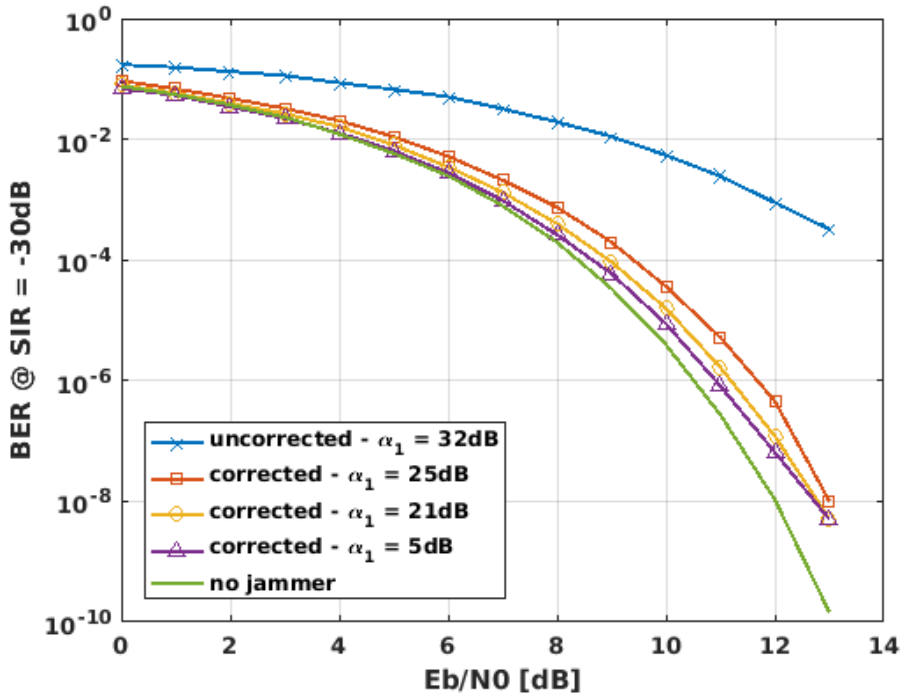

Figure 6.14: Comparison of BER curves for uncorrected and corrected RX gain, for a SIR $= -30\,\text{dB}$

regime. Such a powerful interferer makes the RX unable to decode the received signal, as shown in fig.6.15. We clearly see that without the gain adaptation mechanism, the BER is constant even when the noise power decreases. As noticed in fig.6.14, when the gain decreases the BER is significantly improved. We also see a significant improvement between cases 21 dB and 15 dB curves. The 15 dB gain value was obtained for a SIHR close to 20 dB. When compared with the 5 dB gain BER curve, the gap is very small, accordingly with fig.6.13 remarks. However, as the interferer is very powerful (even after the adapted filter), its contribution is too important to obtain a BER close to its theoretical limit. That is why a large gap exists between the corrected gain BER curve and the theoretical bound.

False Alarm Probability Discussion

Thanks to the BER analysis, let now tackle the problem of choosing the best false alarm probability. Indeed, we saw in the previous section that the P_{fa} had a large influence on the final gain value. With the SIHR, we analyzed that the correct gain value has to be in the range of 18 dB to 21 dB for a SIR equals $-30\,\text{dB}$. According to tab.6.1, in absence of noise the P_{fa} that gives the closest gain value is 5%. We saw that in noisy conditions the gain value increases, which implies that obtained gain value is not optimal. But, when the noise power is important the SIHR influence is much lower than the noise power. It can be seen in fig.6.13, considering the E_b/N_0 case. For a E_b/N_0 of 0 dB, we see that even with a SIHR of 0 dB the BER improvement is small. So, a high amplification in noisy conditions may not be

too harmful for the SOI. When the noise power is small the gain value is closer to its noiseless value. It allows the best trade off between a high gain and a high BER correction.

We realized the same analysis for a SIR equals $-40\,\text{dB}$. These results are presented in tab.6.2. Thanks to fig.6.12, we forecast that the gain value has to be in the range 12 dB to 15 dB. As the interferer is more powerful, each P_{fa} leads to a final gain value closer to the 12 dB to 15 dB (except for $P_{fa} = 0.5$, which is much lower).

$\alpha_1(\infty)$ [dB]		P_{fa} [%]					
		50	**20**	**10**	**5**	**1**	**0.1**
E_b/N_0 [dB]	**0**	5.6	11.0	12.4	13.4	14.7	15.9
	5	4.0	9.1	10.6	11.8	13.6	14.4
	10	4.9	8.3	11.0	11.4	12.4	13.8
	20	4.7	8.5	9.5	10.6	12.3	13.4
	∞	5.2	8.3	9.7	11.1	12.6	14.1

Table 6.2: Summary of Gain values after algorithm convergence for several E_b/N_0 and false alarm probability for a SIR $= -40\,\text{dB}$

Hence, we recommend to use a 5% P_{fa} as is seemed to be the value that allows to obtain the best tradeoff between decreasing the BER while and the preserving the gain as high as

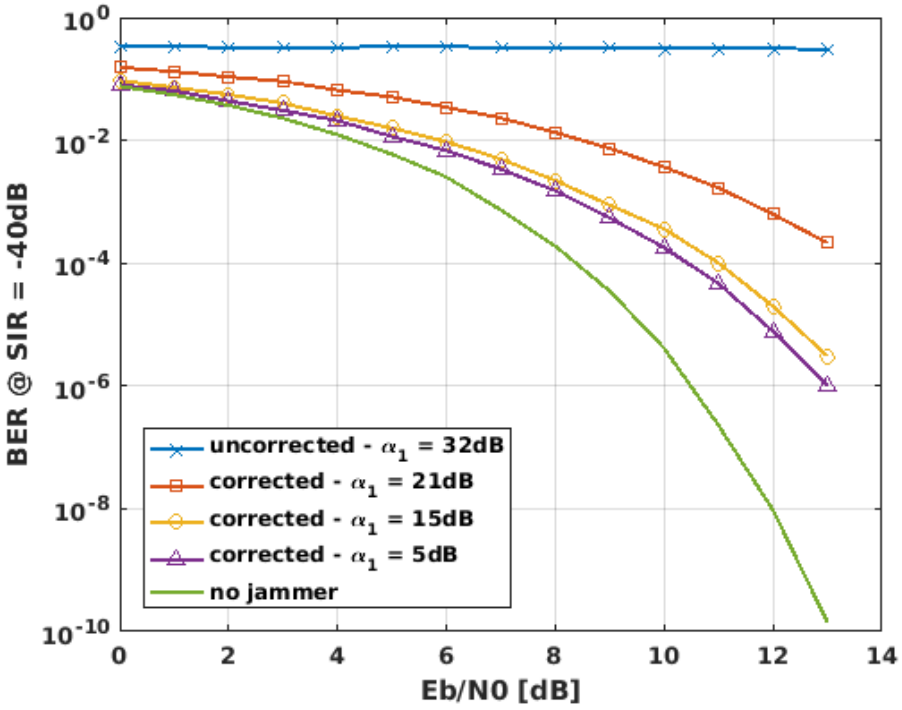

Figure 6.15: Comparison of BER curves for uncorrected and corrected RX gain, for a SIR $= -40\,\text{dB}$

possible.

6.5 Conclusion & Perspectives

In this chapter, we first point out state-of-the-art methods pros and cons. Various possibilities could be adapted to almost suppress unwanted nonlinear perturbations due to blocking signals presence. However, each one rely on the nonlinear model parameters knowledge, which turned out to be inadequate in the FITNESS context. Then, we developed a spectrally aware PMR receiver proof of concept. This mechanism is based on the feedback loop concept, which allows the receiver to adjust its gain and IP3 level to work in a more linear region. Despite the lack of a theoretical expression for our detection method, an adaptive mechanism was proposed. An analysis of our algorithm convergence was presented. We saw that after a short time, a stable gain value can be obtained. However, we cannot guarantee that the obtained value is the best one to limit the nonlinear harmonic power. Finally, a study on the impact of our proposed method on the BER was done. Our most important results are:

a) With this proof of concept, we showed that the BER could be significantly improved even when the receiver is saturated;

b) When an interferer is present, the gain adaptation mechanism improves significantly the receiver BER performance. The higher amplification limit is the ADC maximum dynamic. The lower amplification bound is the gain value that gives the maximum acceptable noise floor (as discussed in eq.(6.5));

c) We introduced the SIHR metric that represents the power of the unwanted harmonic that lays in the SOI bandwidth. We have shown that a well chosen gain value allows to increase the SIHR. The BER evolution is directly linked with the evolution of the SIR. Our gain updating relation gives a value that is close to the optimal SIHR value for a $5\%P_{fa}$;

d) To our best knowledge the gain feedback loop concept is a topic that has not been explored yet, and provide interesting results.

In the other hand, several points that were not discussed in this chapter have to be developed. As a proof of concept, the gain adaptation mechanism is realized on a simple nonlinear receiver. In other words, many parameters were neglected, as for example: quantization effects on detection rate, ADC margins adjustments, or finite number of possible gain values(every front-end analog component is not tunable). Such simplifications may conduct to a significant loss of efficiency of our method in a real receiver, especially the quantification. Nonetheless, ADC margins relaxing (that were not considered in our simulations) may lead to additional improvements that are difficult to evaluate for now. Indeed, as discussed in chapter 2, important PAPR margins are left to ensure an unsaturated digital signal. Thanks to our detection mechanism these margins could be decreased, which allows to increase the gain in a certain

extent to improve the SNR. This was a major requirement expressed in chapter 2. We noticed that, to maximize the tuning effect of our method, the best way is to adapt the gain of the receiver's first analog components as it impacts all the following chain. In our work, we assumed that several stages parameters may be adjusted to produce fine gain and IIP3 tuning, which could not be possible in a real receiver. A mechanism that adapts the RX gain in a fixed set of values could be realized instead. The ideal gain value could be approximated to select the closest gain value. Finally, this method is able to detect a interferer, to detect if the circuit works in a nonlinear regime and identify the reason. So, this method seems to be a good answer to FITNESS requirements.

This work opened several interesting points as perspectives:

1. As we saw, having a theoretical expression for our detection criterion is essential to define an optimal iterative algorithm. We forecast that benefits from this work are a quickest convergence and a gain value the closer of optimality.

2. It is also essential to use this method in a experimental device to relax assumptions we made. This work have to be done in cooperation with CEA lab that can also implement this algorithm in an experimental platform.

3. The current context is devoted to detect a narrowband signal. But working at complex baseband opens possibilities to use our method on OFDM systems. Indeed, the nonlinear receiver is also a problem in the cognitive radio that deals with broadband signals.

Part II - Conclusions

In this thesis the second part, we answered FITNESS requirements that were defined in the first part. As seen in chapter 4, several PMR modulations make difficult the unwanted signal detection to be realized in blind mode. We first studied state-of-the-art methods to perform the detection of phase modulated unwanted signals on carrier, in a general context. These methods are not adapted to FITNESS needs, so we proposed a novel algorithm based on second order cyclic moments. It turns out that our algorithm requires a small number of symbols to provide interesting detection rates. Nevertheless, some remaining work on this method has to be done. The complete mathematical description of our method is a major point that lack to this study. The work presented in chapter 4 led to the publication of a national (GRETSI 2017) and an international paper (WCNC 2018).

Then, we use this new tool in the FITNESS context. As seen in section 2.4, due to its internal devices the analog receiver could not be considered as linear function. Hence, we modeled it as a polynomial. When a unwanted signal is present close to the signal of interest carrier, additional harmonics are created due to the nonlinear behavior. As analyzed in chapter 5, a harmonic lays in the useful signal bandwidth, which degrades system performance. That is why, we used the method defined in section 4.4, to detect particular harmonics that are created only when the receiver works in a nonlinear regime. With the information of nonlinear harmonics presence, we decide if the receiver works or not in its linear region. Main principles and a theoretical analysis of obtained results were presented in chapter 5. We showed that a detection is possible well before the receiver work in a highly nonlinear regime. This analysis was published in an international conference (ICC 2018).

Finally, the method in chapter 4 and its application in chapter 5 are gathered in a final chapter. In chapter 6, we considered that the receiver is able to analyze its spectral environment. Hence, we developed a proof of concept for a mechanism that adapt automatically the receiver parameters. This algorithm is based on the idea that the interferer and/or its nonlinear harmonics detection, allows to identify two scenarios. When a powerful interferer is detected (linearity scenario), the front-end amplification could be adjusted to decrease unwanted harmonics influence. On the other hand, when there is only a useful signal of small power in the received bandwidth (sensitivity scenario), the gain could be increased. We showed through simulations that the presented method is able to adjust dynamically the receiver gain. A theoretical analysis was also performed. Our most important result is that a clever amplification mechanism allows a significant bit-error-rate improvement. As discussed

in chapter 6, several parameters influence can't be tested in a simple manner and requires the development of a receiver full chain model. This is a completely original work that has not been published yet. These results will soon be shared in several scientific communications as a proof of concept.

General conclusions and perspectives

Let take a look to the Minolta definition for cognitive radios [Mitola, 2000]:

> *Cognitive Radio: a radio or system that senses, and is aware of, its operational environment and can dynamically and autonomously adjust its radio operating parameters accordingly.*

Considering this definition, the sensing mechanism designed in this thesis allows an autonomous adjustment of receiver gain, which limits its internal interferences. In the light of the work presented in this thesis, we consider that the proposed system can be called a cognitive PMR radio.

The first part of this thesis was devoted to the PMR spectral environment analysis. We saw is chapter 2 that PMR standards specifications are tight to be addressed only by a analog design. Moreover, as the overall receiver design is already defined, it implies additional constraints on digital answers that could be proposed (e.g. blind mode, fast processing, etc.). Hence, the novelty of the project is to detect when and why the receiver works in a nonlinear regime. This algorithm have to be realized in the digital domain, and could allow to adapt the receiver analog parameters thanks to a feedback loop. The idea to measure the nonlinear harmonic power is new and deserve a deep analysis.

That is why, the chapter 3 is devoted to a state of the art of blind detection methods. Because signal and noise powers statistics are assumed unknown, the energy detector can't be used. Other efficient methods such as matched filter are also discarded due to the lack of knowledge on the signal to detect. It appears that the cyclostationary approach is the most adapted one, as it requires a few information and performs well at low SNR.

With the previous analysis, we go on with this thesis achievements. We saw in chapter 4 that the detection of phase modulated signals is not possible using a cyclic second order moments method. For detecting such signals usual methods are: higher order moments or to use a nonlinear transformation. We showed that such methods require too much symbols to provide good detection rates and a high confidence level. Hence, we proposed a new detection method based on second order statistics. The originality of our algorithm is to be able to detect the presence of a signal by monitoring a cyclic frequency where no energy is present in

theory. This algorithm proved to be able to detect a cyclic energy when the theoretical value is zero. This method can be performed in a semi-blind mode and require very few symbols to detect a signal's presence. We evaluated through simulations that this method provides good detection rates at 0 dB. Our detector is also resilient to the channel selectivity, and to a bad synchronization, as theoretically and experimentally shown.

This new tool is then applied in the FITNESS context. In chapter 5, we modeled the receiver as a polynomial due to its analog components, which have a nonlinear behavior. We saw that the presence of a PMR signal in a channel close to the signal of interest carrier frequency creates additional harmonics. The method developed in chapter 4 was applied to detect cyclic harmonics due the nonlinear regime of the receiver. A theoretical analysis of this mechanism is provided. Besides the use of our detector is not mandatory, it allows nonetheless to perform a detection with a small number of symbols, and without a noise variance estimation technique. With the information of nonlinear harmonics presence, we are able to decide if the receiver works or not in its linear region. Through simulations, we showed that a detection is possible well before a degradation of the useful signal. This study was realized in cooperation with the CEA, and led to a communication [Grollier et al., 2018].

In chapter 6, we detailed main principles of state-of-the-art method to decrease IMD3 harmonic influence. There are few state of the art solutions on this topic, that are recalled in the beginning of the chapter. Such solutions often tightens analog requirements, which is not affordable in the FITNESS context. Hence, we propose a completely new method based on the feedback loop principle. Based on our work in chapter 4 and in chapter 5, we propose a new method for the receiver to adapt its parameters in chapter 6. The adaptation concept is based on the Friis nonlinear formula. This relation implies that a gain decrease implies that the circuit becomes more linear. Then, we presented a mechanism to adapt the gain level. This method efficiency was shown through simulations, and we saw that it leads to a significant Bit-Error-Rate improvement. As this work is recent, there is still no scientific communications on this topic. However, a communication and a journal paper are planed based on obtained results.

Nonetheless, the work presented over this thesis could be continued. Several perspectives were tackled in previous chapters, so let now concentrate on main ones:

a) The first point that should be developed is the estimator $\hat{J}_{L,N}(\alpha)$ (proposed in chapter 4) theoretical description. Such an expression may allow to link the criterion value to the interferer's power.

b) This development is also a major interest for the feedback mechanism developed in chapter 6. The feedback algorithm we proposed cannot grant a convergence to the best gain value. Moreover, the convergence speed could be improved using the gradient descent method, which require the knowledge of $\hat{J}_{L,N}(4f_{c2})$.

c) It could also be interesting to implement this method on a demonstrator to show its reliability in an effective receiver.

d) In chapter 5 and chapter 6 we assumed that the received additive noise is complex AWGN.

But, as it goes through the nonlinear receiver, its statistical properties and distribution necessary changed. So, state of the art method statistical properties, and our detector statistics as well, are different. The new model should be expressed as in eq.(6.15), where $x(t) = \sum_{i=1}^{2} y_i(t) + w(t)$:

$$p(t) = \alpha_1 x(t) + \alpha_2 x(t)^2 + \alpha_3 x(t)^3 \tag{6.15}$$

Hence, the same work has to be done taking the new model eq.(6.15) into consideration.

APPENDIX A

Demonstration relative to Chapter 4

We propose here to show that considering $\delta_{t_1} = 0$ in eq.(3.2) does not lead to a loss of generality. Let us consider the general CAF definition eq.(3.28), in the case of a cycloergodic process. The received signal will be $y(t) = x(t - \Delta_{t_1})$, which CAF expression is given in eq.(A.1)

$$R^{\alpha}_{yy}(\tau) = \langle x(t - \Delta_{t_1} - \frac{\tau}{2}) x^*(t - \Delta_{t_1} \frac{\tau}{2}) e^{-j2\pi\alpha t} \rangle_t \tag{A.1}$$

A simple variable change $u = t - \Delta_{t_1}$ leads to eq.(A.2).

$$\begin{aligned} R^{\alpha}_{yy}(\tau) &= e^{j2\pi\alpha\Delta_{t_1}} \langle x(u - \frac{\tau}{2}) x^*(u + \frac{\tau}{2}) e^{-j2\pi\alpha u} \rangle_u & \text{(A.2)} \\ &\triangleq e^{j2\pi\alpha\Delta_{t_1}} R^{\alpha}_{xx}(\tau) & \text{(A.3)} \end{aligned}$$

In most methods presented in this document the CAF energy measure is realized thanks to the $|.|^2$ operation. Hence, we notice that the CAF energy of $x(t)$ and $y(t)$ are identical, which is enough to justify the model simplification.

$$|R^{\alpha}_{yy}(\tau)|^2 = |R^{\alpha}_{xx}(\tau)|^2 \tag{A.4}$$

APPENDIX B

Nonlinear Harmonics Cyclic Frequency Search

We propose to derive here the theoretical expression of a BPSK signal through a nonlinear system in order to search for its cyclic frequencies. Let first define the input signal in eq.(B.1), in agreement with the chapter 5.

$$y_1(t) = z_R(t)\cos(2\pi f_{c1} t) \tag{B.1}$$

We assumed here that $z_R(t) = \sum_{k=-\infty}^{\infty} a_k h(t - kT_1)$, where a_k are BPSK symbols, which explains the absence of imaginary part in eq.(B.1). Such an assumption allows to reduce the number of terms to develop, in order to obtain more convenient expressions. The idea is to show that a nonlinear distortion produces several terms having a cyclic frequency $4f_{c1}$. These terms belongs to the most powerful one.

The nonlinear system is the following one:

$$p(t) = \alpha_1 y_1(t) + \alpha_3 y_1^3(t) \tag{B.2}$$

As we saw in chapter 4, to realize the search for cyclic frequencies, one has to develop the expression $p(t)p(t-\tau)$. From eq.(B.2) the eq.(B.3) expression is straightforward.

$$p(t)p(t-\tau) = \alpha_1^2 y_1(t)y_1^2(t-\tau) + \alpha_3^2 y_1^3(t)y_1^3(t-\tau) + \alpha_1\alpha_3 y_1(t)y_1^2(t-\tau) + \alpha_1\alpha_3 y_1^2(t)y_1(t-\tau) \tag{B.3}$$

We prefer to develop each terms one by one replacing eq.(B.1) into eq.(B.3). It gives following expressions from eq.(B.4) to eq.(B.7), where $\omega_1 = 2\pi f_{c1}$:

$$y_1(t)y_1(t-\tau) = \frac{1}{2} z_R(t)z_R(t-\tau)\Big(\cos(\omega_1(2t-\tau) + \cos(\omega_1\tau)\Big) \tag{B.4}$$

$$\begin{aligned} y_1^3(t)y_1(t-\tau) = \frac{1}{8} z_R^3(t)z_R(t-\tau)\Big(&\cos(\omega_1(4t-\tau)) + \cos(\omega_1(2t+\tau) \\ &+ \cos(\omega_1(2t-\tau) + \cos(\omega_1\tau)\Big) \end{aligned} \tag{B.5}$$

$$y_1(t)y_1^3(t-\tau) = \frac{1}{8}z_R(t)z_R^3(t-\tau)\Big(\cos(\omega_1(4t-3\tau)) + \cos(\omega_1(2t-3\tau) + \cos(\omega_1(2t-\tau) + \cos(\omega_1\tau)\Big) \quad \text{(B.6)}$$

$$y_1^3(t)y_1^3(t-\tau) = \frac{1}{32}z_R^3(t)z_R^3(t-\tau)\Big(\cos(\omega_1(6t-3\tau)) + \cos(\omega_1(4t-3\tau) + \cos(\omega_1(4t-\tau) + \cos(\omega_1(2t-3\tau) + \cos(\omega_1(2t-\tau) + \cos(\omega_1(2t+\tau) + \cos(\omega_1\tau) + \cos(3\omega_1\tau)\Big) \quad \text{(B.7)}$$

As we see, terms in eq.(B.4) are only proportional to the linear amplification α_1^2, when others expressions depends on α_3. Let study these last three terms frequency components to determine which frequencies are due to the RX nonlinear behavior. In eq.(B.5), eq.(B.6) and eq.(B.7), harmonics at baseband and at $2\omega_1$ gets mixed up with same harmonics in eq.(B.4). So, most powerful harmonics linked to the nonlinear gain have a frequency equal $4\omega_1$. If we apply the expectancy operation in eq.(B.3), we obtain $R_{yy}^{4f_1}(\tau)$ in eq.(B.8) the CAF expression at cyclic frequency $4f_1$:

$$\begin{aligned} R_{yy}^{4f_1}(\tau) = & \frac{1}{8}\alpha_1\alpha_3 E\left[z_R^3(t)z_R(t-\tau)\cos(\omega_1(4t-\tau))e^{-\jmath 2\pi 4f_1 t}\right] \\ & + \frac{1}{8}\alpha_1\alpha_3 E\left[z_R(t)z_R^3(t-\tau)\cos(\omega_1(4t-3\tau))e^{-\jmath 2\pi 4f_1 t}\right] \\ & + \frac{1}{32}\alpha_3^2 E\left[z_R^3(t)z_R^3(t-\tau)\cos(\omega_1(4t-3\tau))e^{-\jmath 2\pi 4f_1 t}\right] \\ & + \frac{1}{32}\alpha_3^2 E\left[z_R^3(t)z_R^3(t-\tau)\cos(\omega_1(4t-\tau))e^{-\jmath 2\pi 4f_1 t}\right] \end{aligned} \quad \text{(B.8)}$$

In eq.(B.7) some harmonic at $6\omega_1$ were not considered since their power is much less than $4\omega_1$ components. So, tracking the $6\omega_1$ harmonic becomes useless as the detection rate will be lower than those obtained at $4\omega_1$. In addition, to make such a measure, the system sampling frequency as to be greater than $6\omega_1$, which is an additional constraint in comparison to the $4\omega_1$ monitoring.

The same method could be applied on a QPSK signal, but with $y_1(t)$ modeled as:

$$y_1(t) = z_R(t)\cos(2\pi f_{c1}t) - z_I(t)\sin(2\pi f_{c1}t) \quad \text{(B.9)}$$

Many additional terms would be added, but the previous analysis remain valid as created harmonics could not be different.

Bibliography

[Antoni, 2007] Antoni, J. (2007). Cyclic spectral analysis in practice. *Mechanical Systems and Signal Processing*, 21(2):597 – 630.

[Baldini et al., 2011] Baldini, G., Picchi, O., Luise, M., Sturman, T. A., Vergari, F., Moy, C., Braysy, T., and Dopico, R. (2011). The euler project: application of software defined radio in joint security operations. *IEEE Communications Magazine*, 49(10):55–62.

[Barkat, 2005] Barkat, M. (2005). *Signal Detection and Estimation*. Artech House radar library. Artech House.

[Baudoin and Venard, 2013] Baudoin, G. and Venard, O. (2013). *Radiocommunications numériques: Tome 1, Principes, modélisation et simulation*. Technique Et Ingenierie. Dunod.

[Boiteau and Martret, 1998] Boiteau, D. and Martret, C. L. (1998). A general maximum likelihood framework for modulation classification. In *Acoustics, Speech and Signal Processing, 1998. Proceedings of the 1998 IEEE International Conference on*, volume 4, pages 2165–2168 vol.4.

[Boyles and Gardner, 1983] Boyles, R. and Gardner, W. (1983). Cycloergodic properties of discrete- parameter nonstationary stochastic processes. *IEEE Transactions on Information Theory*, 29(1):105–114.

[Brandon et al., 2014] Brandon, M., Ariaudo, M., Traverso, S., Bouvier, J., Gautier, J. L., and Fijalkow, I. (2014). Joint linearity and efficiency improvement for a high power amplifier. *IEEE Microwave and Wireless Components Letters*, 24(12):884–886.

[Bräysy et al., 2010] Bräysy, T., Lehtomäki, J., Calvet, B., Delmas, S., and Moy, C. (2010). Cognitive techniques for finding spectrum for public safety services. In *Military Communications and Information Systems Conference, MCC'10*, page 9 pages, Wroclaw, Poland.

[Ciblat et al., 2000] Ciblat, P., Chevreuil, A., and Loubaton, P. (2000). alpha;-repetition/modulation and blind second-order identification. *IEEE Transactions on Signal Processing*, 48(11):3153–3161.

[Ciblat et al., 2002] Ciblat, P., Loubaton, P., Serpedin, E., and Giannakis, G. B. (2002). Asymptotic analysis of blind cyclic correlation-based symbol-rate estimators. *IEEE Transactions on Information Theory*, 48(7):1922–1934.

[Cripps, 2006] Cripps, S. (2006). *RF Power Amplifiers for Wireless Communications, Second Edition*. Artech House, 685 Canton Street Norwood, MA 02062.

[Dandawate and Giannakis, 1994a] Dandawate, A. V. and Giannakis, G. B. (1994a). Statistical tests for presence of cyclostationarity. *IEEE Transactions on Signal Processing*, 42(9):2355–2369.

[Dandawate and Giannakis, 1994b] Dandawate, A. V. and Giannakis, G. B. (1994b). Statistical tests for presence of cyclostationarity. *IEEE Transactions on Signal Processing*, 42(9):2355–2369.

[Dunlop and Smith, 1994] Dunlop, J. and Smith, D. G. (1994). *Telecommunications engineering / J. Dunlop and D.G. Smith*. Chapman & Hall London, 3rd ed. edition.

[ETSI, 2002] ETSI (2002). Terrestrial trunked radio(tetra); data(v+d); part 15: Tetra frequency bands, duplex spacing and channel numbering. ETSI TS 100 392-15 v1.2.1.

[ETSI, 2007] ETSI (2007). Electromagnetic compatibility and radio spectrum matters (erm); land mobile service; radio equipment intended for the transmission of data (and/or speech) using constant or non-constant envelope modulation and having an antenna connector; part 1: Technical characteristics and methods of measurement. ETSI TR 102.580 V1.1.1.

[ETSI, 2011] ETSI (2011). Electromagnetic compatibility and radio spectrum matters (erm); land mobile service; radio equipment intended for the transmission of data (and/or speech) using constant or non-constant envelope modulation and having an antenna connector; part 1: Technical characteristics and methods of measurement. ETSI EN 300 113-1 V1.7.1.

[ETSI, 2013] ETSI (2013). Terrestrial trunked radio(tetra); voice plus data(v+d); part 2: Air interface (ai). ETSI TS 100 392-2 V3.6.1.

[Faulkner, 2002] Faulkner, M. (2002). Dc offset and im2 removal in direct conversion receivers. *IEE Proceedings - Communications*, 149(3):179–184.

[FITNESS, 2017] FITNESS (2017). Fitness scope. http://lisite.isep.fr/minarc/minarc-projects/fitness/. Accessed: 2017-02-28.

[Gardner, 1994] Gardner, W. (1994). *Cyclostationarity in communications and signal processing*. Electrical engineering, communications and signal processing. IEEE Press.

[Gardner, 1988a] Gardner, W. A. (1988a). Signal interception: a unifying theoretical framework for feature detection. *IEEE Transactions on Communications*, 36:897–906.

[Gardner, 1988b] Gardner, W. A. (1988b). *Statistical spectral analysis, A non probabilistic theory*. Prentice-Hall, Englewood Cliffs,New Jersey.

[Gardner et al., 2006] Gardner, W. A., Napolitano, A., and Paura, L. (2006). Cyclostationarity: Half a century of research. *Signal Processing*, 86(4):639 – 697.

[Gardner and Spooner, 1992] Gardner, W. A. and Spooner, C. M. (1992). Signal interception: performance advantages of cyclic-feature detectors. *IEEE Transactions on Communications*, 40(1):149–159.

[Gardner and Spooner, 1994] Gardner, W. A. and Spooner, C. M. (1994). The cumulant theory of cyclostationary time-series. i. foundation. *IEEE Transactions on Signal Processing*, 42(12):3387–3408.

[Germain, 2014] Germain, M. (2014). Introduction ̀la pmr. Technical report, RFC Editor.

[Ghorbani and Sheikhan, 1991] Ghorbani, A. and Sheikhan, M. (1991). The effect of solid state power amplifiers (sspas) nonlinearities on mpsk and m-qam signal transmission. In *1991 Sixth International Conference on Digital Processing of Signals in Communications*, pages 193–197.

[Ghozzi, 2008] Ghozzi, M. (2008). *Cyclostationarity-based test for detection of vacant frequency bands*. Theses, Université Rennes 1.

[Gouldieff et al., 2018] Gouldieff, V., Nafkha, A., Grollier, N., Palicot, J., and Daumont, S. (2018). Cyclic autocorrelation based spectrum sensing:theoretical derivation framework. In *2018 25th International Conference on Telecommunications (ICT)*.

[Grollier and Houcke, 2017] Grollier, N. and Houcke, S. (2017). Détection de signaux qpsk sur porteuse en utilisant les statistiques cycliques d'ordre 2. In *GRETSI 2017 : 26ème colloque du Groupement de Recherche en Traitement du Signal et des Images*.

[Grollier and Houcke, 2018] Grollier, N. and Houcke, S. (2018). On carrier qpsk signal detector based on second order cyclic-moments. In *2018 IEEE Wireless Communications and Networking Conference (WCNC)*, pages 1–6.

[Grollier et al., 2018] Grollier, N., Houcke, S., and Pelissier, M. (2018). Enhanced spectrally aware rf front end receiver under non-linearity. In *2018 IEEE International Conference on Communications (ICC)*.

[Hayes, 1996] Hayes, M. (1996). *Statistical digital signal processing and modeling*. John Wiley & Sons.

[Haykin, 1996a] Haykin, S. (1996a). *Adaptive Filter Theory (3rd Ed.)*. Prentice-Hall, Inc., Upper Saddle River, NJ, USA.

[Haykin, 1996b] Haykin, S. (1996b). *Adaptive Filter Theory (3rd Ed.)*. Prentice-Hall, Inc., Upper Saddle River, NJ, USA.

[Haykin, 2005] Haykin, S. (2005). Cognitive radio: brain-empowered wireless communications. *IEEE Journal on Selected Areas in Communications*, 23(2):201–220.

[Hill and Bodie, 2001] Hill, D. A. and Bodie, J. B. (2001). Carrier detection of psk signals. *IEEE Transactions on Communications*, 49(3):487–496.

[Houcke, 2002] Houcke, S. (2002). *Séparation autodidacte d'une mélange de sources émettant à débits inconnus et éventuellement différents*. PhD thesis, UPEM - Université Paris-EST Marne-la-Vallée (Université Paris-Est). Th. doct. : Traitement du signal pour les communications, Université Paris-Est, 2002.

[Johnson and Kotz, 1972] Johnson, N. and Kotz, S. (1972). *Distributions in statistics: continuous multivariate distributions*. Wiley series in probability and mathematical statistics: Applied probability and statistics. Wiley.

[Jouini et al., 2012] Jouini, W., Moy, C., and Palicot, J. (2012). Decision making for cognitive radio equipment: analysis of the first 10 years of exploration. *EURASIP Journal on Wireless Communications and Networking*, 2012(26):40 p. http://jwcn.eurasipjournals.com/content/2012/1/26#sec7.

[Jung, 2013] Jung, Y. (2013). Estimation of inverse models applied to power amplifier predistortion. The series name "Linköping Studies in Science and Technology. Licentiate Thesis" is incorrect. The correct sereis name is "Linköping Studies in Science and Technology. Thesis".

[Kay, 2009] Kay, S. M. (2009). *Fundamentals Of Statistical Processing, Volume 2: Detection Theory*. Prentice-Hall signal processing series. Pearson Education.

[Keehr and Hajimiri, 2008] Keehr, E. A. and Hajimiri, A. (2008). Equalization of third-order intermodulation products in wideband direct conversion receivers. *IEEE Journal of Solid-State Circuits*, 43(12):2853–2867.

[Kenington, 2000] Kenington, P. (2000). *High-linearity RF Amplifier Design*. Artech House microwave library. Artech House.

[Ketterling, 2004] Ketterling, H.-P. A. (2004). *Introduction to digital professional mobile radio*. Artech House, 685 Canton Street Norwood, MA 02062.

[Kim et al., 2007] Kim, K., Akbar, I. A., Bae, K. K., Um, J. S., Spooner, C. M., and Reed, J. H. (2007). Cyclostationary approaches to signal detection and classification in cognitive radio. In *2007 2nd IEEE International Symposium on New Frontiers in Dynamic Spectrum Access Networks*, pages 212–215.

[Laot, 1997] Laot, C. (1997). *"Egalisation autodidacte et turbo-égalisation. Application aux canaux sélectifs en fréquence*. PhD thesis, INST Bretagne. Thèse de doctorat dirigé par Glavieux, Alain Traitement du signal et télécommunicaitons Rennes 1 1997.

[Larson, 1997] Larson, L. E. (1997). *RF and microwave circuit design for wireless communications*. Mobile communication series. Artech House, Boston, MA.

[Lolis, 2011] Lolis, L. (2011). *Agile Bandpass Sampling RF Receivers for low power Applications*. Theses, Université Sciences et Technologies - Bordeaux I.

[Macchi et al., 1993] Macchi, O., da rochai, C. A. F., and Travassos-Romanof, J. M. (1993). égalisation adaptative autodidacte par rt́roprd́iction et prd́iction. In *GRETSI 1993 : 14ème colloque du Groupement de Recherche en Traitement du Signal et des Images*.

[Max, 1981] Max, J. (1981). *Méthodes et techniques de traitement du signal et applications aux mesures physiques: Principes généraux et méthodes classiques*. Méthodes et techniques de traitement du signal et applications aux mesures physiques. Masson.

[Mazo, 1978] Mazo, J. E. (1978). Jitter comparison of tones generated by squaring and by fourth-power circuits. *The Bell System Technical Journal*, 57(5):1489–1498.

[Mitola, 2000] Mitola, J. (2000). *Cognitive Radio — An Integrated Agent Architecture for Software Defined Radio*. DTech thesis, Royal Institute of Technology (KTH), Kista, Sweden.

[Mitola and Maguire, 1999] Mitola, J. and Maguire, G. Q. (1999). Cognitive radio: making software radios more personal. *IEEE Personal Communications*, 6(4):13–18.

[Muhammad et al., 2005] Muhammad, K., Ho, Y. C., Mayhugh, T., Hung, C. M., Jung, T., Elahi, I., Lin, C., Deng, I., Fernando, C., Wallberg, J., Vemulapalli, S., Larson, S., Murphy, T., Leipold, D., Cruise, P., Jaehnig, J., Lee, M. C., Staszewski, R. B., Staszewski, R., and Maggio, K. (2005). A discrete time quad-band gsm/gprs receiver in a 90nm digital cmos process. In *Proceedings of the IEEE 2005 Custom Integrated Circuits Conference, 2005.*, pages 809–812.

[Muraoka et al., 2008] Muraoka, K., Ariyoshi, M., and Fujii, T. (2008). A novel spectrum-sensing method based on maximum cyclic autocorrelation selection for cognitive radio system. In *2008 3rd IEEE Symposium on New Frontiers in Dynamic Spectrum Access Networks*, pages 1–7.

[Narieda and Hada, 2017] Narieda, S. and Hada, T. (2017). Signal cyclostationarity detection based spectrum sensing using simple diversity combining technique and its implementation. *Wireless Personal Communications*, 96(1):909–924.

[Parsons, 2001] Parsons, J. D. (2001). *The Mobile Radio Propagation Channel*. John Wiley & Sons, Ltd.

[Perez, 1998] Perez, R., editor (1998). *Series page*, volume 1 of *Wireless Communications Design Handbook*. Academic Press.

[Porat and Friedlander, 1989] Porat, B. and Friedlander, B. (1989). Blind adaptive equalization of digital communication channels using high-order moments. In *International Conference on Acoustics, Speech, and Signal Processing,*, pages 1372–1375 vol.2.

[Proakis, 2001] Proakis, J. (2001). *Digital Communications*. McGraw-Hill series in electrical and computer engineering : communications and signal processing. McGraw-Hill.

[Raab et al., 2002] Raab, F. H., Asbeck, P., Cripps, S., Kenington, P. B., Popovic, Z. B., Pothecary, N., Sevic, J. F., and Sokal, N. O. (2002). Power amplifiers and transmitters for rf and microwave. *IEEE Transactions on Microwave Theory and Techniques*, 50(3):814–826.

[Razavi, 2011] Razavi, B. (2011). *RF Microelectronics (2Nd Edition) (Prentice Hall Communications Engineering and Emerging Technologies Series)*. Prentice Hall Press, Upper Saddle River, NJ, USA, 2nd edition.

[Rebeiz et al., 2015] Rebeiz, E., Ghadam, A. S. H., Valkama, M., and Cabric, D. (2015). Spectrum sensing under rf non-linearities: Performance analysis and dsp-enhanced receivers. *IEEE Transactions on Signal Processing*, 63(8):1950–1964.

[Rebeiz et al., 2012] Rebeiz, E., Urriza, P., and Cabric, D. (2012). Experimental analysis of cyclostationary detectors under cyclic frequency offsets. In *2012 Conference Record of the Forty Sixth Asilomar Conference on Signals, Systems and Computers (ASILOMAR)*, pages 1031–1035.

[Reichert, 1992] Reichert, J. (1992). Automatic classification of communication signals using higher order statistics. In *Acoustics, Speech, and Signal Processing, 1992. ICASSP-92., 1992 IEEE International Conference on*, volume 5, pages 221–224 vol.5.

[Rouphael, 2014] Rouphael, T. J. (2014). *Chapter 8 - Receiver Architectures*. Academic Press, Boston.

[Ru et al., 2010] Ru, Z., Klumperink, E. A. M., and Nauta, B. (2010). Discrete-time mixing receiver architecture for rf-sampling software-defined radio. *IEEE Journal of Solid-State Circuits*, 45(9):1732–1745.

[Saleh, 1981] Saleh, A. A. M. (1981). Frequency-independent and frequency-dependent nonlinear models of twt amplifiers. *IEEE Transactions on Communications*, 29(11):1715–1720.

[Spooner, 2001] Spooner, C. M. (2001). On the utility of sixth-order cyclic cumulants for rf signal classification. In *Conference Record of Thirty-Fifth Asilomar Conference on Signals, Systems and Computers (Cat.No.01CH37256)*, volume 1, pages 890–897 vol.1.

[Tang, 2005] Tang, H. (2005). Some physical layer issues of wide-band cognitive radio systems. In *First IEEE International Symposium on New Frontiers in Dynamic Spectrum Access Networks, 2005. DySPAN 2005.*, pages 151–159.

[Tong et al., 1995] Tong, L., Xu, G., Hassibi, B., and Kailath, T. (1995). Blind channel identification based on second-order statistics: a frequency-domain approach. *IEEE Transactions on Information Theory*, 41(1):329–334.

[Traverso et al., 2009] Traverso, S., Ariaudo, M., Fijalkow, I., l. Gautier, J., and Lereau, C. (2009). Decision-directed channel estimation and high i/q imbalance compensation in ofdm receivers. *IEEE Transactions on Communications*, 57(5):1246–1249.

[Tubbax et al., 2005] Tubbax, J., Come, B., der Perre, L. V., Donnay, S., Engels, M., Man, H. D., and Moonen, M. (2005). Compensation of iq imbalance and phase noise in ofdm systems. *IEEE Transactions on Wireless Communications*, 4(3):872–877.

[Turunen et al., 2016] Turunen, V., Kosunen, M., Kallioinen, S., Pärssinen, A., and Ryynänen, J. (2016). The effects of non-linearity in spectrum sensing receivers. *International Journal of Microwave and Wireless Technologies*, FirstView:1–9.

[UC, 2018] UC, T. (2018). Tetrapol institutional website. http://www.tetrapol.com. Accessed: 2018-06-11.

[Urkowitz, 1967] Urkowitz, H. (1967). Energy detection of unknown deterministic signals. *Proceedings of the IEEE*, 55(4):523–531.

[Valkama et al., 2006] Valkama, M., hagh ghadam, A. S., Anttila, L., and Renfors, M. (2006). Advanced digital signal processing techniques for compensation of nonlinear distortion in wideband multicarrier radio receivers. *IEEE Transactions on Microwave Theory and Techniques*, 54(6):2356–2366.

[Valkama et al., 2001] Valkama, M., Renfors, M., and Koivunen, V. (2001). Advanced methods for i/q imbalance compensation in communication receivers. *IEEE Transactions on Signal Processing*, 49(10):2335–2344.

[Valkama et al., 2005] Valkama, M., Renfors, M., and Koivunen, V. (2005). Blind signal estimation in conjugate signal models with application to i/q imbalance compensation. *IEEE Signal Processing Letters*, 12(11):733–736.

[Villegas, 2007] Villegas, M. (2007). *Radiocommunications numériques: Conception de circuits intégrés RF et micro-ondes*. Radiocommunications numériques. Dunod.

[Windisch and Fettweis, 2007] Windisch, M. and Fettweis, G. (2007). Blind estimation and compensation of i/q imbalance in ofdm receivers with enhancements through kalman filtering. In *2007 IEEE/SP 14th Workshop on Statistical Signal Processing*, pages 754–758.

[Yucek and Arslan, 2009] Yucek, T. and Arslan, H. (2009). A survey of spectrum sensing algorithms for cognitive radio applications. *Commun. Surveys Tuts.*, 11(1):116–130.

[Zou et al., 2009] Zou, Q., Mikhemar, M., and Sayed, A. H. (2009). Digital compensation of cross-modulation distortion in software-defined radios. *IEEE Journal of Selected Topics in Signal Processing*, 3(3):348–361.

UNIVERSITE BRETAGNE LOIRE / MATHSTIC

IMT Atlantique
Bretagne-Pays de la Loire
École Mines-Télécom

Titre : Identification aveugle de l'environnement spectral au plus près de la chaine d'acquisition pour un système PMR

Mots clés : Détection aveugle, Non linéarités, Récepteur PMR, Cyclostationnarité

Résumé : Cette thèse a été préparée à l'IMT atlantique dans le contexte du projet FITNESS. Ce projet Européen vise à moderniser les radios PMR (Professional Mobile Radio), utilisées par les services de sûretés. L'objectif est de développer un nouveau récepteur compatible avec les 4 normes européennes, tout en ajoutant de nouvelles fonctionnalités. Les contributions de cette thèse à FITNESS concernent la rétrocompatibilité du nouveau récepteur avec les standards actuels. Un filtre de sélection de canal de fréquence centrale reconfigurable a été utilisé pour gérer cette interopérabilité. Toutefois on notera que sa bande passante est trop large et que plusieurs canaux de communications insuffisamment atténués serons présents au niveau des convertisseurs. Pour relâcher les contraintes de linéarité et les marges de numérisation, nous proposons de rendre le récepteur conscient de son environnement spectral. L'intérêt de cette méthode a été développé dans une première partie de la thèse. Une méthode de détection aveugle basée sur les propriétés cyclostationnaires du signal de communication a été proposée. Nous utilisons ensuite cet outil pour détecter la présence d'harmoniques indésirables créés lors d'un fonctionnement en régime non linéaire du récepteur. Nous montrons qu'il est ainsi possible de détecter très tôt le mode de fonctionnement du récepteur. Enfin, basé sur les deux études précédentes nous proposons une méthode permettant d'adapter automatiquement les paramètres de la chaine analogique. Cette preuve de concept basé sur une boucle de rétroaction permet une amélioration significative du taux d'erreur binaire tout en relâchant les contraintes au niveau analogique.

Title : Spectral Environment Blind Identification for PMR System the Closer of Analog Receiver

Keywords : Blind detection, Nonlinearities, PMR receiver, Cyclostationarity

Abstract: This thesis was prepared at IMT Atlantique, in the context of the FITNESS project. This European project aims to modernize PMR (Professional Mobile Radio) radios, used by security services. The objective is to develop a new receiver compatible with the 4 European standards, while adding new features. The contributions of this thesis to FITNESS concern the backwards compatibility of the new receiver with current standards. A reconfigurable central frequency channel selection filter was used to manage this interoperability. However, it should be noted that its bandwidth is too large and that several insufficiently attenuated communication channels are present at the A/D converters input. To relax linearity constraints and digitization margins, we propose to make the receiver aware of its spectral environment. The interest of this method has been developed in a first part of this document. A method for blind detection based on the cyclostationary properties of the communication signal has been proposed. We then use this tool to detect the presence of unwanted harmonics created during non-linear operation of the receiver. We show that it is possible to detect the operating mode of the receiver before the useful signal degradation. Finally, based on the two previous studies, we propose a method to automatically adapt the parameters of the analog receiver. This proof of concept based on a feedback loop allows a significant improvement in the bit error rate while relaxing constraints at the analog level.